Volume Mesh Generation CFD Framework for Hypersonic Heat Flux Predictions

Joel A. McQuaid and Christoph Brehm
University of Maryland



Advanced Modeling & Simulation (AMS) Seminar Series
NASA Ames Research Center, May 30th, 2024

NASA EPSCoR RA Award (no. 80NSSC19M0144) with Dr. Eric Stern
NASA ACCESS (award no. 80NSSC21K1117) with Dr. Eric Stern.
Office of Naval Research (award no. N00014-23-1-2167) with Dr. Eric Marineau.
Naval Air Warfare Center Aircraft Division (award no. N00421-22-2-0001) with Dr. Joshua Butler and Dr. William Tyson.

Introduction

- Hypersonic flight has been under study as early as 1948
- Various rocket-powered flight vehicles were designed to test the vehicle designs at these extreme conditions
  - RTV-G-4 Bumper (1948)
  - X-15 (1959)
  - X-51 (2010)
  - HTV-2 (2011)
- HTV-2 was flown to Mach 20, then spent 200 seconds flying in the atmosphere before succumbing to aerodynamic heating



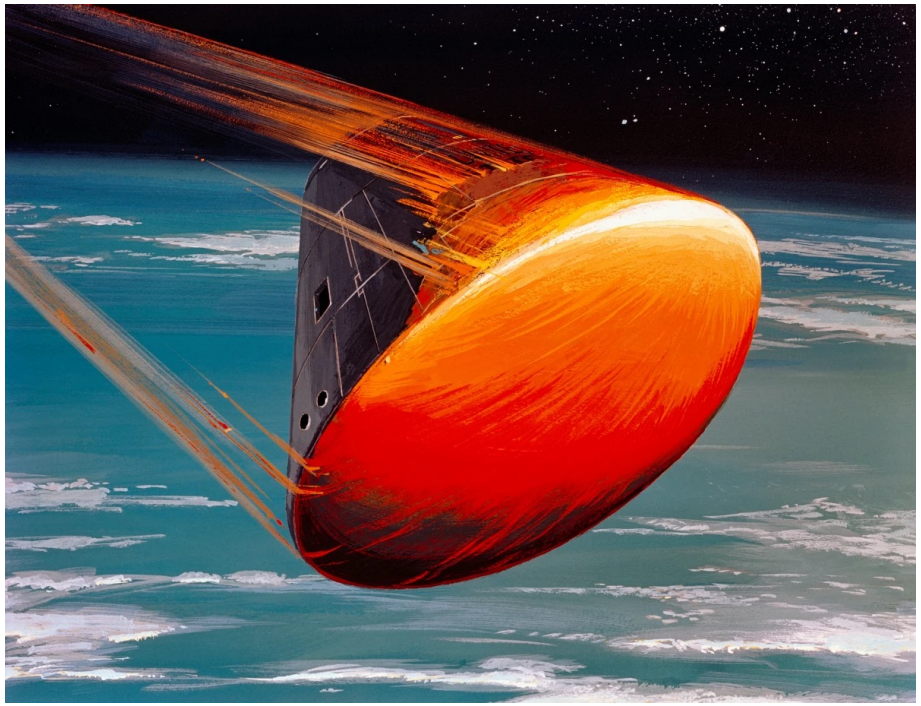




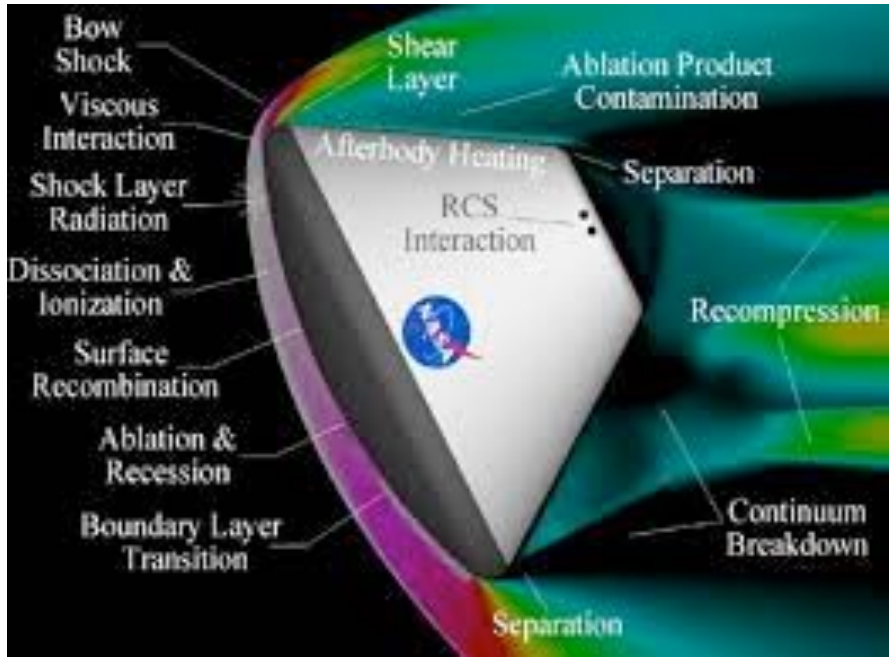
NASA NESC (2014, May 28). X-15 Flight 3-65-97 Accident Analysis: A Fresh Look at the Role of the MH-96 "Self-Adaptive" Flight Control System. https://nescacademy.nasa.gov/video/afbbfa1bb74243aeab139db4c110c2021d
University of Colorado Boulder (2022, March 30). CU Boulder awarded major Department of Defense research grant for hypersonics. https://www.colorado.edu/aerospace/2022/03/30/cu-boulder-awarded-major-department-defense-research-grant-hypersonics
Wikimedia Foundation. (2010, February 25). DARPA Falcon Project. https://en.wikipedia.org/wiki/DARPA_Falcon_Project

Introduction

- Sustained hypersonic flight is still not commercially viable after decades of research
- Two significant hurdles remain (to name a few)
  - How can we mitigate aerodynamic heating effects to design reusable hypersonic vehicles?
  - What kind of propulsion system is capable of sustained hypersonic flight?







NASA JSC. (1968, August). Art Concept - Apollo VIII - Command Module (CM) - Re-Entry Orientation. https://images.nasa.gov/details-S68-55292

National Air and Space Museum. (1970). Gemini Heat Shield, Ablated. https://airandspace.si.edu/collection-objects/heat-shield-gemini/nasm_A19781814000

Introduction

- Entry vehicle heat flux can be approximated with (Earth entry):

$$\dot{q} = (1.83E-4)u_{\infty}^{3}\sqrt{\frac{\rho_{\infty}}{R_n}}$$

- Heat load is a strong function of the entry velocity
- How do we mitigate aerodynamic heating?
  - Ablative heat shields (graphite, FiberForm, PICA, SLA, etc.)
  - Transpiration cooling
  - Geometric optimizations
- Heat shields need to be replaced after each flight to maintain structural integrity

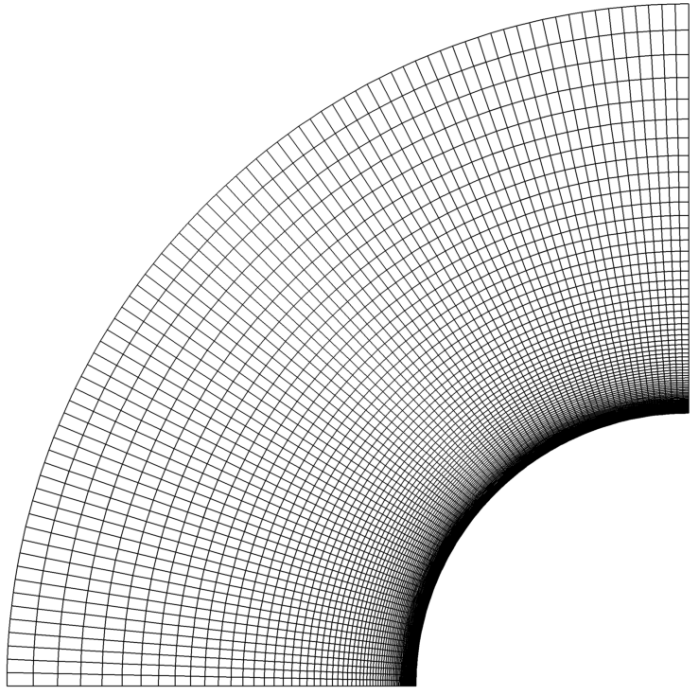
Material	Graphite	FiberForm	PICA	SLA
Max. Temp (K)	~3200	~3000	?	~1100

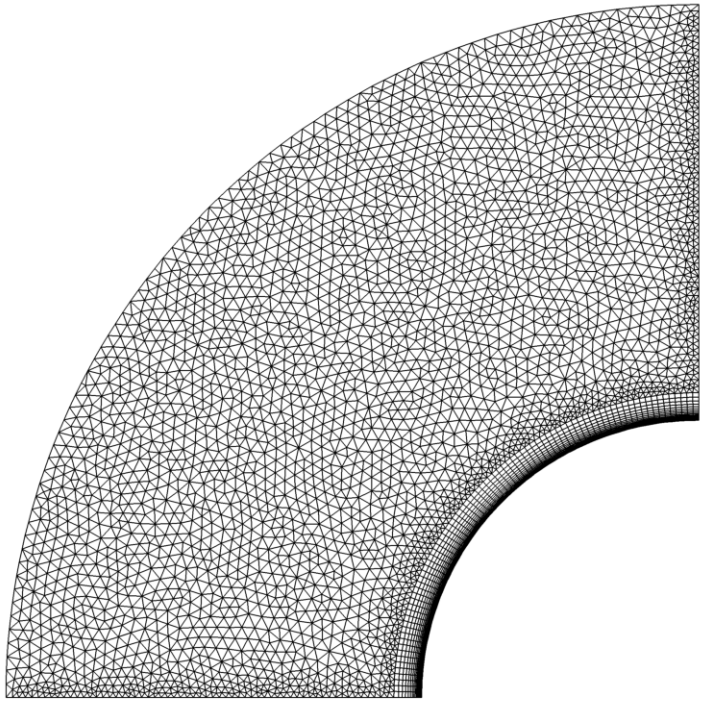
Motivation

- Accurate surface heat flux predictions is critical to hypersonic vehicle design and analysis
- Surface heat flux is a highly sensitive quantity, particularly with respect to:
  - Shock alignment with grid
  - Mesh generation
  - Mesh element topology
  - Convective/viscous schemes (specifically near-wall dissipation)
  - Boundary conditions
  - Etc.
- In the context of high enthalpy environments, typical of fluid ablation interaction (FAI) applications, additional sensitivity stems from the employed reaction mechanism and mixture transport properties

Background

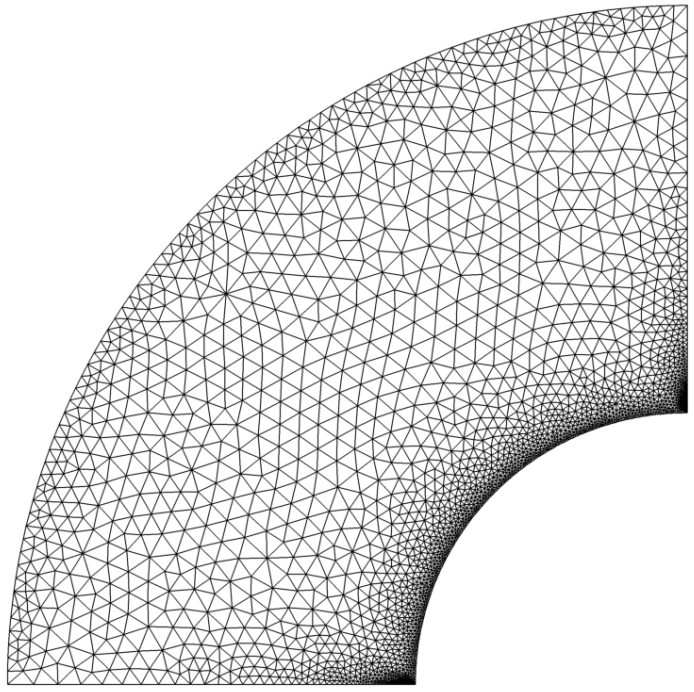
Body-fitted (Structured)

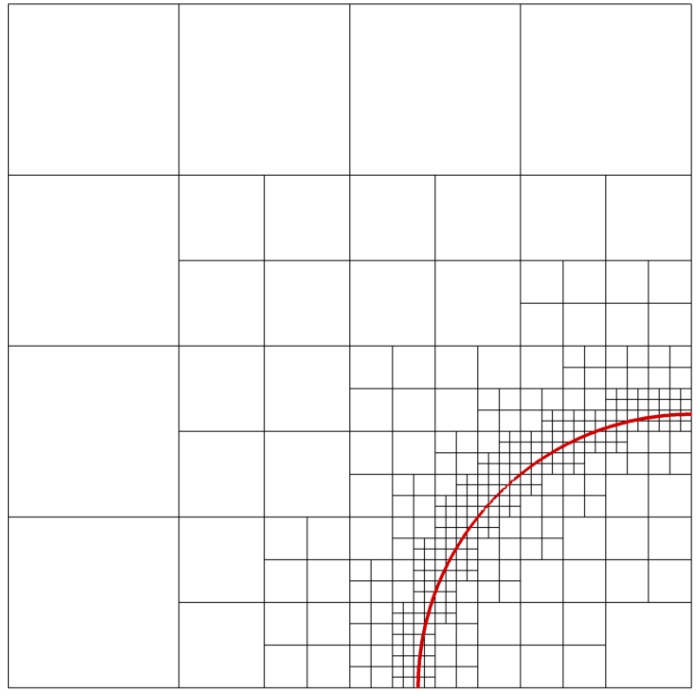




Body-fitted (Quasi-unstructured)

Body-fitted (Unstructured)





Cartesian (Block-structured)

Background

- For laminar viscous flow applications, IBM solvers can be significantly more expensive than body-conformal solvers
  - Inability to employ high aspect ratio cells which are very computationally efficient for laminar boundary layers
- In transitional/turbulent flows, the need for sufficient streamwise resolution makes the relative costs more comparable
  - i.e. for DNS, LES, WMLES, etc.

Estimated fully-resolved IBM grid requirements for 3D Re-entry vehicle

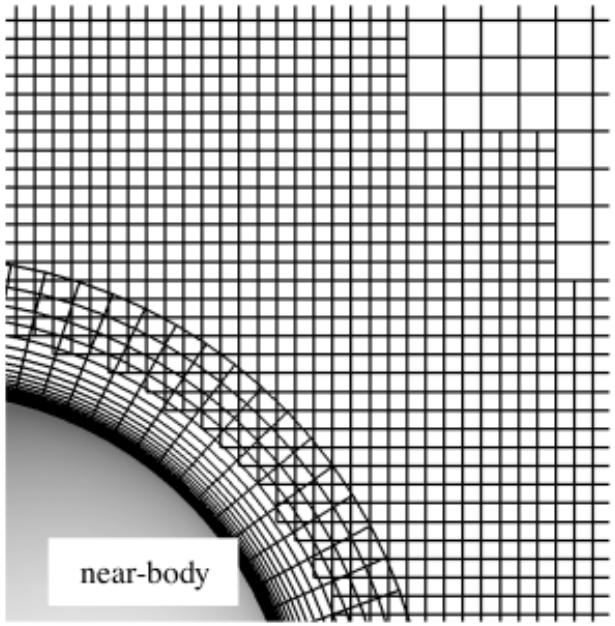
Spacing Requirement	Minimum Spacing	Total Points Required
"Transitional"	1.0×10^{-02}	$1.86 \times 10^{+06}$
Inviscid	5.0×10^{-03}	$5.89 \times 10^{+06}$
Viscous	1.0×10^{-06}	$8.43 \times 10^{+12}$

*Taken from work of Meakin et al. (2007)

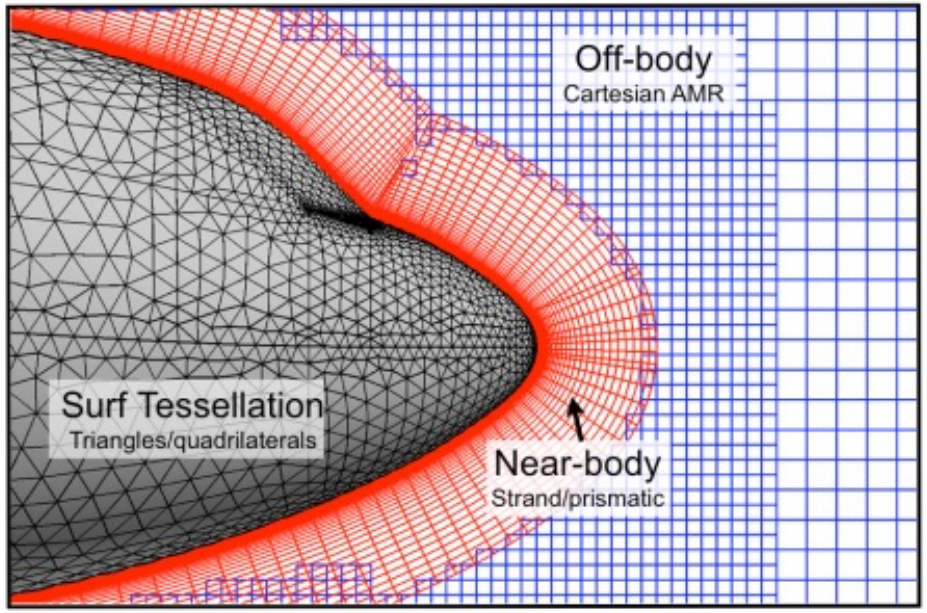
- Based on the Orion CEV test case (included in thesis)
  - Body-fitted mesh size: 4M (Hollis 2009, DPLR)
  - NBS-Cart solver (this work): 12.5M (McQuaid et al. CAF 2023); over-resolved based on grid study

Near Body/Strand Grid Solvers

- The solution to this issue (for laminar boundary layers) is a hybrid grid framework
  - Body-conformal grid to capture boundary layer
  - Cartesian grid to track off-body flow structures
  - Overset coupling between both solvers
- Only 1 Cartesian/strand grid solver is capable of simulating high speed flows for heating predictions (Atkins 2022)
  - Limited to 2D only
  - Mesh motion achieved via pre-defined topology changes (rather than being driven by an MR solver)



*Taken from work of Meakin et al. (2007)



*Taken from work of Wissink et al. (2009)

- Used for:
  - Transitional/turbulent flows for low-speed (Ma<1) rotorcraft applications
  - Research almost exclusively limited to perfect gas models
  - Heat flux comparisons are rarely shown

Objective

- Develop automated solver capabilities within the CHAMPS framework capable of automatic volume mesh generation and accurate heat flux predictions in consideration of laminar boundary layers
- The NBS solver development
  - **Wall-modeled NBS coupling (NBS-IBM solver)**
    a) Validation of solver coupling for simple 2D applications
  - **Overset 2D NBS coupling (NBS-Cart solver)**
    a) Validation of solver coupling for simple 2D applications
    b) Coupled framework between the CHAMPS NBS solver and KATS-MR solver for 2D FAI studies
  - **Overset 3D NBS coupling (NBS-Cart solver)**
    a) Extension of NBS solver to 3D applications
    b) Development of higher order, memory optimized convective schemes for 3D NBS scale resolving simulations

Contributions of PhD Dissertation

- Trajectory-based aerothermodynamics simulations
  - Constantly changing shock characteristics and wake structures induces accuracy losses if no grid augmentation is implemented
  - How do you robustness move grid points to track flow structures without sacrificing near-wall grid quality?
  - **NBS-Cart: AMR tracks both shock and wake structure during runtime with no user intervention; independent of NBS grid resolution**
- High-fidelity scale-resolving simulations (i.e. BOLT)
  - Iterative simulation process between dissipative upwinding and central schemes to arrive at final solution state
  - Complex vehicles with body-fitted codes often reduce to low order finite-volume methods
  - Iterative process on grid tailoring to shock front to reduce numerical noise (see Vu et. al Scitech 2024, US3D)
  - **NBS-Cart: Maintain higher order accuracy on Cartesian solver and accurate wall-normal gradient reconstructions on NBS; good solution with a single simulation**

Governing Equations

- Compressible Navier-Stokes equations
  - Additional terms for capturing finite-rate effects marked in red
  - 2-temperature model for reacting flow cases
  - NBS solves same governing equations as Cartesian solver
  - Validation for Earth/Mars entry

$$W = \frac{\partial \boldsymbol{U}}{\partial t} + \boldsymbol{\nabla} \cdot (\boldsymbol{F} - \boldsymbol{F_v}) \quad \boldsymbol{W} = \begin{bmatrix} \dot{\boldsymbol{w}}_1 \\ \vdots \\ \dot{\boldsymbol{w}}_s \\ \boldsymbol{0} \\ \boldsymbol{0} \\ \boldsymbol{0} \\ \boldsymbol{0} \\ \boldsymbol{Q_{t2v} + Q_{c2v}} \end{bmatrix}$$

$$\boldsymbol{U} = [\rho, \rho u, \rho v, \rho w, \rho e_T]^T$$

$$\boldsymbol{F^1} = \begin{bmatrix} \rho u \\ \rho u^2 + p \\ \rho uv \\ \rho uw \\ \rho u e_T \\ \rho u e_v \end{bmatrix} \quad \boldsymbol{F^2} = \begin{bmatrix} \rho v \\ \rho vu \\ \rho v^2 + p \\ \rho vw \\ \rho v e_T \\ \rho v e_v \end{bmatrix} \quad \boldsymbol{F^3} = \begin{bmatrix} \rho w \\ \rho wu \\ \rho wv \\ \rho w^2 + p \\ \rho w e_T \\ \rho w e_v \end{bmatrix}$$

$$\boldsymbol{F_v^1} = \begin{bmatrix} -J_{1,x} \\ \vdots \\ -J_{s,x} \\ \tau_{xx} \\ \tau_{xy} \\ \tau_{xz} \\ f_v^1 \\ f_v^4 \end{bmatrix} \quad \boldsymbol{F_v^2} = \begin{bmatrix} -J_{1,y} \\ \vdots \\ -J_{s,y} \\ \tau_{yx} \\ \tau_{yy} \\ \tau_{yz} \\ f_v^2 \\ f_v^5 \end{bmatrix} \quad \boldsymbol{F_v^3} = \begin{bmatrix} -J_{1,z} \\ \vdots \\ -J_{s,z} \\ \tau_{zx} \\ \tau_{zy} \\ \tau_{zz} \\ f_v^3 \\ f_v^6 \end{bmatrix}$$

$$f_v^1 = u\tau_{xx} + v\tau_{xy} + w\tau_{xz} - q_x - q_{v,x} - \sum_{i=1}^{ns} J_{i,x} h_i$$

$$f_v^2 = u\tau_{yx} + v\tau_{yy} + w\tau_{yz} - q_y - q_{v,y} - \sum_{i=1}^{ns} J_{i,y} h_i$$

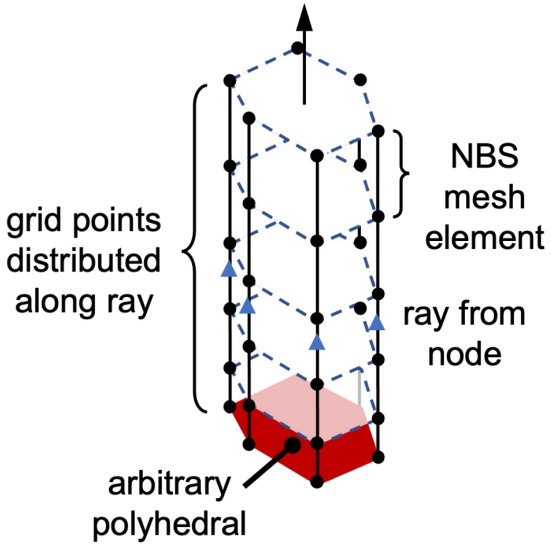
$$f_v^3 = u\tau_{zx} + v\tau_{zy} + w\tau_{zz} - q_z - q_{v,z} - \sum_{i=1}^{ns} J_{i,z} h_i$$

$$f_v^4 = -q_{v,x} - \sum_{i=1}^{ns} J_{i,x} e_{v,i} \quad f_v^5 = -q_{v,y} - \sum_{i=1}^{ns} J_{i,y} e_{v,i}$$

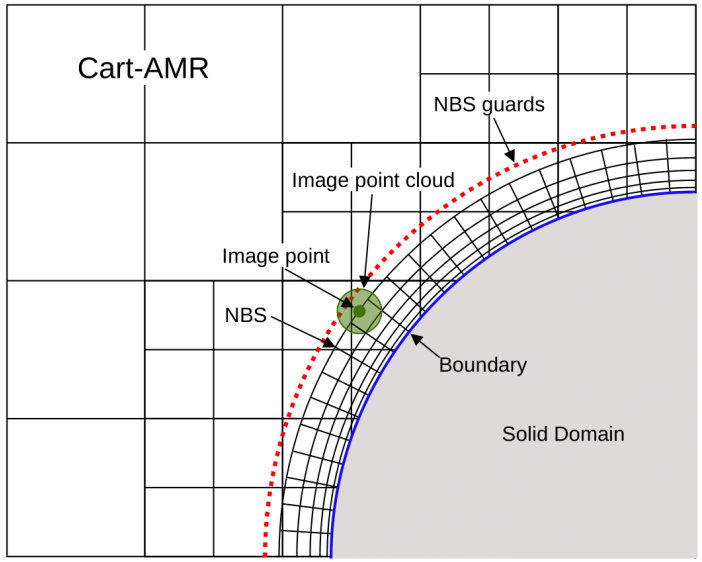
$$f_v^6 = -q_{v,z} - \sum_{i=1}^{ns} J_{i,z} e_{v,i}$$

NBS Solver Overview

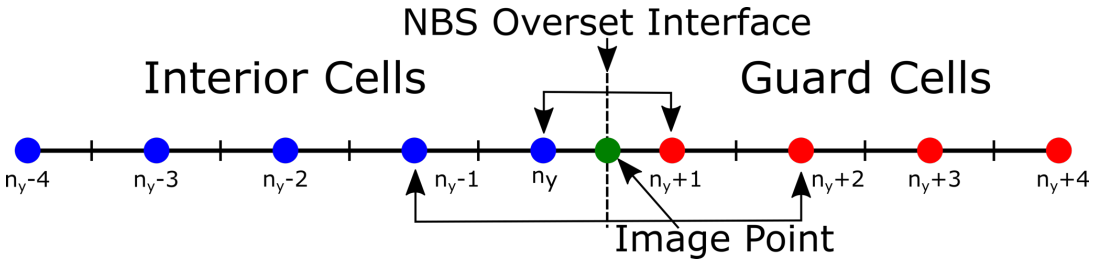
- CHAMPS Cartesian grid solver requires a surface grid to be provided
- NBS mesh generation is built via wall-normal extrusion of this surface grid into the shock layer
  - In 2D, this solver is treated as a fully structured, generalized curvilinear grid
  - Numerical schemes employ grid transformation metrics for flux evaluation in the computational space
- Cartesian to NBS coupling achieved via image point sampling



(1) Mesh generation



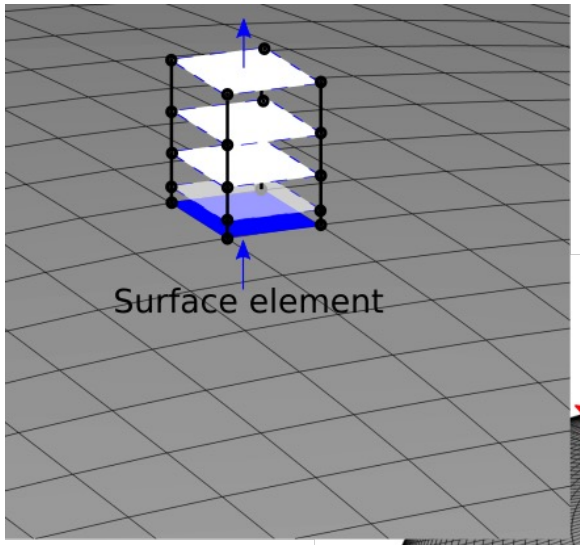
(2) Image point initialization

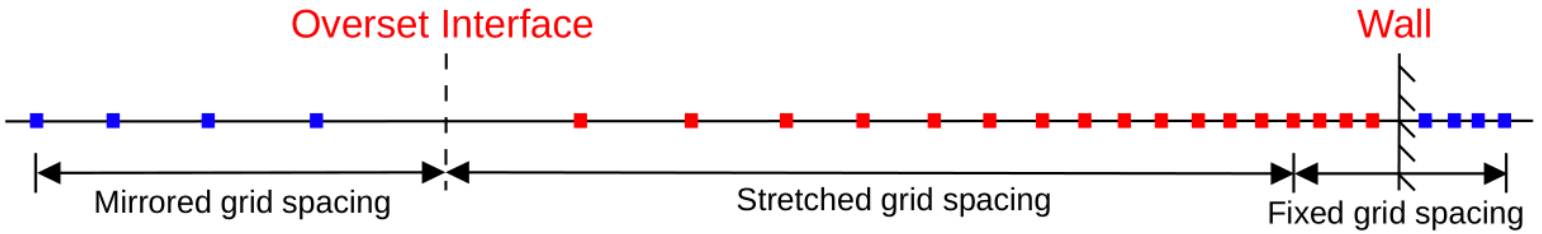


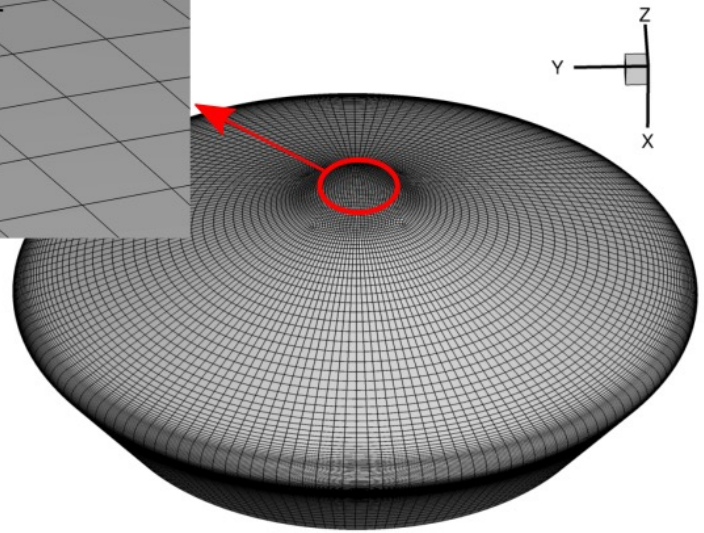
(3) Guard filling stencil

NBS Grid Generation

- Sample grid generation on the fore body of the MSL capsule
  - Quadrilateral surface grid employed
- Fixed cell spacing at wall and mirrored spacing at overset interface to minimize solution reconstruction errors and guarantee wall orthogonality

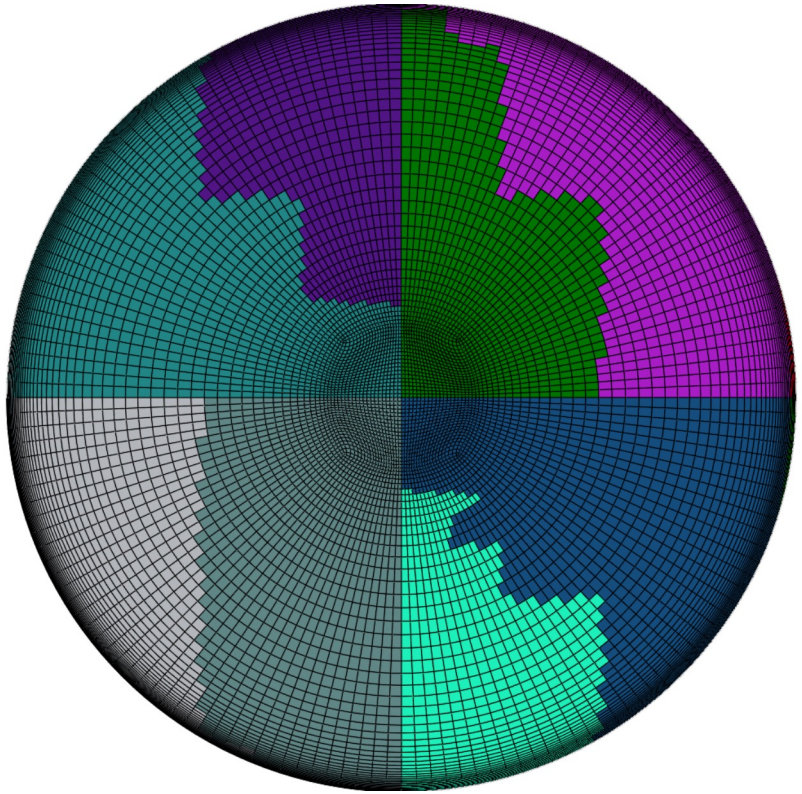




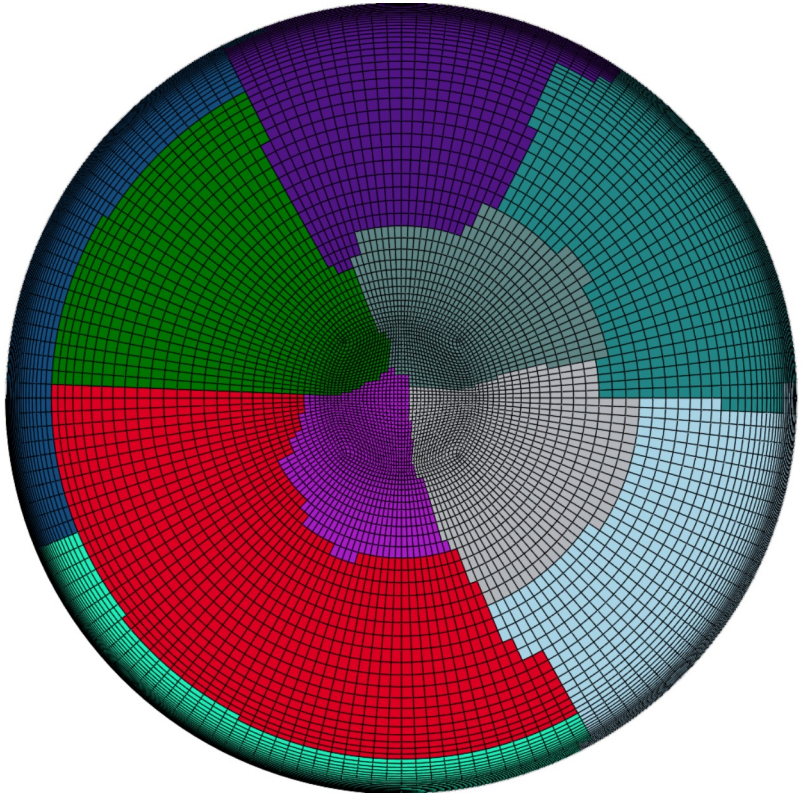


NBS Partitioning and MPI Communication

- NBS partitioning handled with METIS to enforce contiguous partitions (Karypis et al. 1997)
- Sample partition map on MSL capsule
- Partitioning is performed across all available processors; sequential solve with Cartesian solver



Cartesian volume partition



NBS surface partition

NBS-Cart Numerics

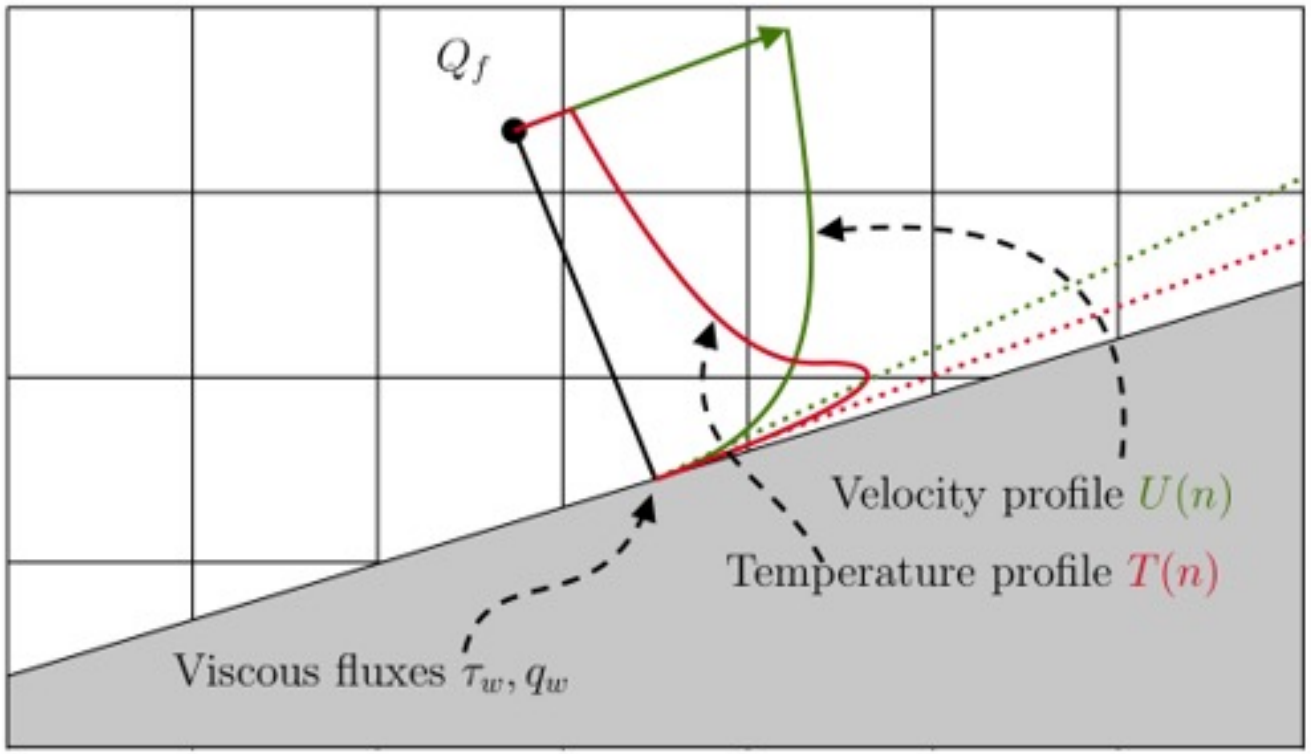
- Cartesian solver
  - 5th order weighted essentially non-oscillatory (WENO-Z) scheme
    - Steger-warming flux function
  - 2nd order centered viscous fluxes
  - Time integration achieved via 3rd order 4-stage strong stability preserving Runge-Kutta scheme (SSPRK34)
- NBS
  - 2nd order Monotonic Upstream-centered Scheme for Conservation Laws (MUSCL)
    - Modified Steger-Warming scheme
  - 2nd order centered viscous fluxes
  - Time integration achieved via line implicit DPLR algorithm

- **Significant differences in NBS and Cartesian spatial scales**
  - Necessitates explicit time integration for Cartesian solver to remain efficient
  - CFL condition dictated by NBS stability

Wall-modeled NBS Solver Coupling (2D)

NBS Wall-Model Coupling

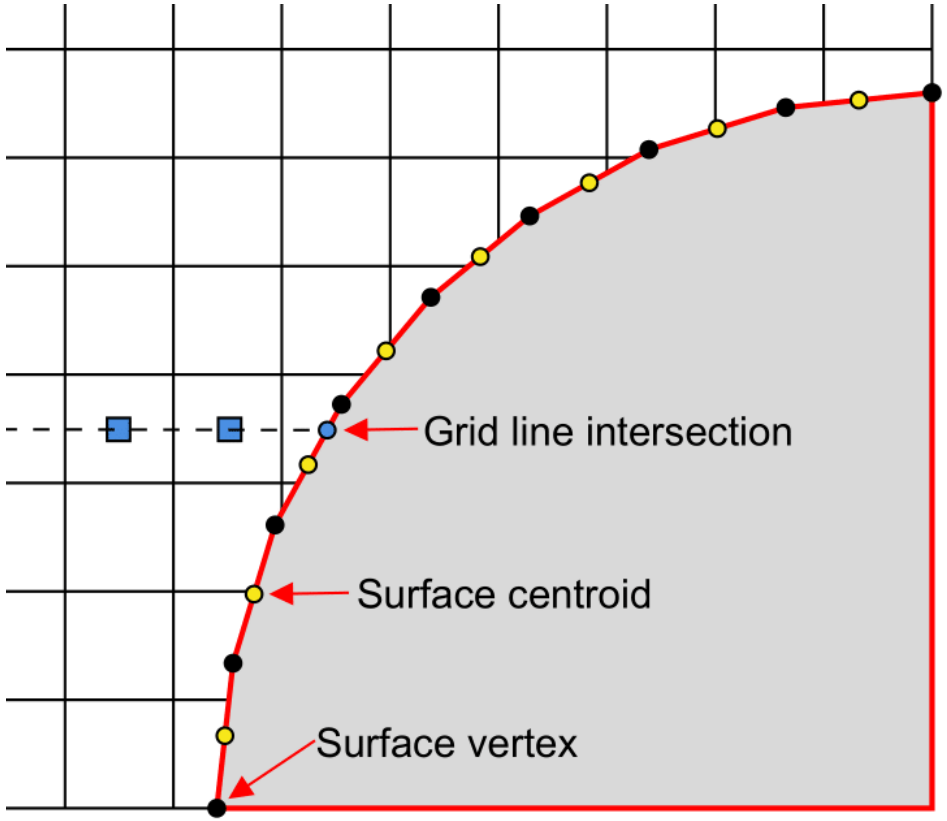
- NBS samples the solution from the IBM solver which refines the upper portion of the boundary layer
- Computed NBS surface viscous fluxes are provided back to the Cartesian solver for inclusion in the viscous flux stencil

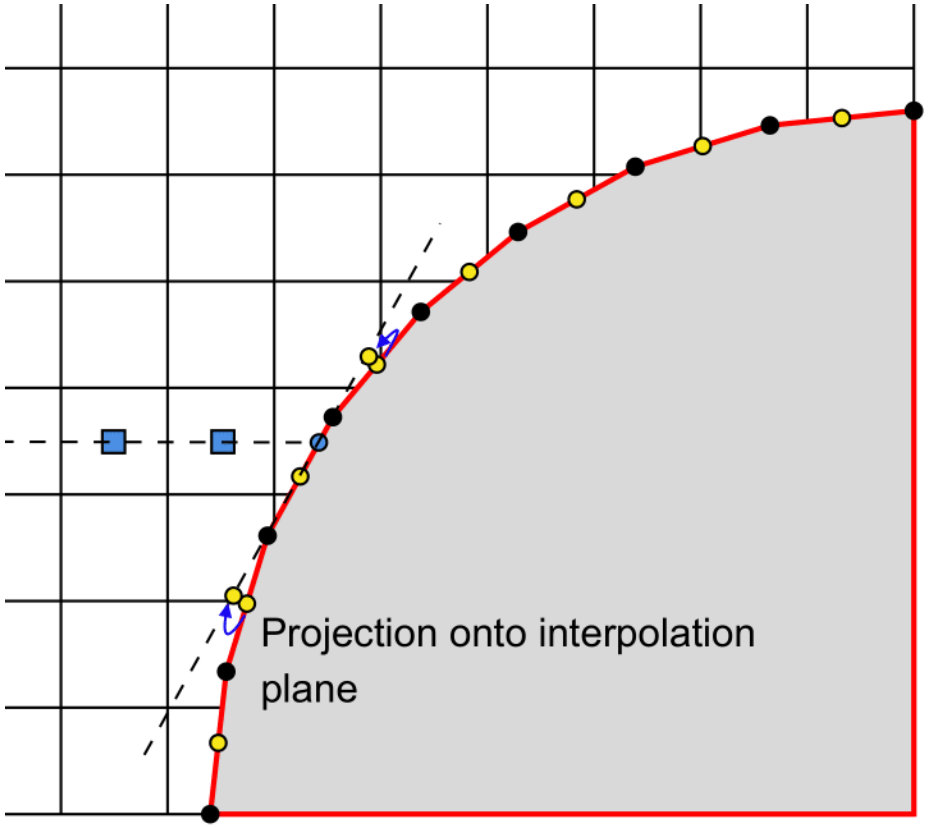


Taken from the work of van Noordt et al. (2021)

NBS Wall-Model Coupling

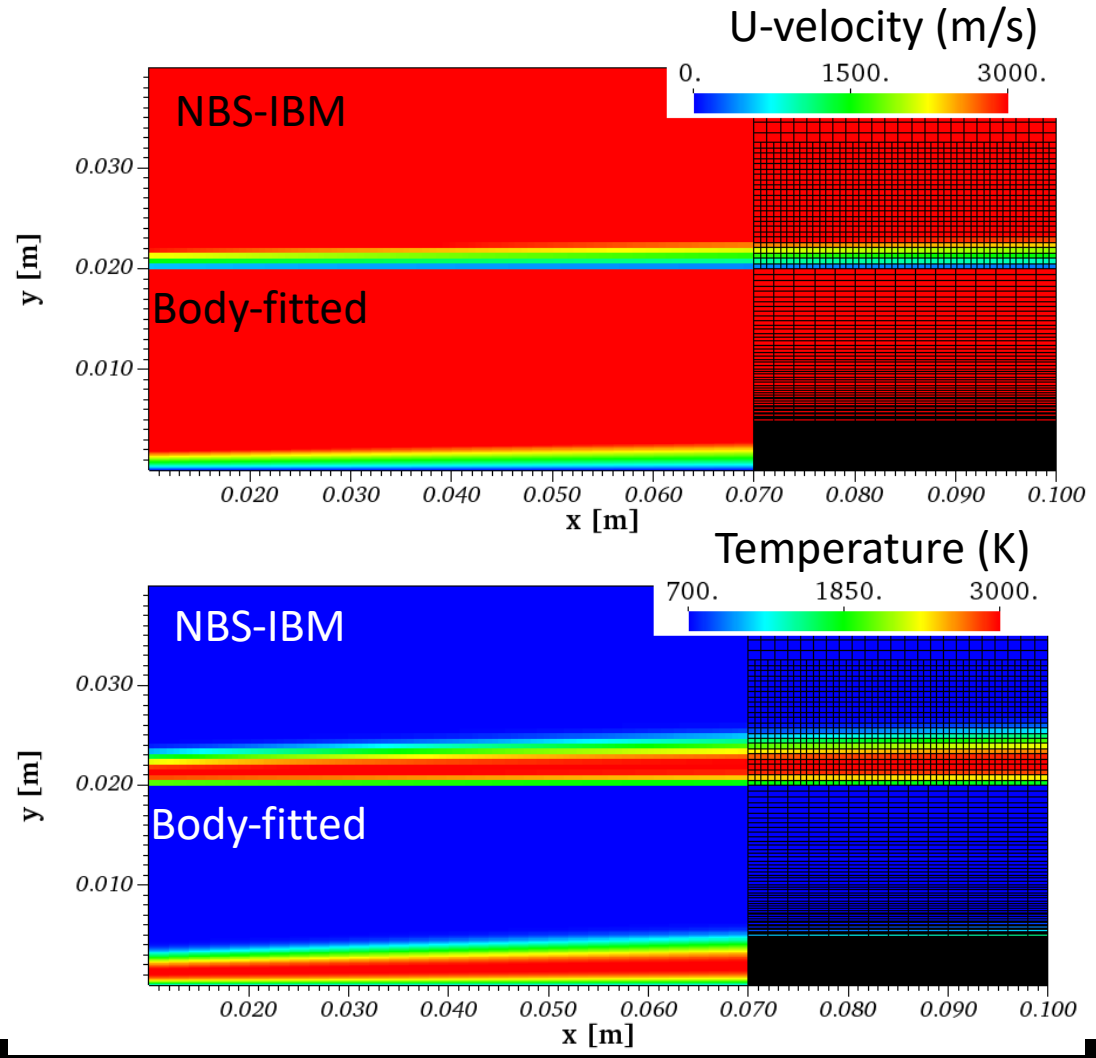
- NBS samples the solution from the IBM solver which refines the upper portion of the boundary layer
- Computed NBS surface viscous fluxes are provided back to the Cartesian solver for inclusion in the viscous flux stencil





Mach 8.5 Flat Plate

- Initialized with similarity solution; 1-species perfect gas mixture
- Used to compare boundary layer profiles between NBS-IBM solver and CHAMPS body-fitted solver
- **Focus:** Can the NBS-IBM solver can capture the correct BL profile on an under-resolved Cartesian grid?

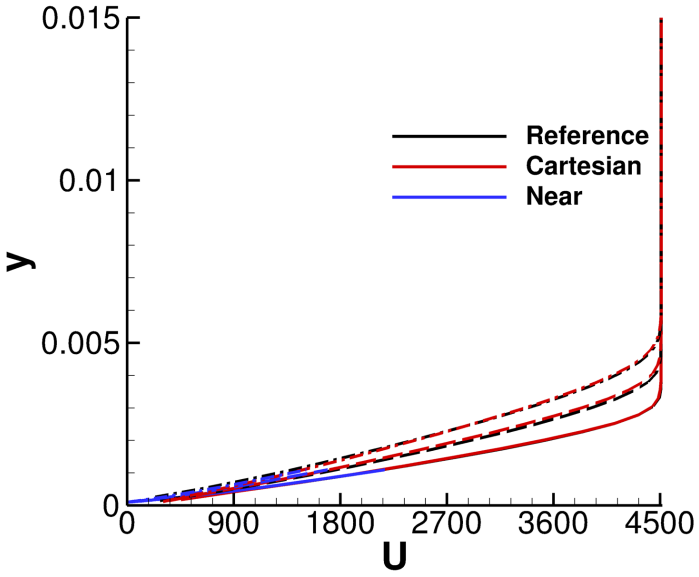


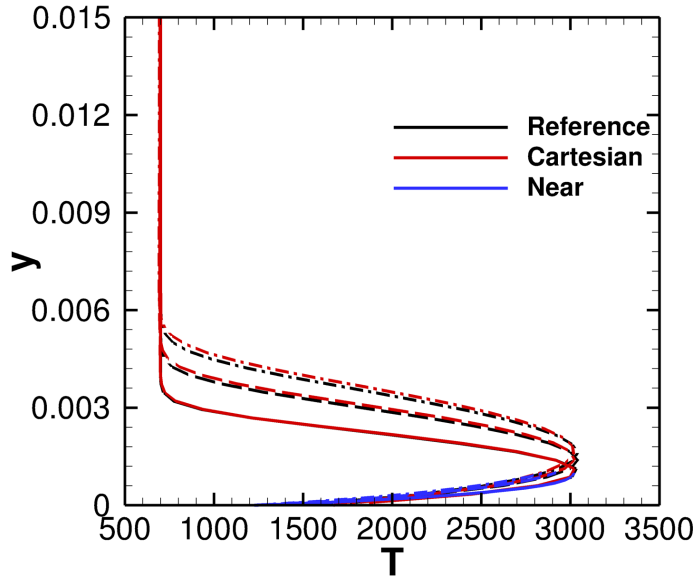
Flow conditions

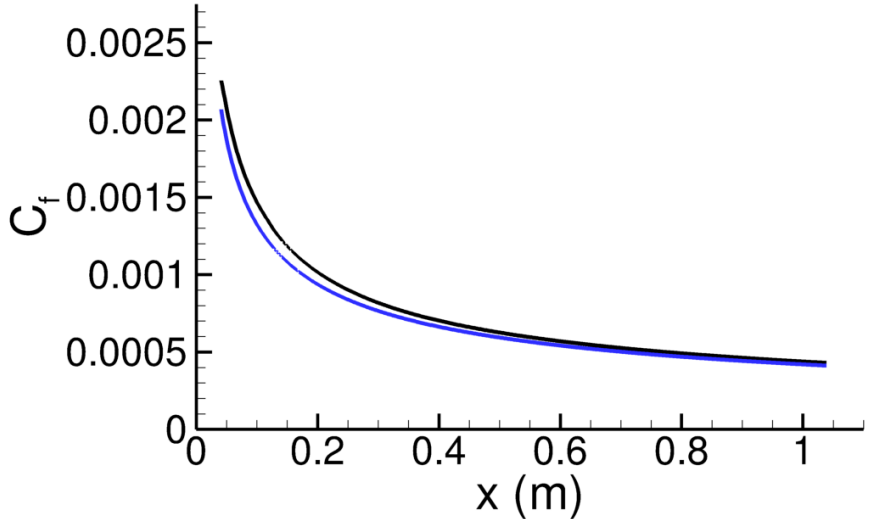
Parameter	Value
M_∞	8.5
p_∞ (Pa)	2932
u_∞ (m/s)	4509
T_∞ (K)	700
T_w (K)	1225
Re_∞ (1/m)	1.983E6

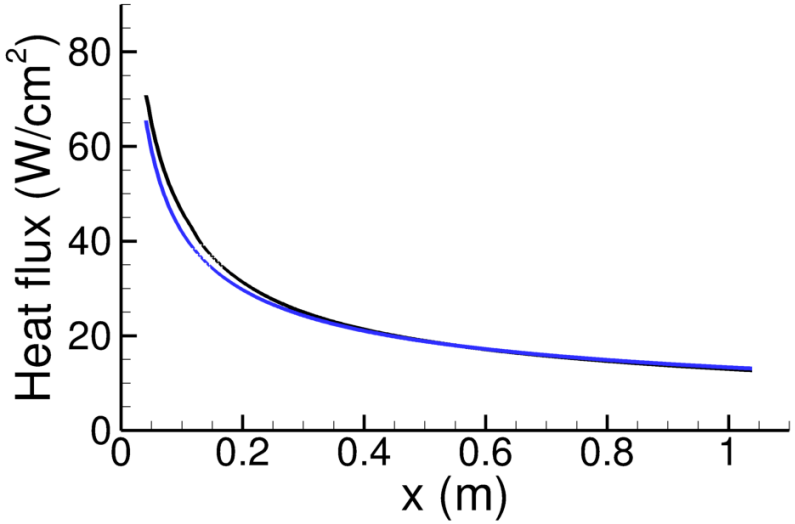
Mach 8.5 Flat Plate

- Reference – CHAMPS body-fitted solution
  - Solid, dashed, and dot-dashed lines – x = 0.1, 0.2, and 0.3 m







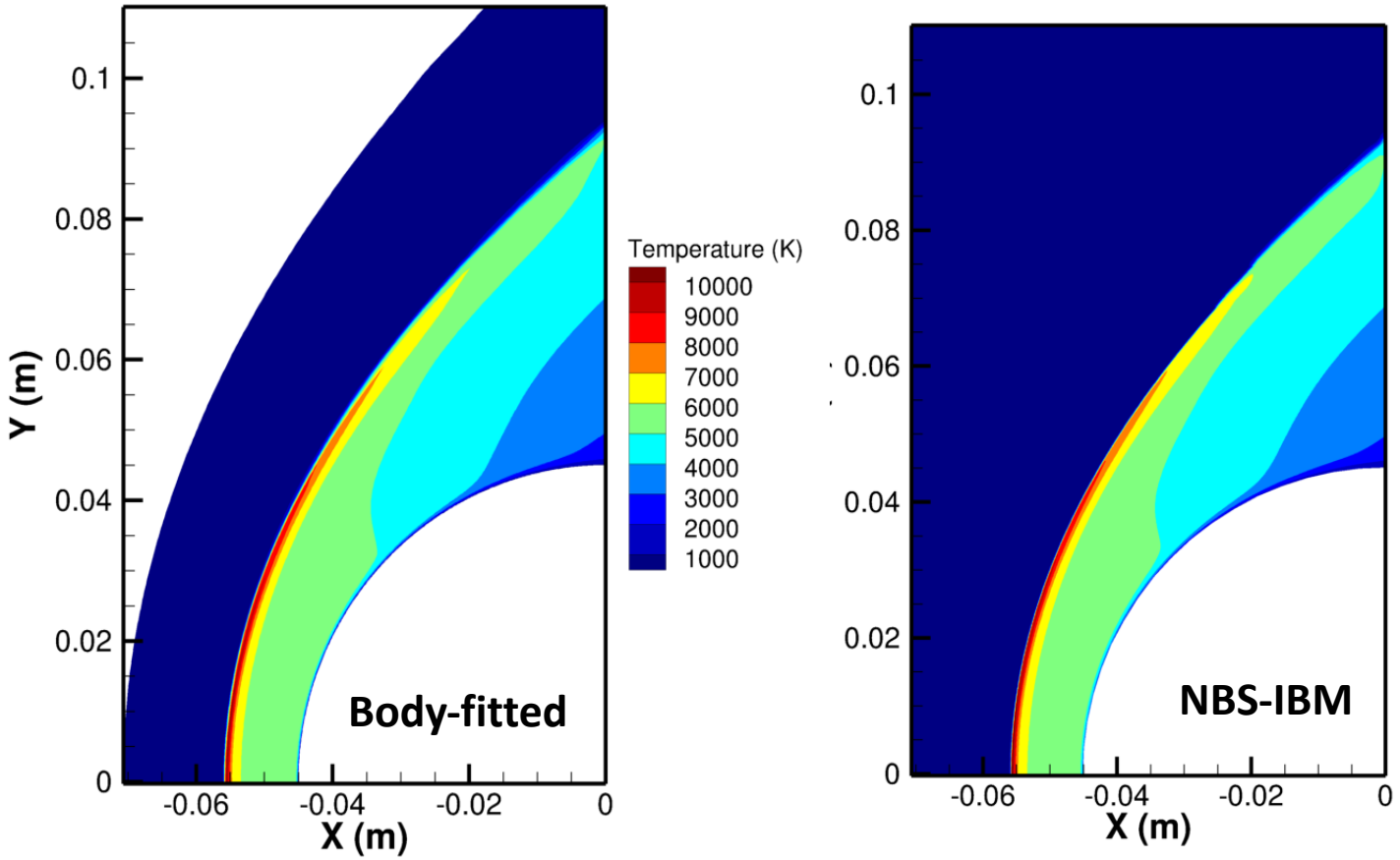


Mach 8.7 Cylinder

- Studied experimentally by Karl et al. (2003), run 627 in the HEG wind tunnel
- Simulated numerically by Nastac et al. (2021) using FUN3D (body-fitted solution)
- 5-species air model
  - N_2, O_2, NO, N, O
- **Focus:** Can the NBS-IBM solver can capture the correct BL profile when considering high temperature effects?

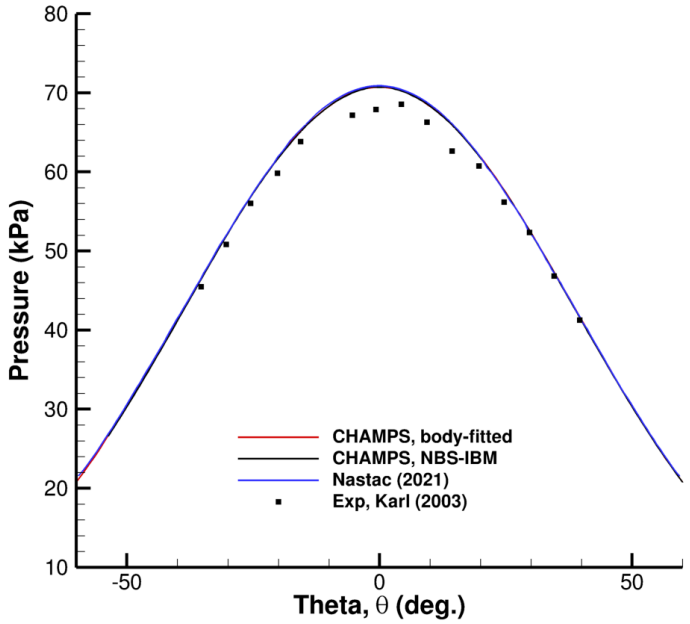
Flow conditions

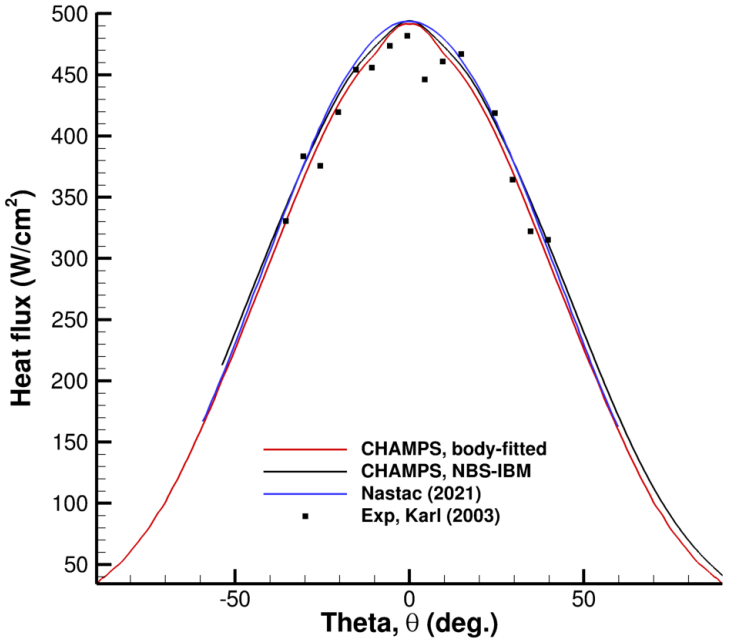
Parameter	Value
M_∞	8.7
p_∞ (Pa)	648.66
u_∞ (m/s)	4776
T_∞ (K)	694
T_w (K)	300
Re_∞ (1/m)	4.770E5
$\vec{Y}$	(0.7356, 0.1340, 0.0509, 0.0, 0.0795)

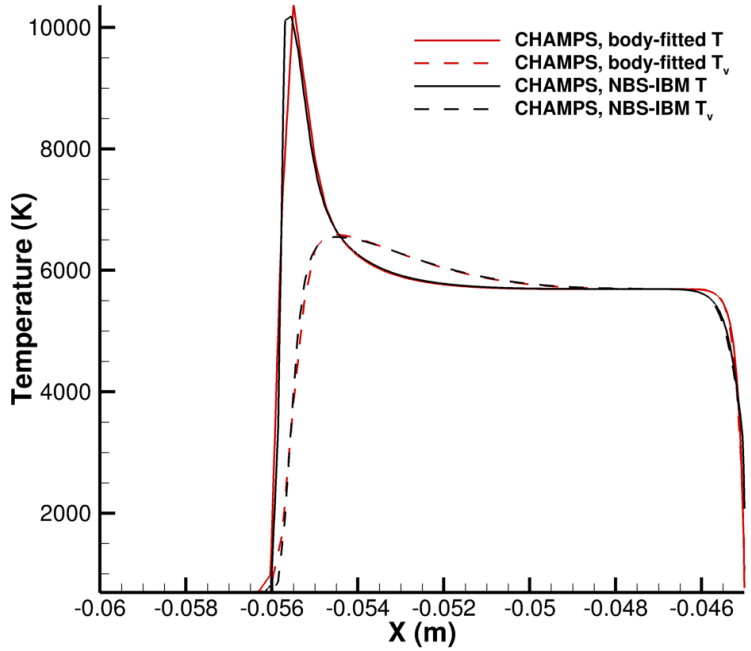


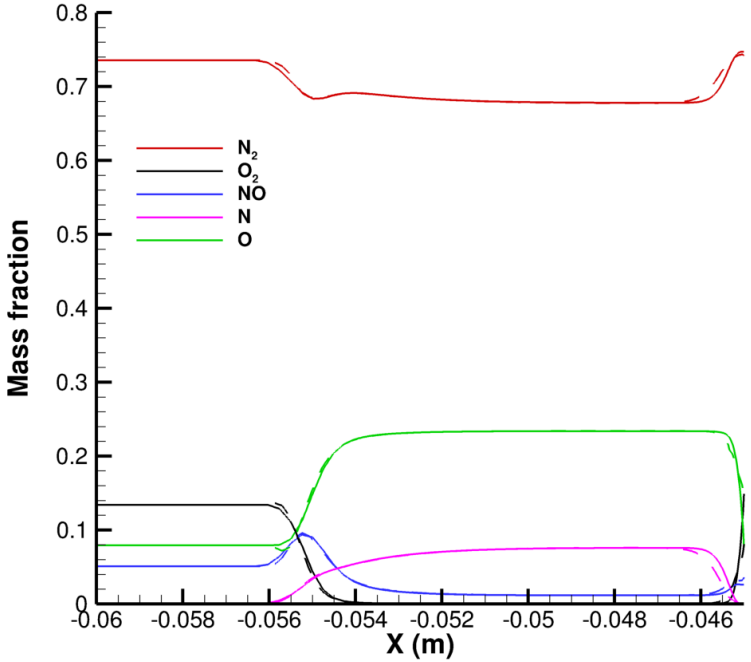
Mach 8.7 Cylinder

- Good agreement in all quantities versus CHAMPS body-fitted solution
- Predicts accurate surface heat flux









NBS-IBM Conclusions

- Generally yields good results but it still requires the use of the immersed interface
  - Requires more resolution at the wall since the coupling point is within the boundary layer

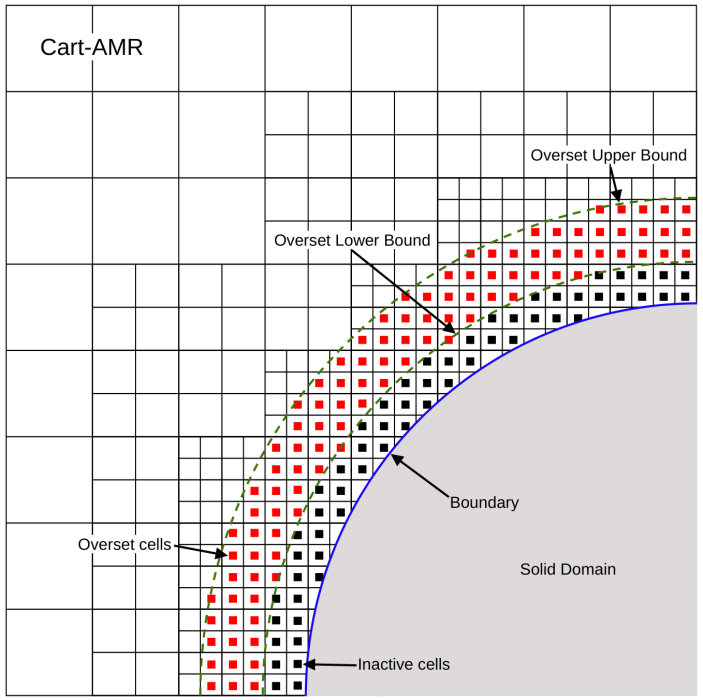
$$\delta_{laminar} = \frac{5x}{\sqrt{Re_x}} \qquad \delta_{turbulent} \approx \frac{0.37x}{Re_x^{1/5}}$$

  - Consider the Mach 8.5 flat plate previously (Re = 2E6 1/m). At x=0.5 m, the laminar BL thickness is: 2.5 mm (vs. 11.7 mm for a turbulent BL)
    - We generally require 8 points in the BL **(Cartesian grid spacing of 3.125E-4 m)**
  - Requires irregular point treatments in the IBM solver which is prone to robustness issues
  - Yet to identify consistent solution for setting the convective boundary condition on the IBM solver
    - Strong impact on heat flux magnitude
- In consideration of this, the overset NBS solver was developed to improve solver robustness and further reduce computational cost

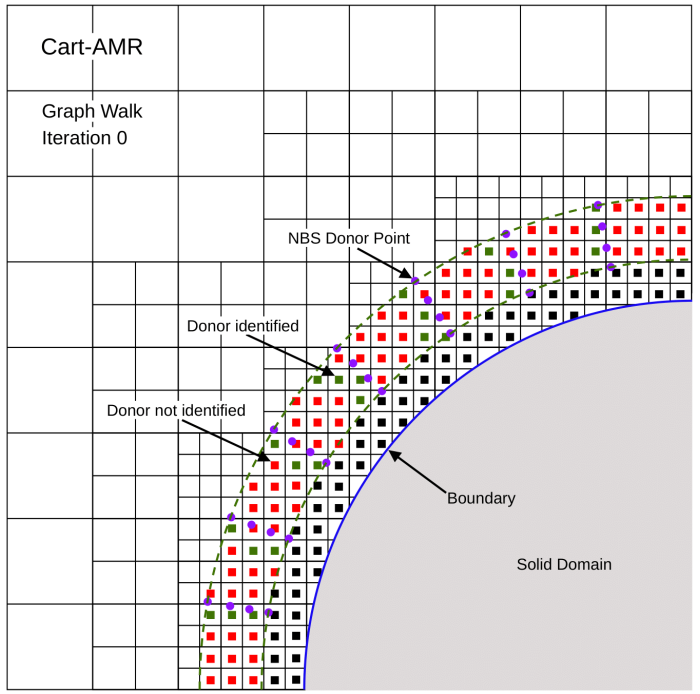
Overset NBS Solver Coupling (2D)

NBS-Cart Overset Interpolation

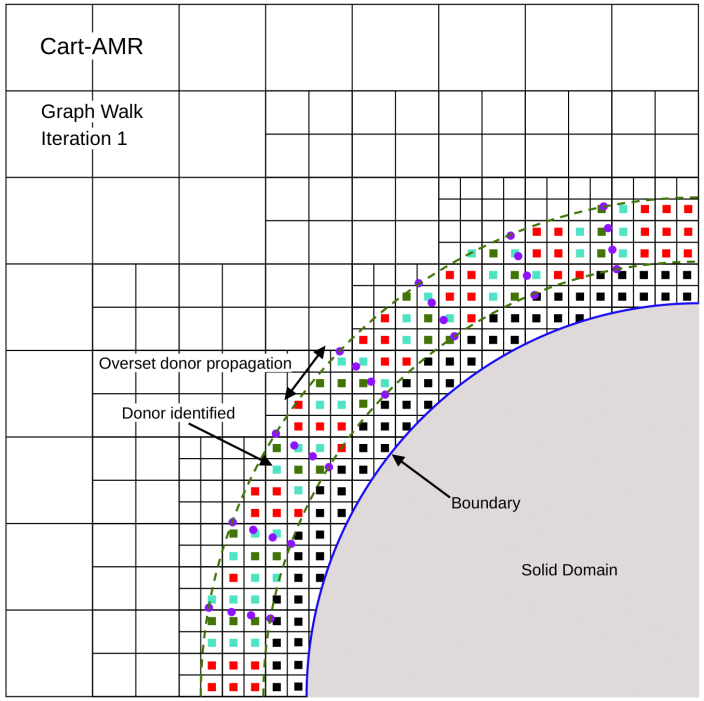
- NBS to Cartesian coupling achieved via overset interpolation
- Identification of upper and lower bound is dependent on maximum stencil width of the Cartesian convective/viscous schemes
- Interpolation coefficients computed to 2nd order accuracy with WLSQR



(1) Cartesian cell identification



(2) Initial donor point identification



(3) Graph walking for donor propagation

Cartesian Solver Shock Capturing

- Formulation of WENO scheme is critical to suppressing post-shock artifacts on non-aligned grids
  - Complete removal of artifacts generally does not occur
- RUS-WENOZ (WENO local Rusanov flux)

$$\hat{f}_i^{\pm} = f_i \pm \lambda_i W_i$$

- GRUS-WENOZ (WENO global Rusanov flux) – as recommended by Shu and Osher

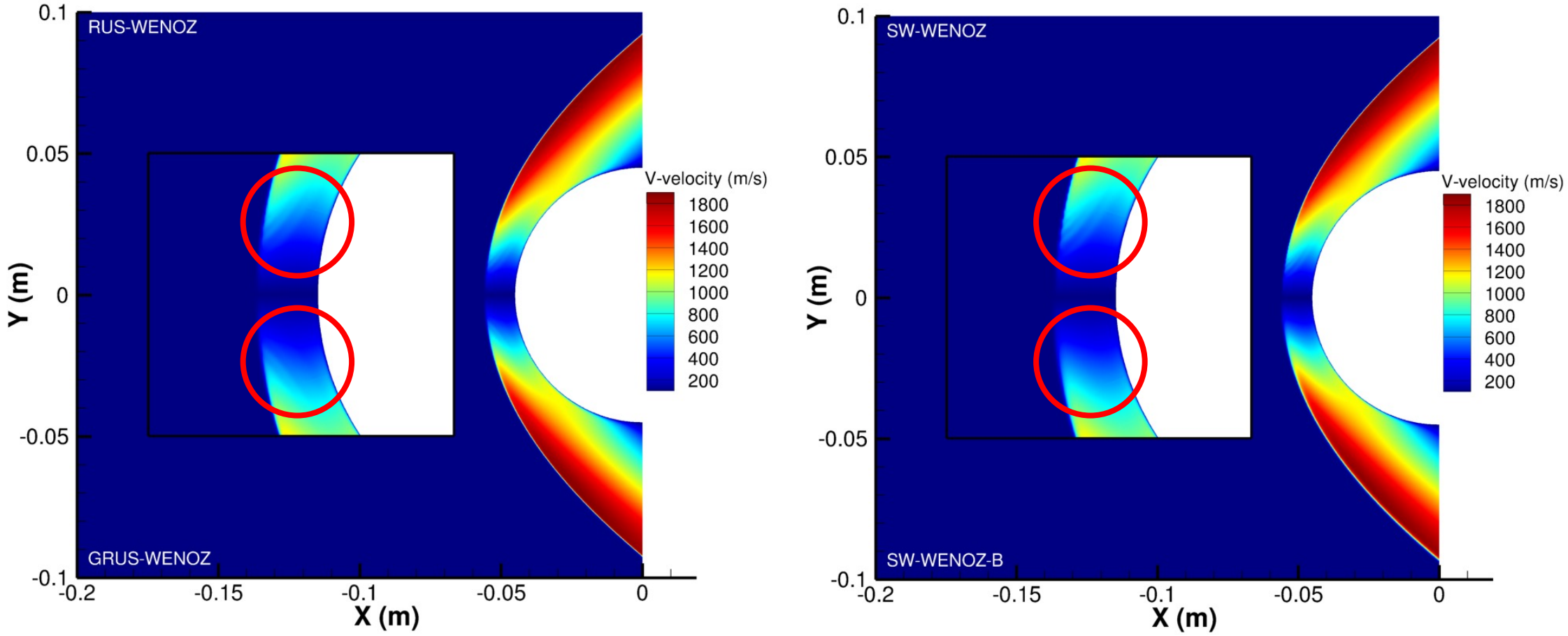
$$\hat{f}_i^{\pm} = f_i \pm \max(\lambda_{i-2:i+3})\, W_i$$

- SW-WENOZ (WENO w/ Steger-Warming flux)
- SW-WENOZ-B (WENO w/ 1st order blending)
  - Uses Ducros sensor for shock detection (Ducros et al. 1999)
  - Reduction to first order scheme at shock front

$$\widehat{f_i^{\pm}} = (1-\alpha)\widehat{f_i}^{WENO} + \alpha \widehat{f_i^{O1}}$$

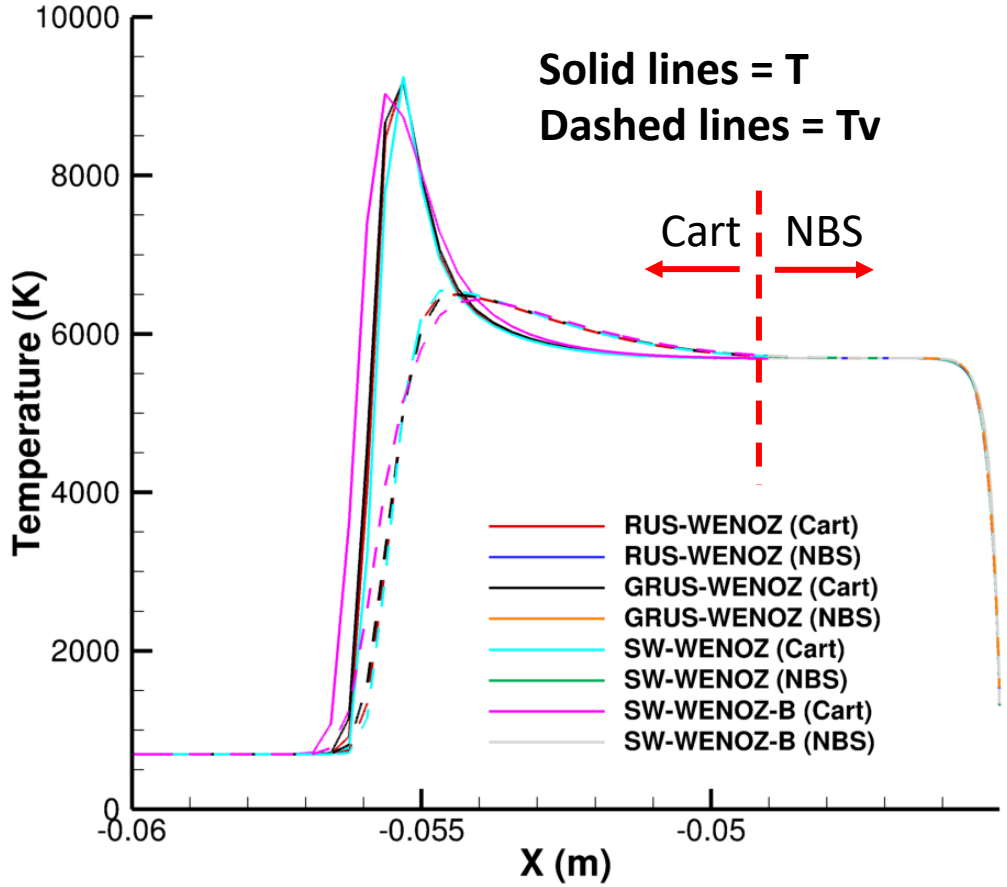
Mach 8.7 Cylinder

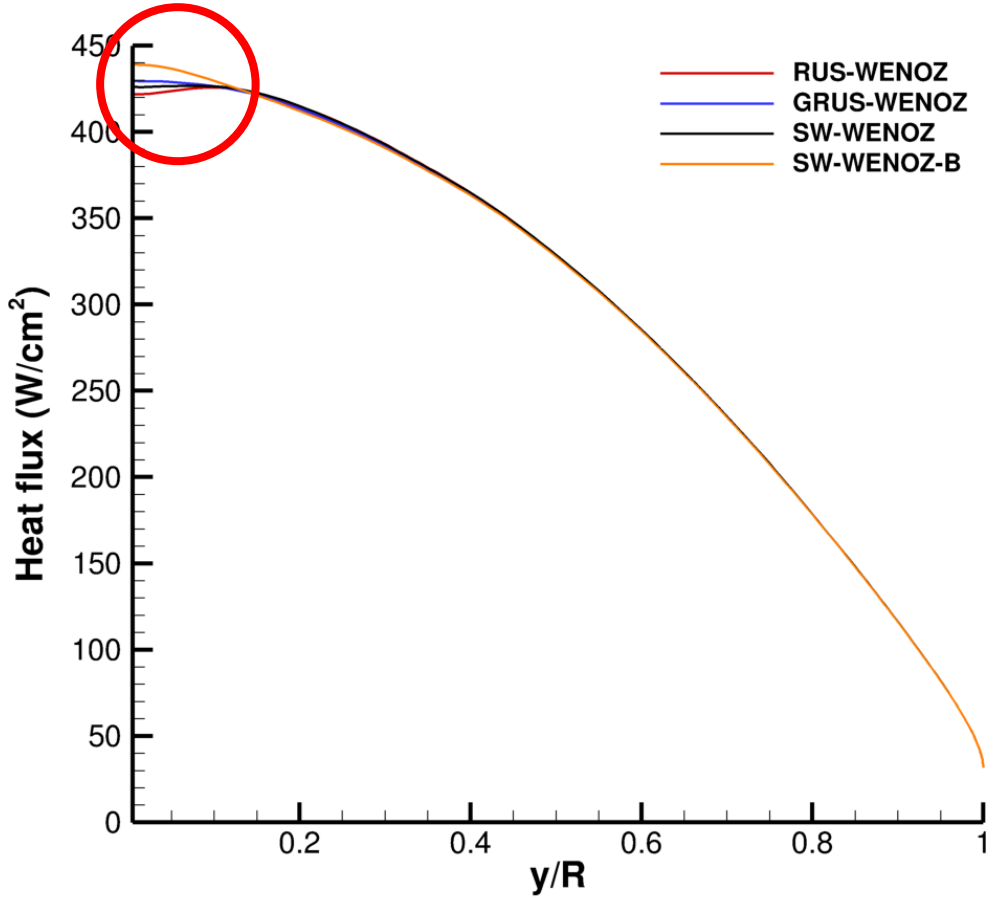
- Same case as before but with the overset interpolation
- Re-simulating this case to test the NBS-Cart solver and the impact of the Cartesian shock capturing approach
- **Focus:** What is the impact of the Cartesian shock-capturing scheme on the NBS surface heat flux?



Mach 8.7 Cylinder

- Reduction to 1st order at shock front results in under-predicted peak temperature and more diffused shock as expected
- Complete removal of stagnation point heating artifact induced by Cartesian shock capturing on non-aligned grids





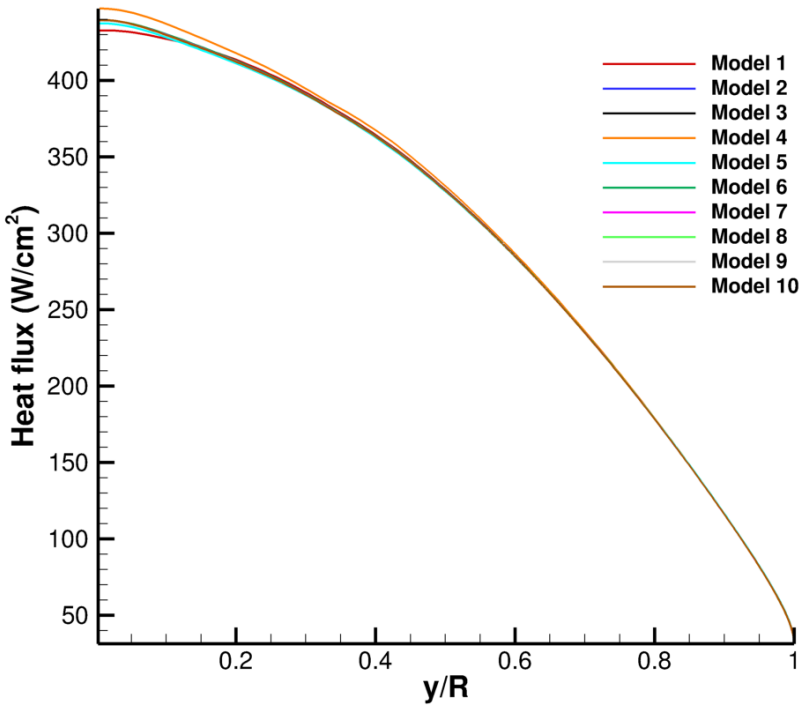
Mach 8.7 Cylinder

- Reduction to 1st order at shock front results in under-predicted peak temperature and more diffused shock as expected
- Complete removal of stagnation point heating artifact induced by Cartesian shock capturing on non-aligned grids

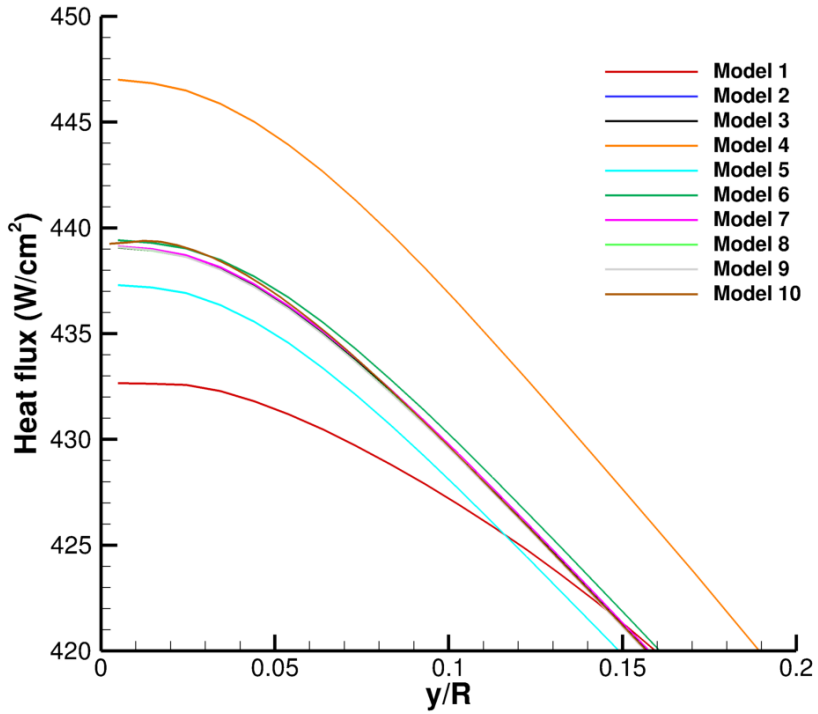
Grid convergence parameters

Model	Δx_{Cart}(m)	α	N_s	N_y	Δx_{NBS}(m)
1	1.5625×10^{-4}	10	160	100	1×10^{-6}
2	3.1250×10^{-4}	8	160	100	1×10^{-6}
3	3.1250×10^{-4}	10	160	100	1×10^{-6}
4	3.1250×10^{-4}	10	160	100	2×10^{-6}
5	3.1250×10^{-4}	10	160	100	5×10^{-7}
6	3.1250×10^{-4}	10	160	50	1×10^{-6}
7	3.1250×10^{-4}	10	160	75	1×10^{-6}
8	3.1250×10^{-4}	10	160	150	1×10^{-6}
9	3.1250×10^{-4}	10	160	200	1×10^{-6}
10	3.1250×10^{-4}	10	320	100	1×10^{-6}

Heat flux grid convergence



Heat flux comparison



Mars2020 Capsule

- 8-species CO2 model for Martian re-entry
  - Code-to-code comparison against US3D (identical reaction mechanisms)
  - Radiative equilibrium, non-catalytic surface
- **Focus:** Validation test case for the NBS radiative equilibrium surface boundary condition

Flow conditions

Parameter	Value
M_∞	22.08
ρ_∞ (kg/m^3)	8.01E-4
u_∞ (m/s)	4856.8
T_∞ (K)	179
T_v (K)	179
Y_{N_2}	0.0315
Y_{CO_2}	0.9685

Convective heating **Enthalpy diffusion** **Re-radiation**

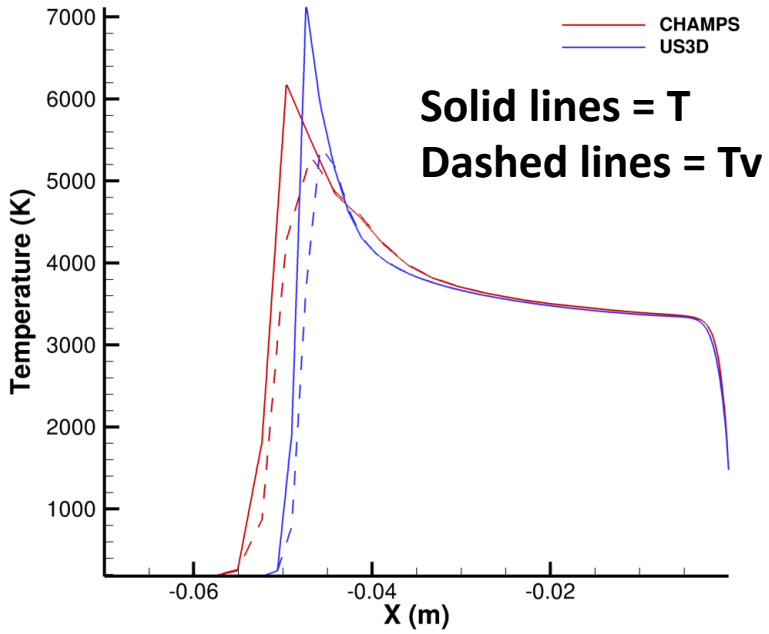
$$0 = \kappa_{tr}\frac{T - T_w}{d\eta} + k_v\frac{T_v - T_w}{d\eta} + \sum_{s=1}^{N_s}\rho D_s h_s \frac{Y_s - Y_{s,w}}{d\eta} - \epsilon\sigma\left(T_w^4 - T_{ref}^4\right)$$

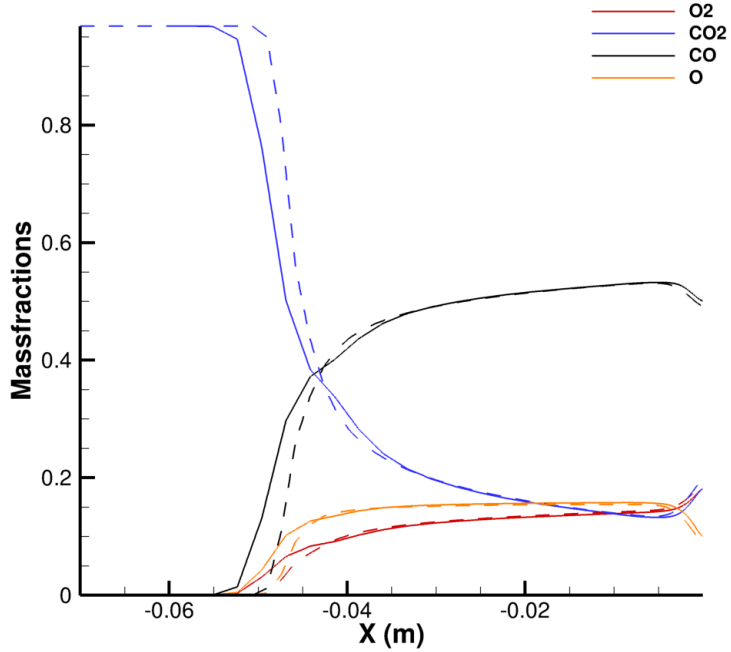
Solved via Newton iterations until error < 10^{-12}

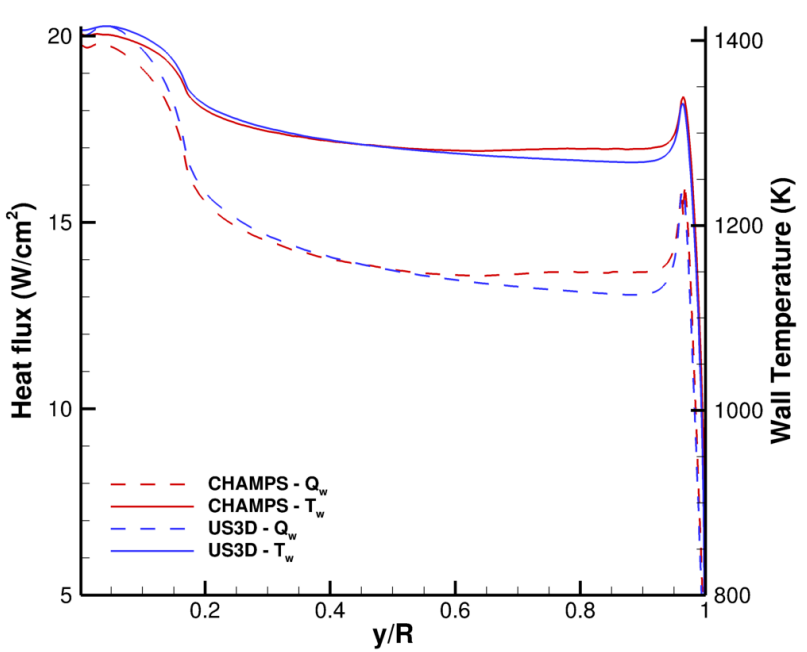
$$T_w^{k+1} = T_w^k - \frac{f(T_w)}{f'(T_w)}$$

Mars2020 Capsule

- Similarly, diffuse shock structure and under-predicted peak temperature due to 1st order shock treatment
- Close agreement on the surface heating and wall temperature profiles







Differences in solutions are presumed to be due to grid resolution

Fluid Ablation Interaction Coupling (2D)

CHAMPS-KATS Coupling

- Coupling was validated initially on the low temperature ablator, camphor
  - 3-species mixture
  - No reactions since Camphor sublimates easily
  - Serves as robustness test of NBS-Cart solver for moving boundary problems with high levels of surface topology changes
- Shift to the high temperature ablator, graphite
  - 11-species model (Argon sometimes added for arc-jet facilities)
  - Lower total recession but more complex reaction mechanism
  - 19-24 reactions depending on selected mechanism
- FAI project was a collaborative work with Aleksander Zibitsker and Dr. Alexandre Martin from the University of Kentucky
  - Employing the Kentucky Aerothermodynamics and Thermal Response System (KATS-MR)

KATS-MR Solver

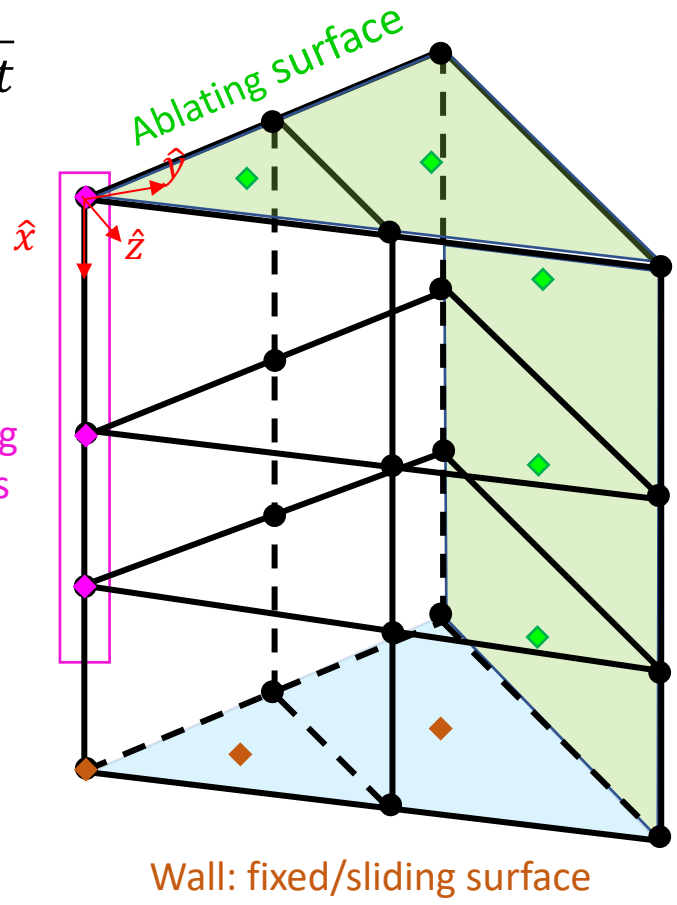
$$\frac{\partial E_s}{\partial t} - \nabla \cdot \left(F_d + F_g\right) = 0$$

- **Kentucky Aerothermodynamics and Thermal Response System (KATS)**
- Governing equation for solid energy:

  Grid flux: $F_g = E_s \bar{\omega}$

  Face averaged velocity: $\bar{\omega}_j = \frac{\Delta \bar{V}_j}{A_j \Delta t}$

- Mesh motion (Radial Basis Function Interpolation):
  - Face centroid recession interpolation at the surface and volume nodes
  - Incorporated constraints in certain motion directions
  - Straightforward implementation on unstructured grids
- Camphor:
  - Gas phase contains 3 non-reactive species: $N_2, O_2, C_{10}H_{16}O$.
  - Surface reactions – single sublimation species (Knudsen-Langmuir model).
- Graphite:
  - Gas phase contains up to 12-species, accounting for dissociation and exchange reactions[1]
  - Gas-surface reactions are modeled with recently developed ACA[2] model.
  - Knudsen-Langmuir model for sublimation species: C, C_2, C_3

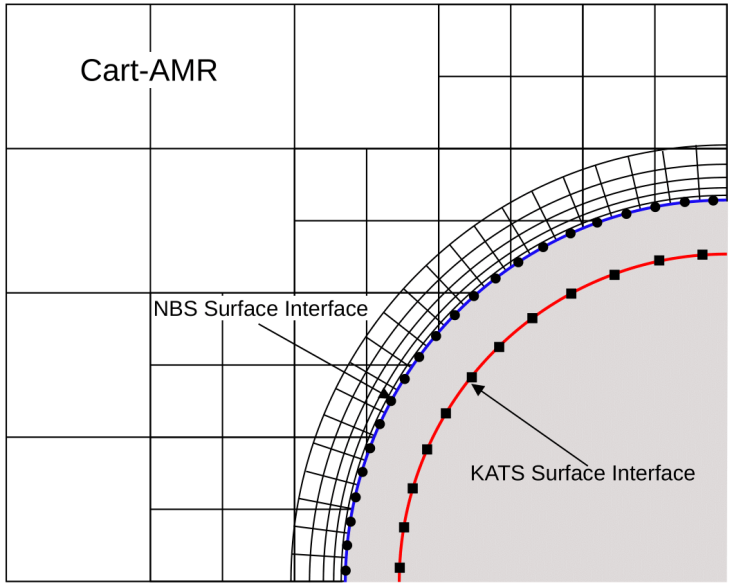


[1]McQuaid, J.A., Zibitsker, A.L., Martin, A. and Brehm, C., 2022. Simulation of Graphite Ablation using an Overset Near Body Solver on an Adaptive Block-Structured Cartesian Off-Body Grid. In *AIAA AVIATION 2022 Forum* (p. 4088).

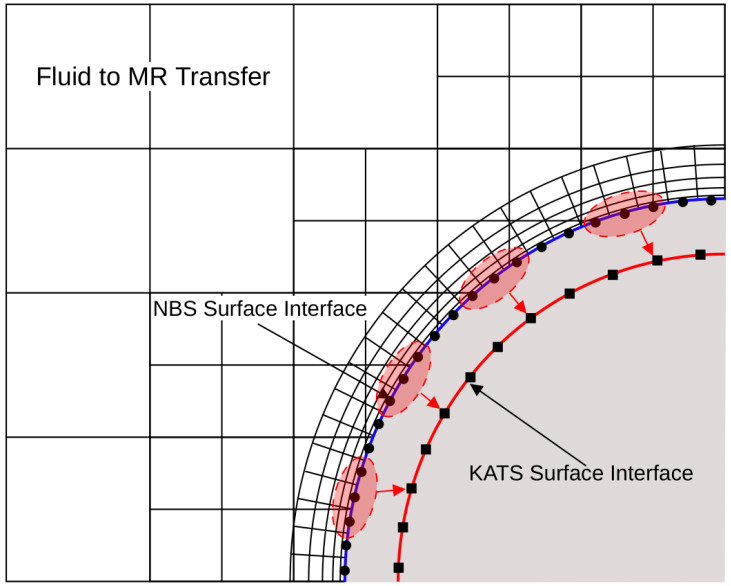
[2]Prata, K.S., Schwartzentruber, T.E. and Minton, T.K., 2022. Air–carbon ablation model for hypersonic flight from molecular-beam data. *AIAA journal*, *60*(2), pp.627-640.

CHAMPS-KATS Coupling Framework

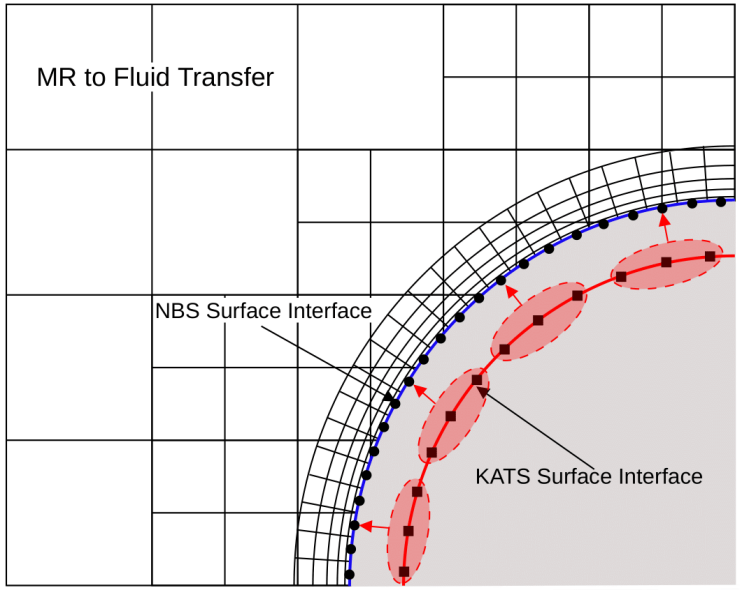
- Designed for mismatched interfacial grid resolutions.
- Interpolation cloud built via nearest neighbor K-d tree lookup.
- Data interpolated between fluid and MR surface centroids using 3rd order interpolating polynomials.
- Communication data structure built and re-built periodically (as required) for mismatched surface partitioning.



FAI coupling overview



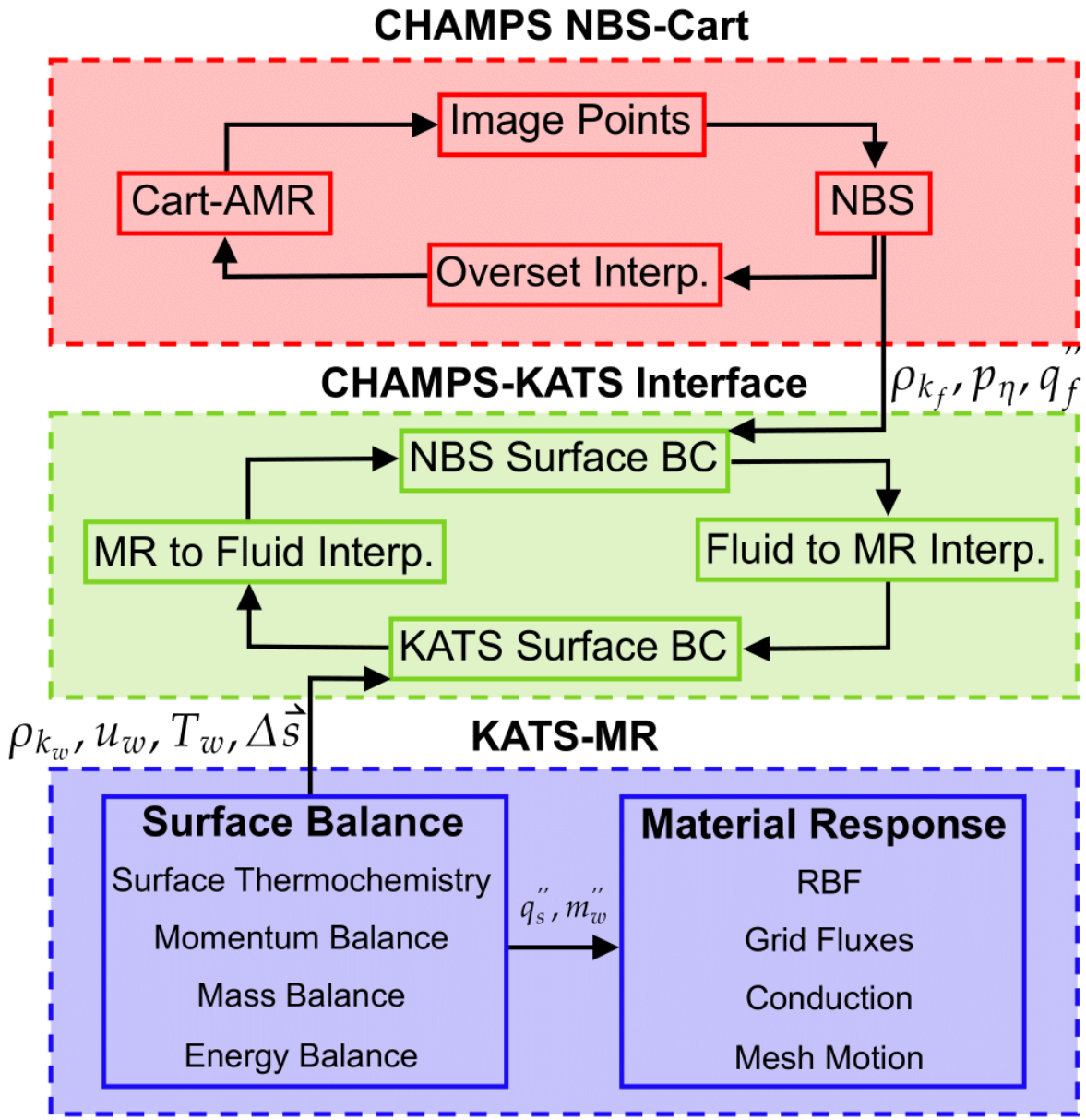
Fluid to MR transfer



MR to fluid transfer

CHAMPS-KATS Coupling Framework

- Fluid to MR transfer:
  - Surface heat flux.
  - Wall-normal momentum in 1st fluid cell.
  - Species densities in 1st fluid cell.
- MR to fluid transfer:
  - Wall temperature.
  - Wall-normal blowing velocity.
  - Wall species densities.
  - Surface recession.
- Provided surface recession is used to update nodal positions of CHAMPS surface grid.
- NBS grid is re-generated from new position and fluid solver is advanced forward in time with updated surface state.



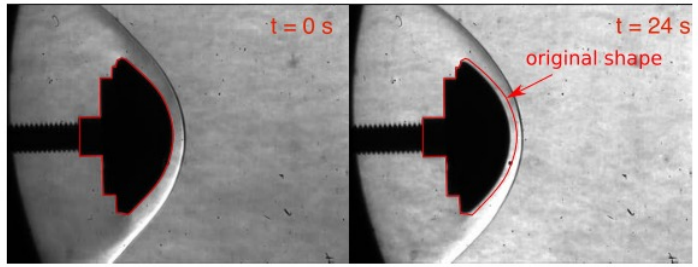
Mach 6 Pheobus Capsule

- Experiment in hypersonic H3 facility at VKI:
  - Mach 6, low-enthalpy flow (~0.5 MJ/kg).
  - Duration: 30 sec
  - Measurement: photogrammetry
- **Focus:** Initial validation of the CHAMPS-KATS FAI coupling framework

Phoebus capsule with a layer of camphor



Experiment at Mach 6 flow (Turchi 2019)

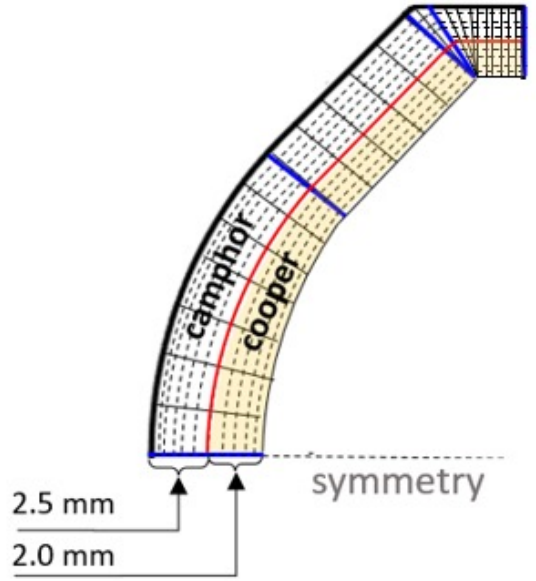


Experimental conditions

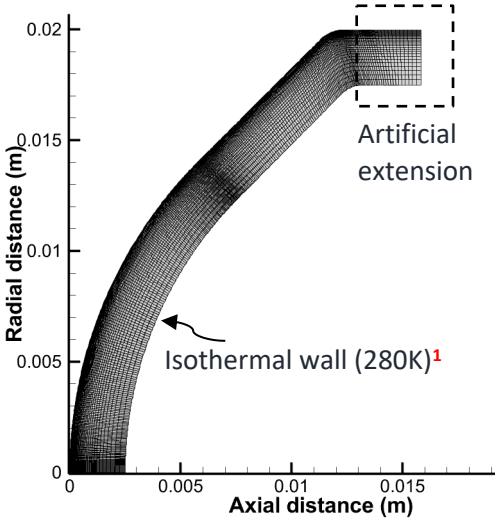
Test	Total Pressure [bar]	Total Temperature [K]	Mach no.
P15	15.647 ± 0.093	524.78 ± 2.31	6
P20	20.569 ± 0.126	487.18 ± 3.91	6
P25	25.660 ± 0.039	511.01 ± 7.04	6

1D/2D discretization: 1DMR/KATS

1DMR discretization[1]



2D-KATS discretization[2]



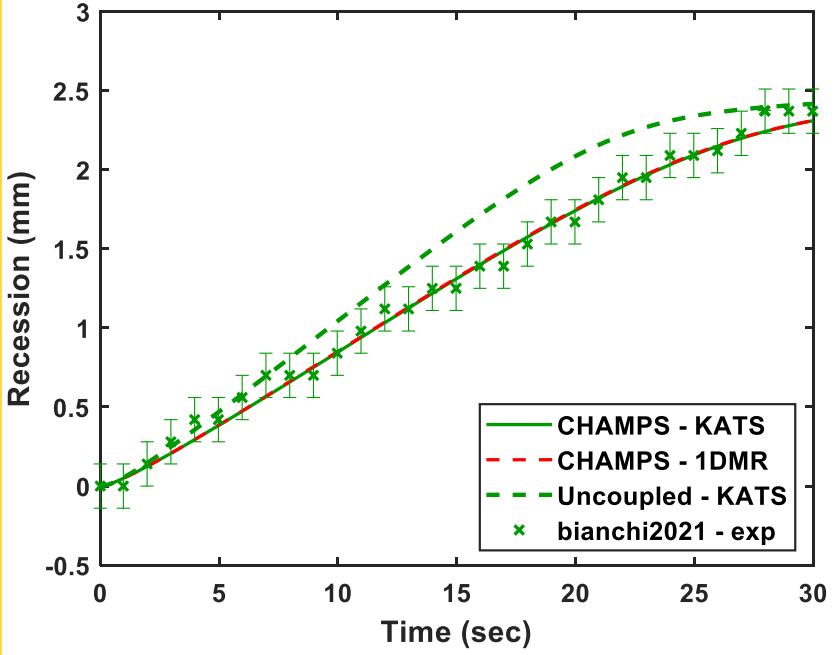
[1]Zibitsker, A.L., McQuaid, J., Brehm, C. and Martin, A., 2022. Fully-Coupled Simulation of Low Temperature Ablator and Hypersonic Flow Solver. In *AIAA SCITECH 2022 Forum* (p. 0676).

[2]Zibitsker, A.L., McQuaid, J.A., Brehm, C. and Martin, A., 2022. Study of a Two-Dimensional Shape Change of Blunt-Body Geometries at Hypersonic Conditions Using Fully Coupled Simulation. In *AIAA AVIATION 2022 Forum* (p. 4006).

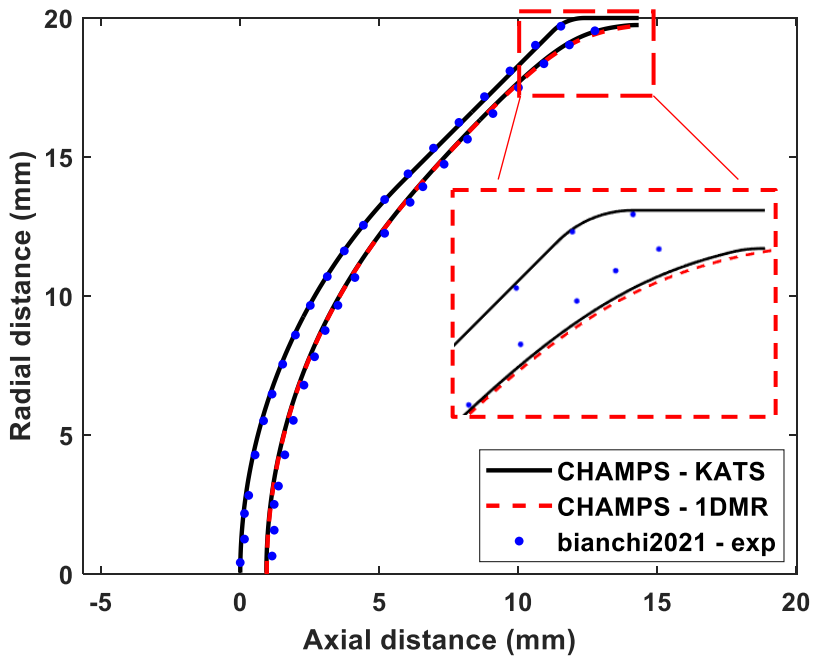
Mach 6 Pheobus Capsule

- Comparison of two geometry discretization approaches:
  - Array of 1DMR ray solvers.
  - Full 2D problem with KATS.
- Accurate prediction of stagnation point recession and shape change with both solvers.

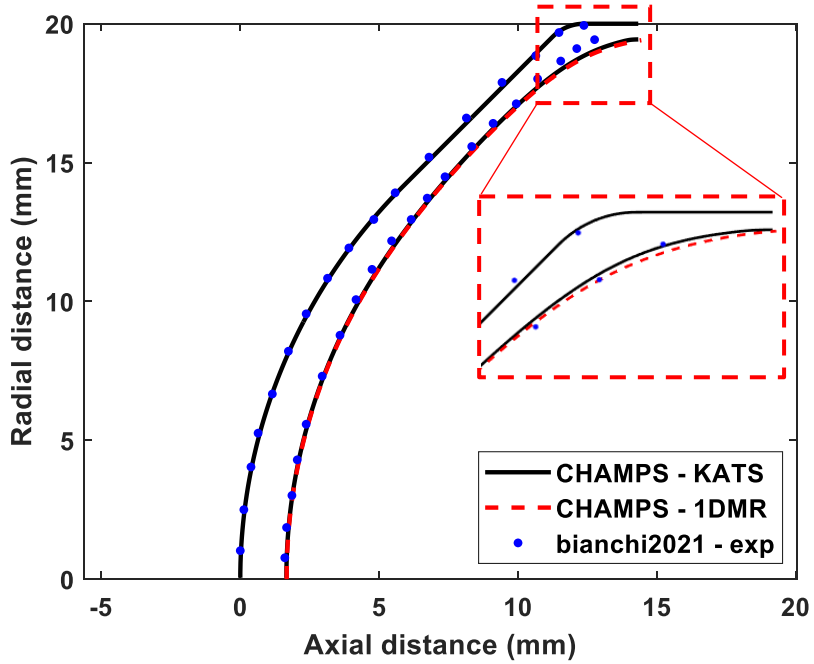
Stagnation point recession



Shape at 11 sec

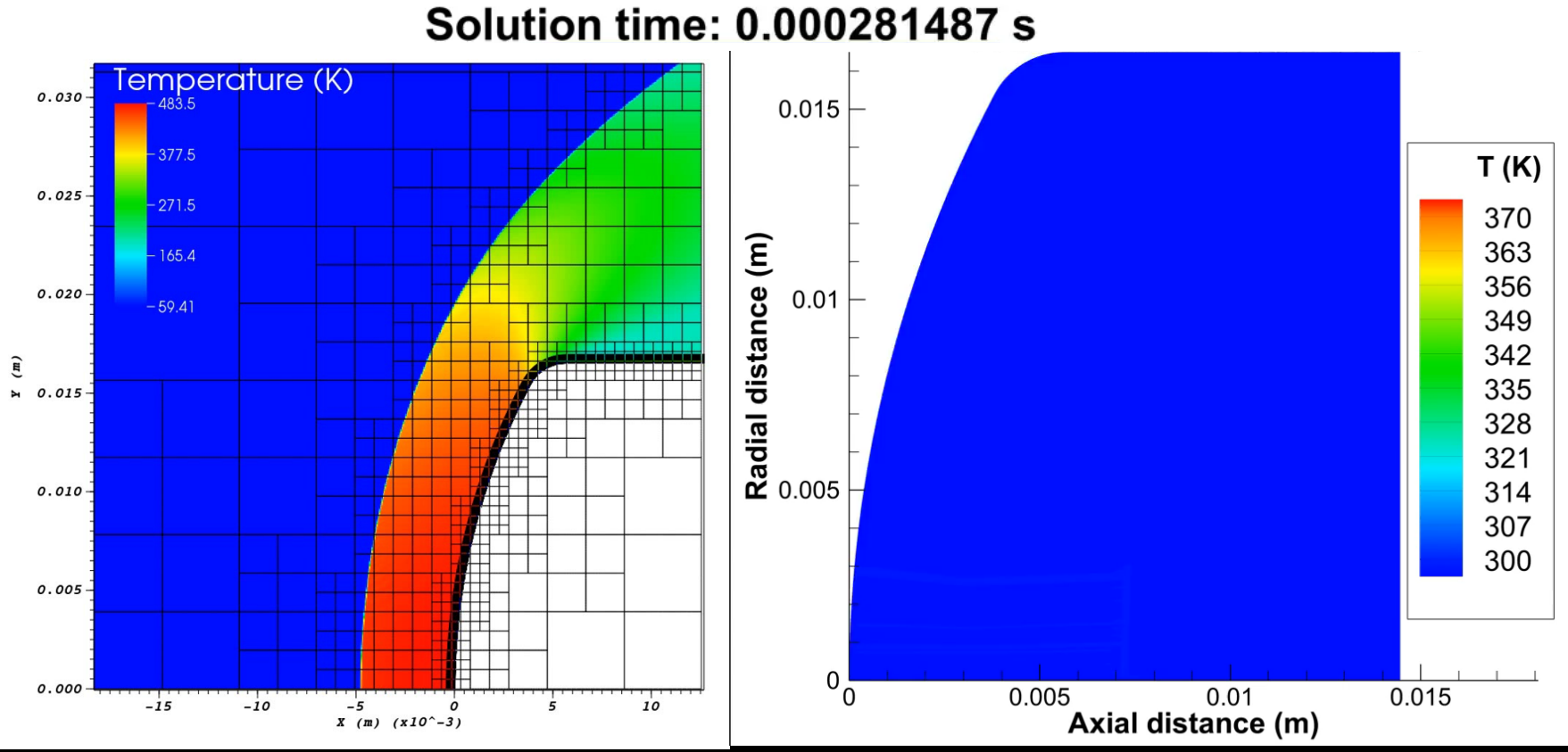


Shape at 19 sec



Mach 6 Iso-Q

- Geometry: Iso-Q; simulated at the same tunnel conditions as the Phoebus capsule
- Test was simulated for a long duration to test the robustness of the coupling under large amounts of surface topology changes
- **Focus:** CHAMPS-KATS FAI robustness test under high levels of surface topology changes

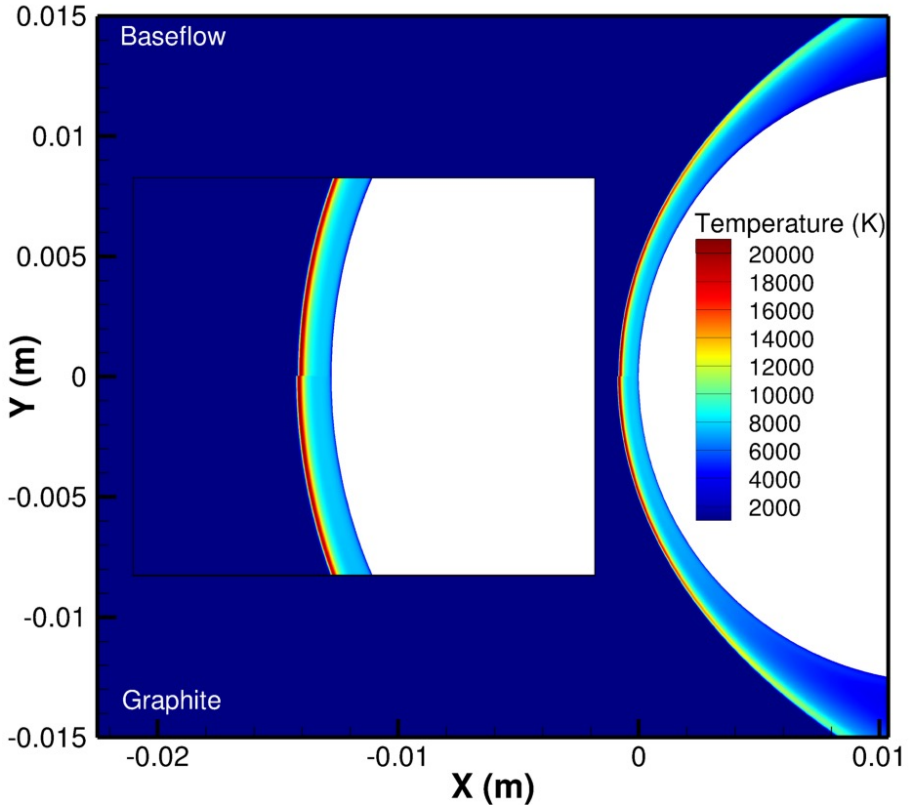


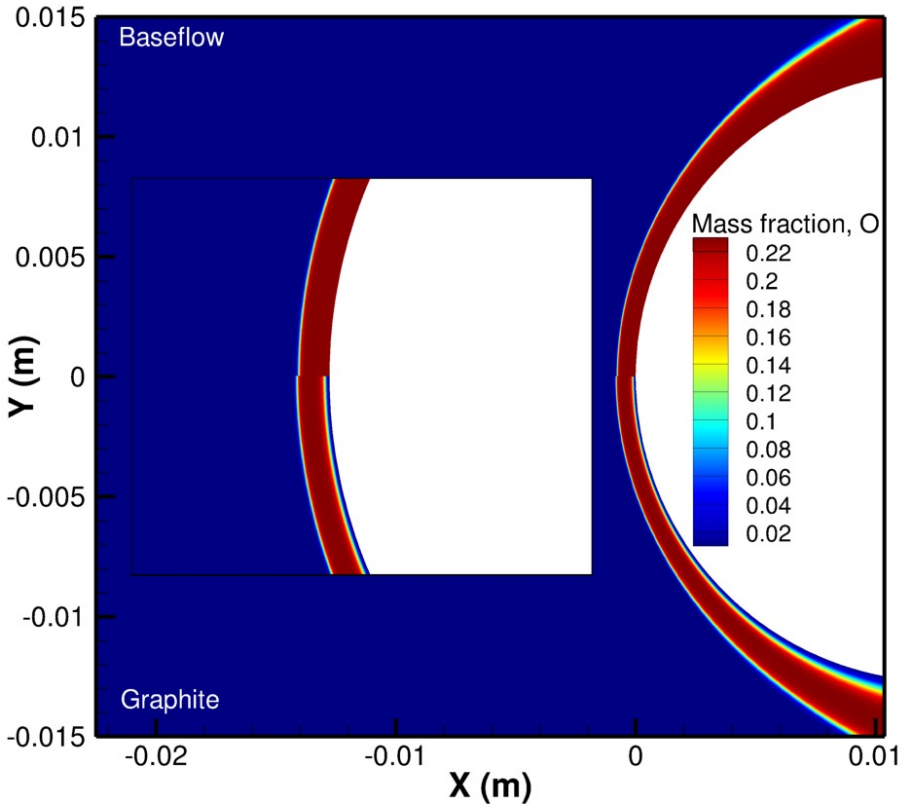
Mach 25.2 9-degree blunt cone

- Mach 25.2 9-degree blune cone ($R_n = 0.0127$ m)
- Steady-state graphite ablation @ 40 km altitude
- Validation against Keenan (1994) using US3D
- **Focus:** Initial validation of the CHAMPS-KATS FAI solver for steady-state graphite ablation

Flow conditions

Parameter	Value
M_∞	25.2
ρ_∞ (kg/m^3)	3.99568E-3
u_∞ (m/s)	8000
T_∞ (K)	250.35
T_w (K)	800
Y_{N_2}	0.7635
Y_{O_2}	0.2365



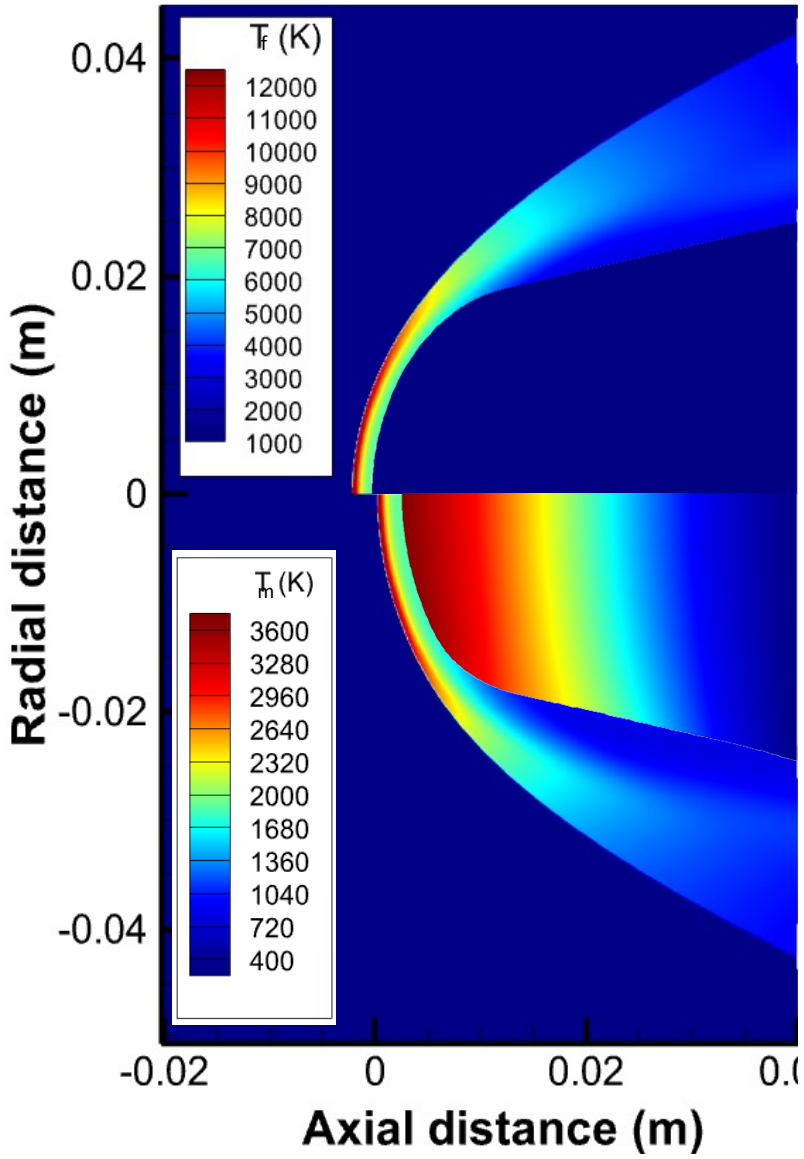


Mach 7 10-degree blunt cone

- High-enthalpy (27 MJ/kg), 30-second duration at arc-jet conditions
- Instrumentation:
  - Recession over time at 0 and 45-degrees
  - Pyrometer at 45-degrees
- Studied previously by several groups: Chen2003, Chen2005, Bianchi2010, Bersbach2022
- **Focus:** Validation of FAI coupling for transient graphite ablation

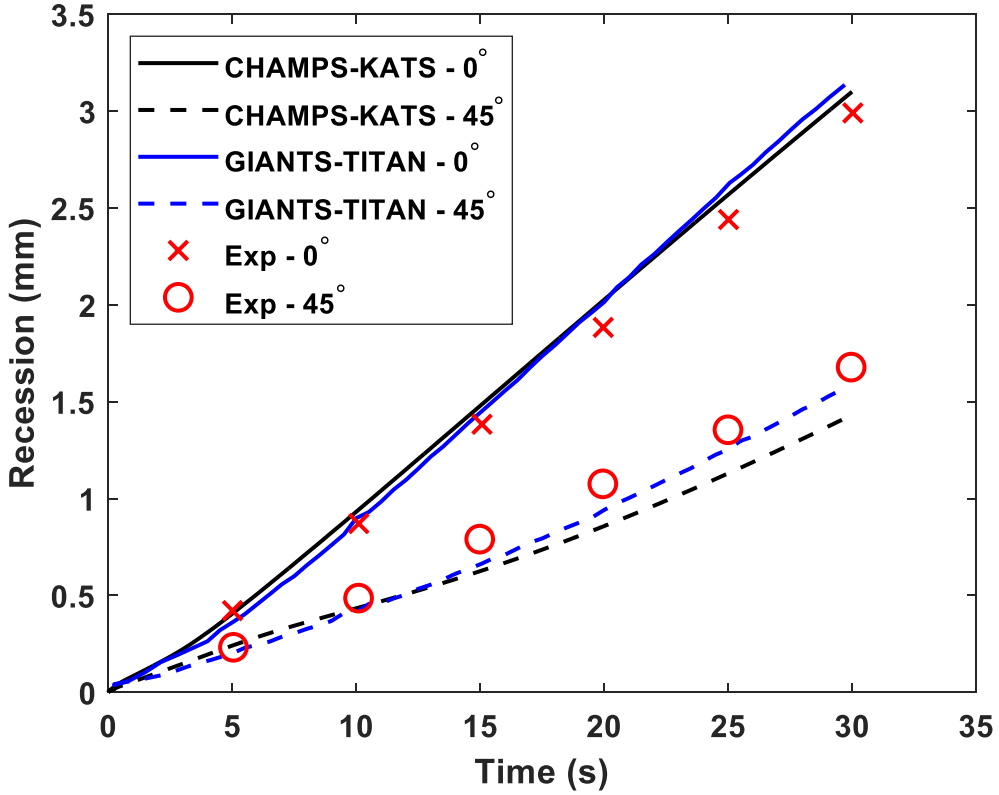
Flow conditions

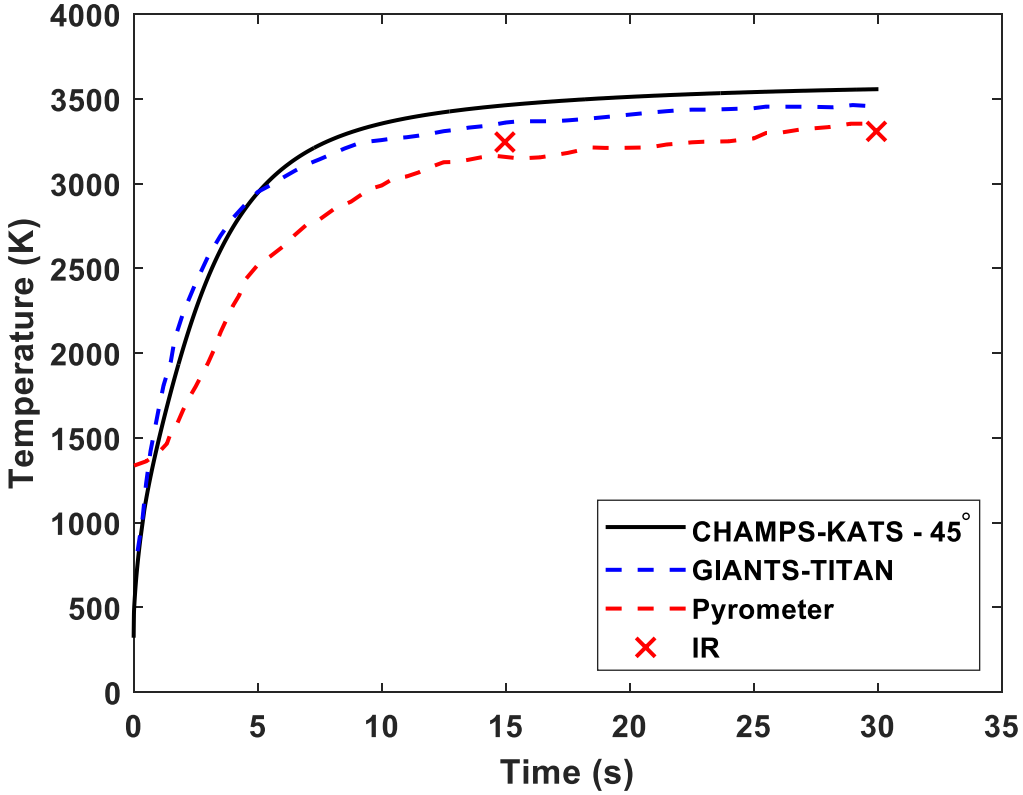
Parameter	Value
ρ_∞ (kg/m^3)	3.00E-3
u_∞ (m/s)	5354
T_∞ (K)	1428
T_w (K)	312
$\vec{Y}(N_2, O_2, NO, N, O)$	0.6169, 0.0, 0.46, 0.1212, 0.2583
Duration (s)	30



Mach 7 10-degree blunt cone

- Comparison to reference data for recession time history and surface temperature response
- Numerical results from GIANTS-TITAN coupling plotted as well





NBS-Cart Overview

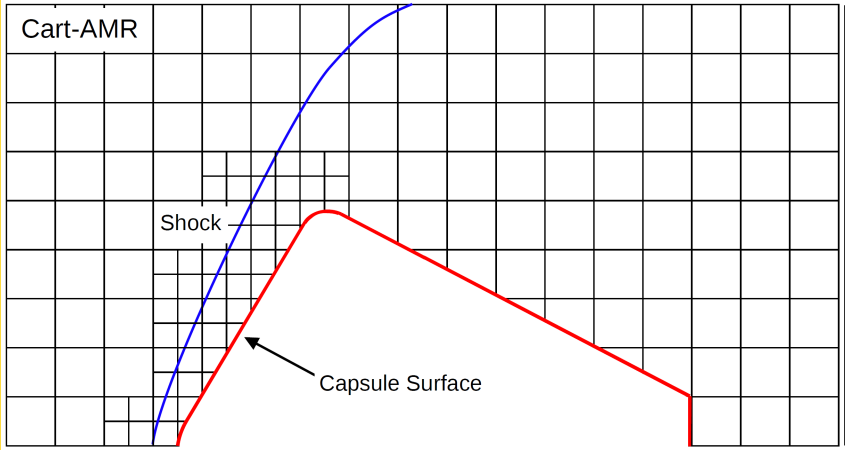
- Automated volume mesh generation was achieved and validated across a wide range of low and high enthalpy test cases
- NBS-Cart solver provides accurate heat flux predictions under various hypersonic conditions
- Numerical scheme proposed and validated for hypersonic shock capturing on non-aligned grids
- NBS remains robust and accurate under thermochemical ablation environments where high levels of surface topology changes are experienced

- **Next steps:**
  - Demonstrate that the NBS-Cart solver is an effective tool for real-world applications
  - Must be capable of simulating complex entry conditions at non-zero angles of attack
  - Must be capable of scale-resolving simulations such that it may be used as a baseflow computational tool for transition predictions

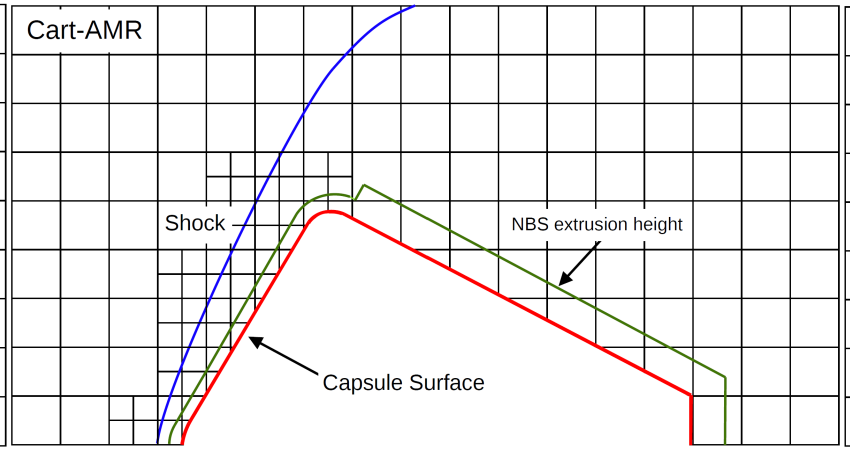
Overset NBS Solver Coupling (3D)

NBS Grid Generation

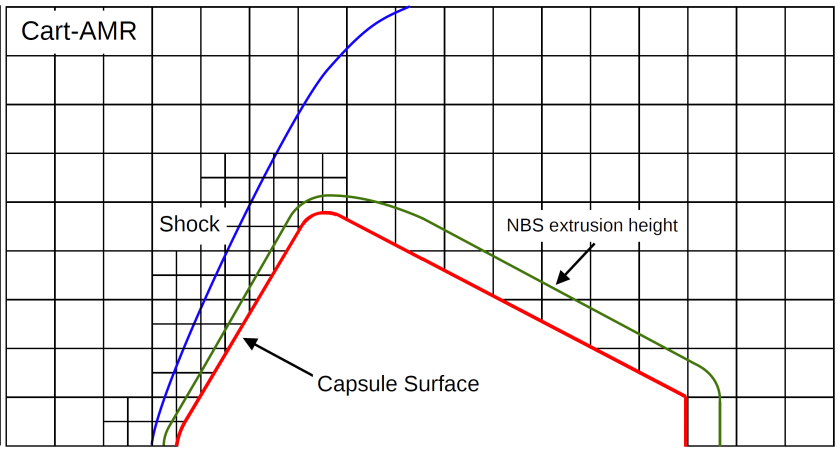
- In 3D, it becomes very important to reduce the computational cost as much as possible
- Typical NBS grid generation approach is modified for variable extrusion
  - Variable Cartesian boundary refinement is employed to reduce computational cost
  - Fine grid maintained in geometric regions with close proximity to shock fronts
  - NBS extrusion is now a function of the local Cartesian cell size at the surface



(1) Generation of Cartesian grid



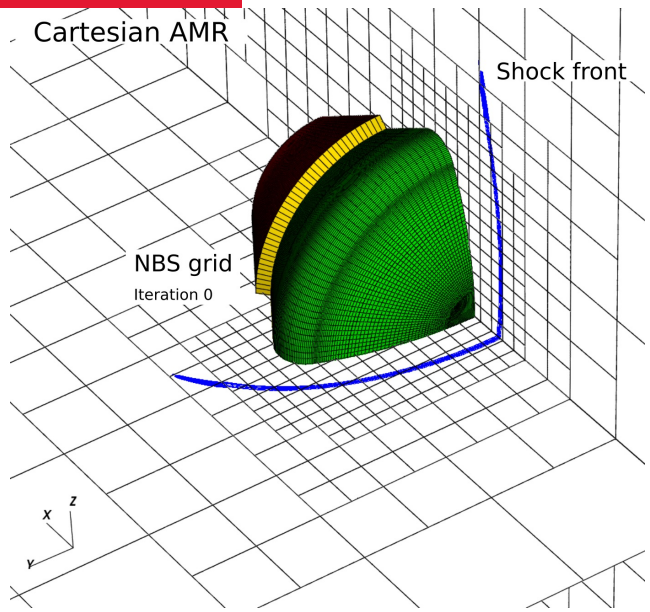
(2) Identify local NBS extrusion height

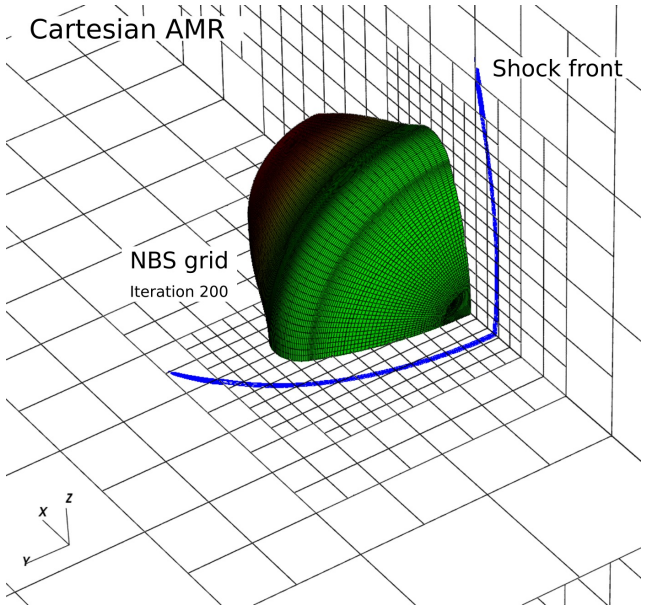


(3) Smoothing of NBS extrusion height

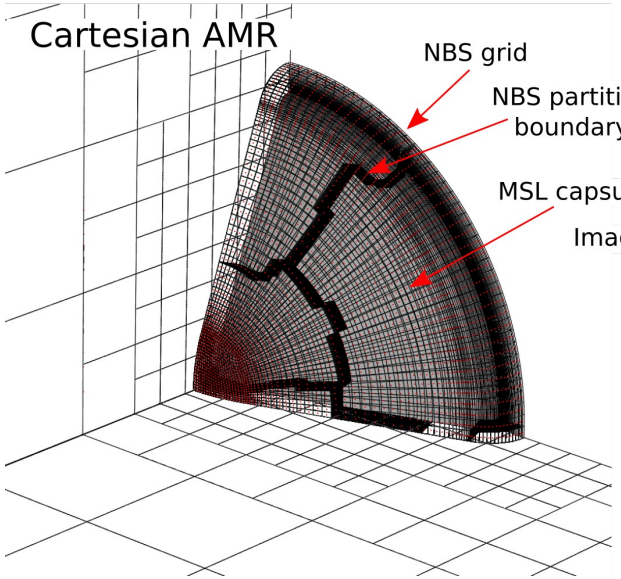
NBS-Cart Solver Overview

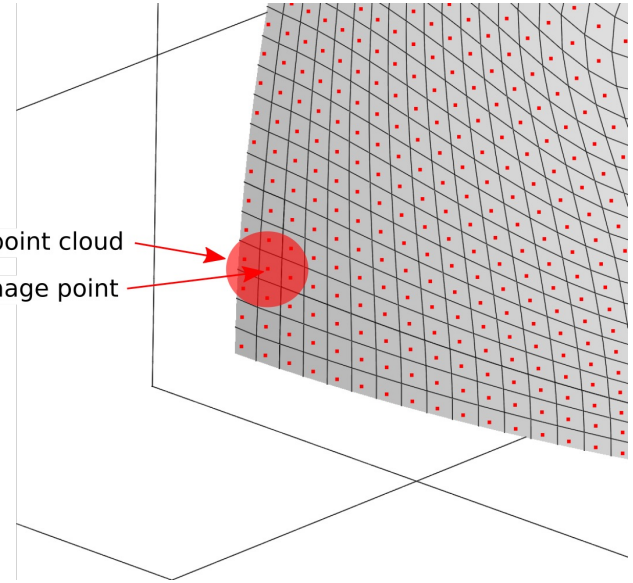
NBS grid generation and smoothing





NBS to Cartesian Coupling



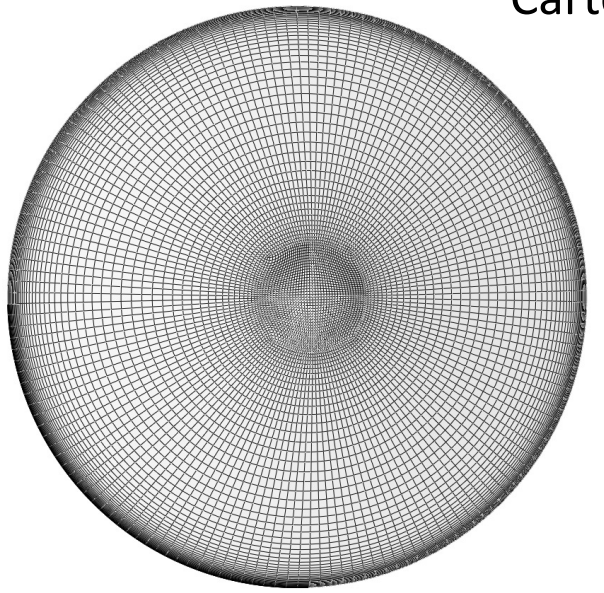


MSL Capsule, Perfect Gas

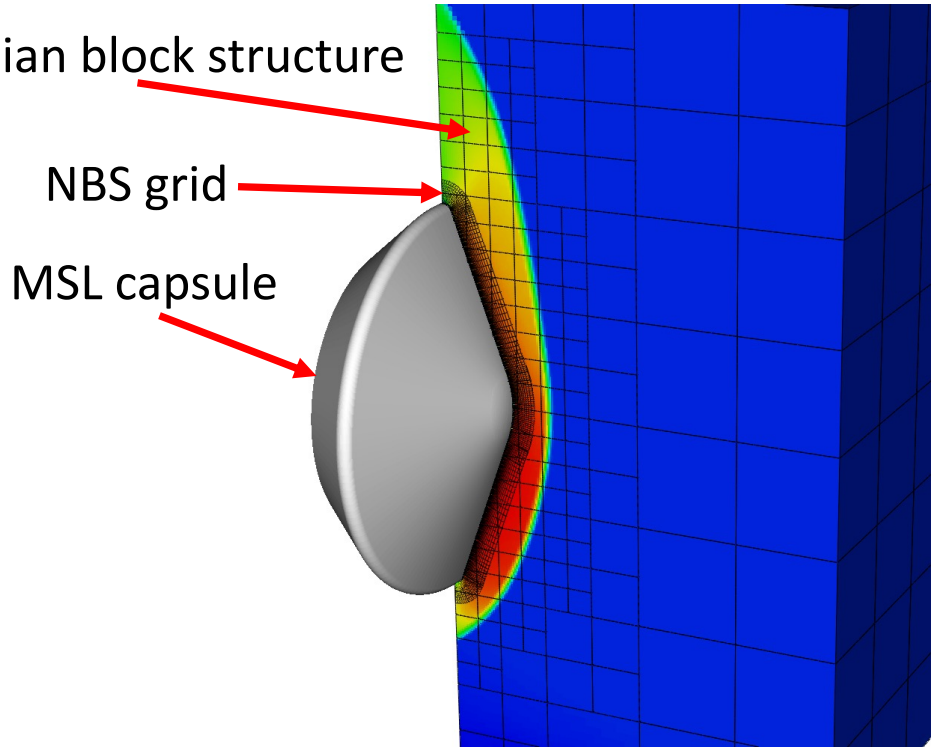
- MSL capsule simulated at angles of attack between 0 and 16-degrees in 4-degree increments
- Validation against body-fitted solver of Chen et al. (2018)
- Validation against experimental campaign of Hollis and Collier (2008)
- **Focus:** Investigation of Cartesian shock-capturing in 3D and validation of NBS solver in 3D

Flow conditions

Parameter	Value
M_∞	9.47
p_∞ (Pa)	167.9
u_∞ (m/s)	1405.59
T_∞ (K)	54.8
T_w (K)	294.44
Re_∞ (1/m)	4.32E6

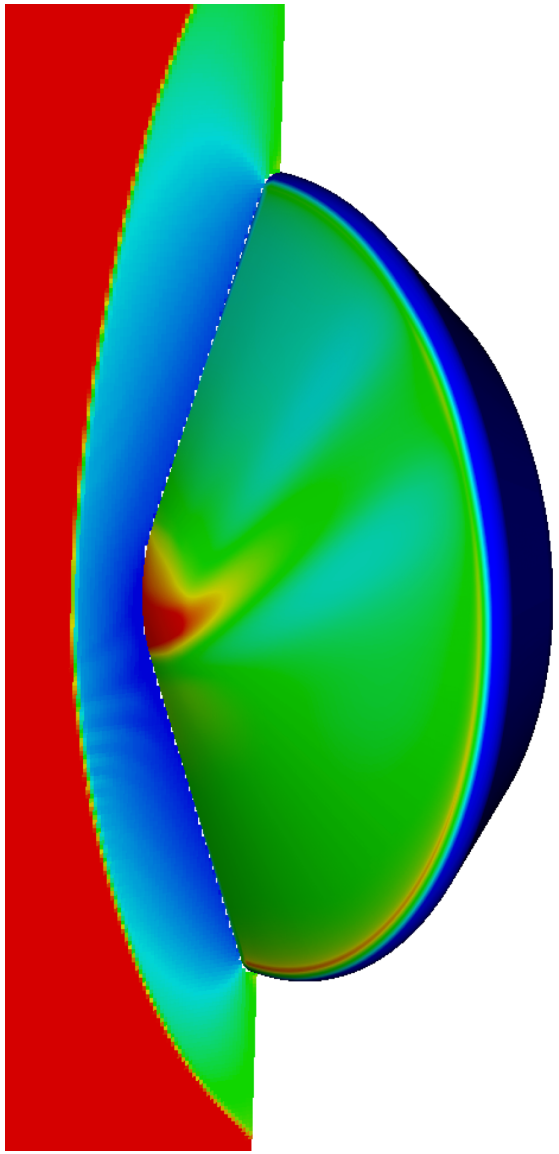


MSL surface grid

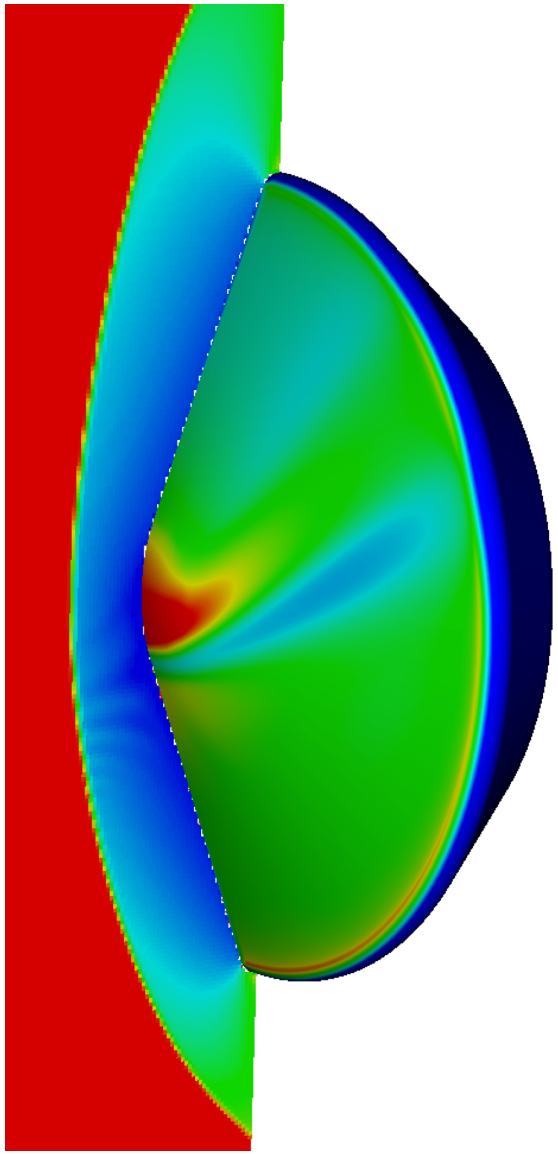


MSL Capsule, Perfect Gas

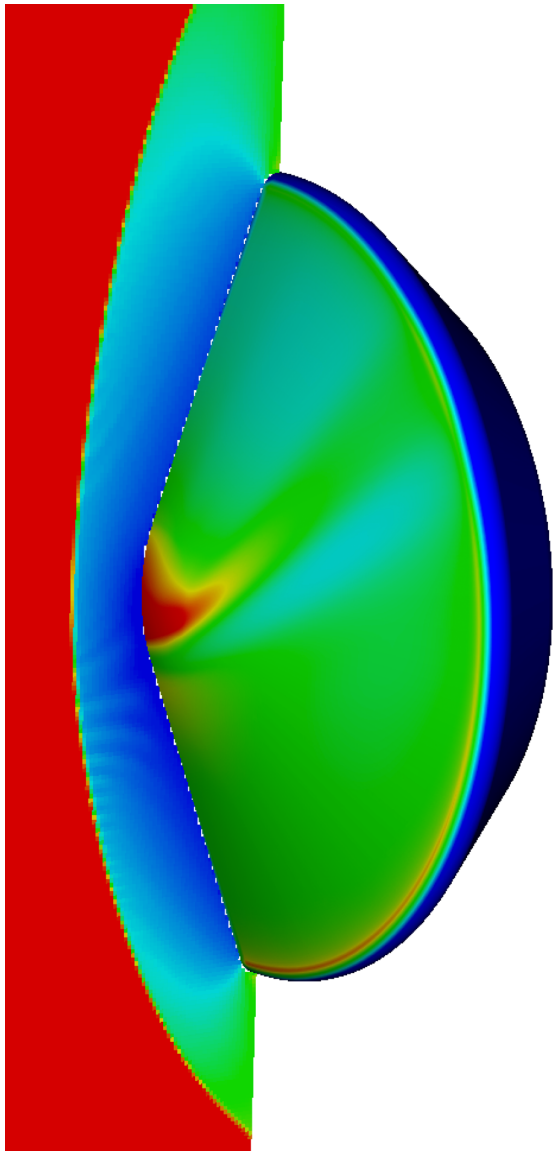
RUS-WENOZ



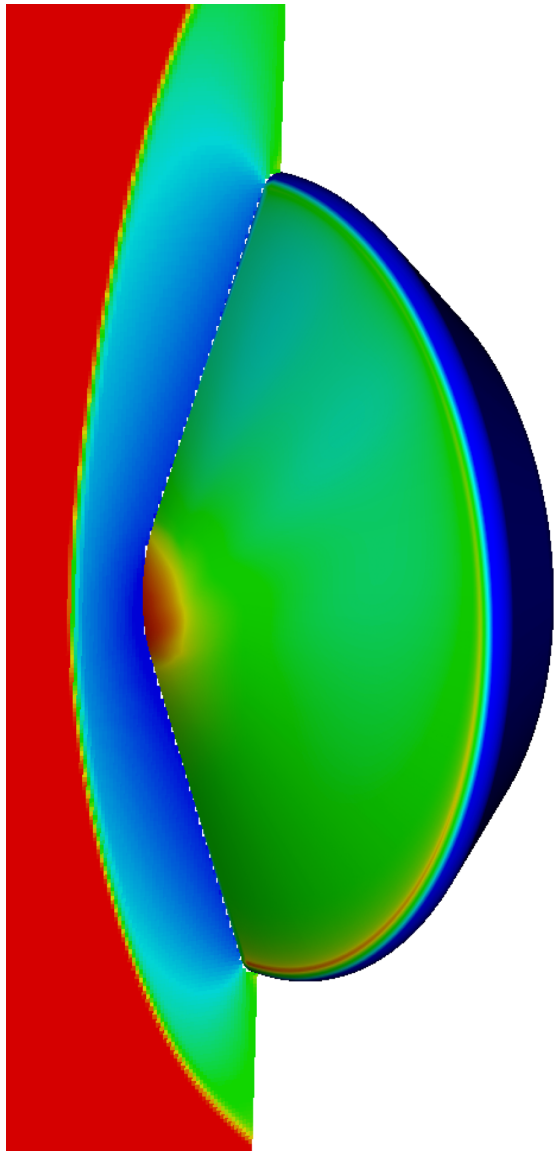
GRUS-WENOZ



SW-WENOZ

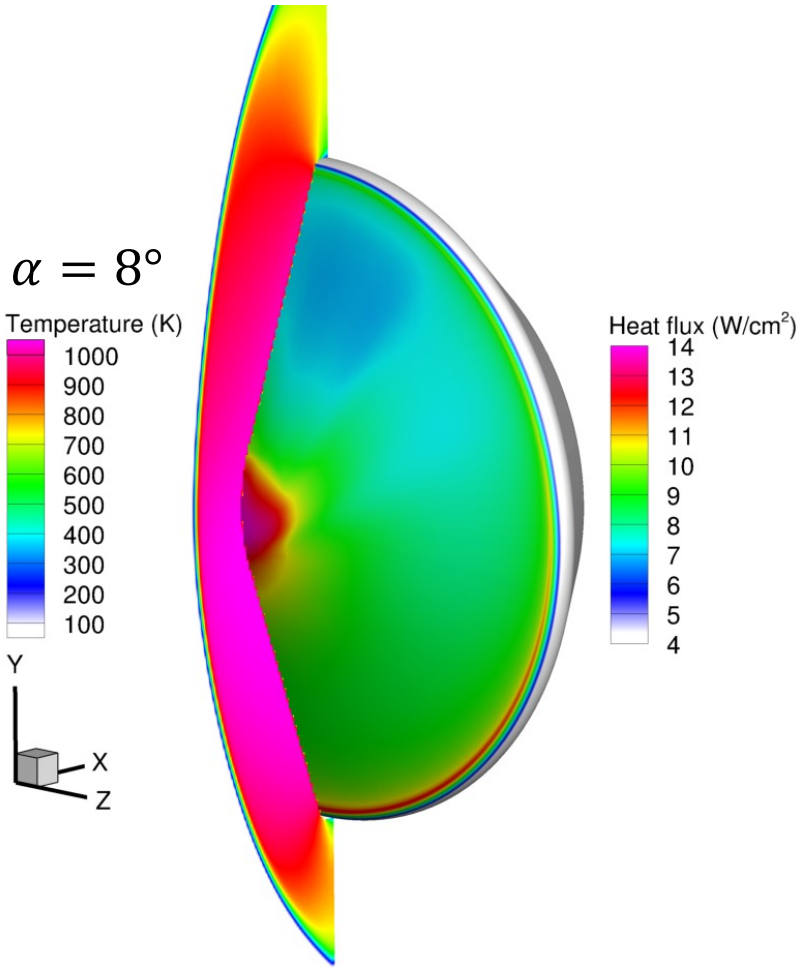


SW-WENOZ-B

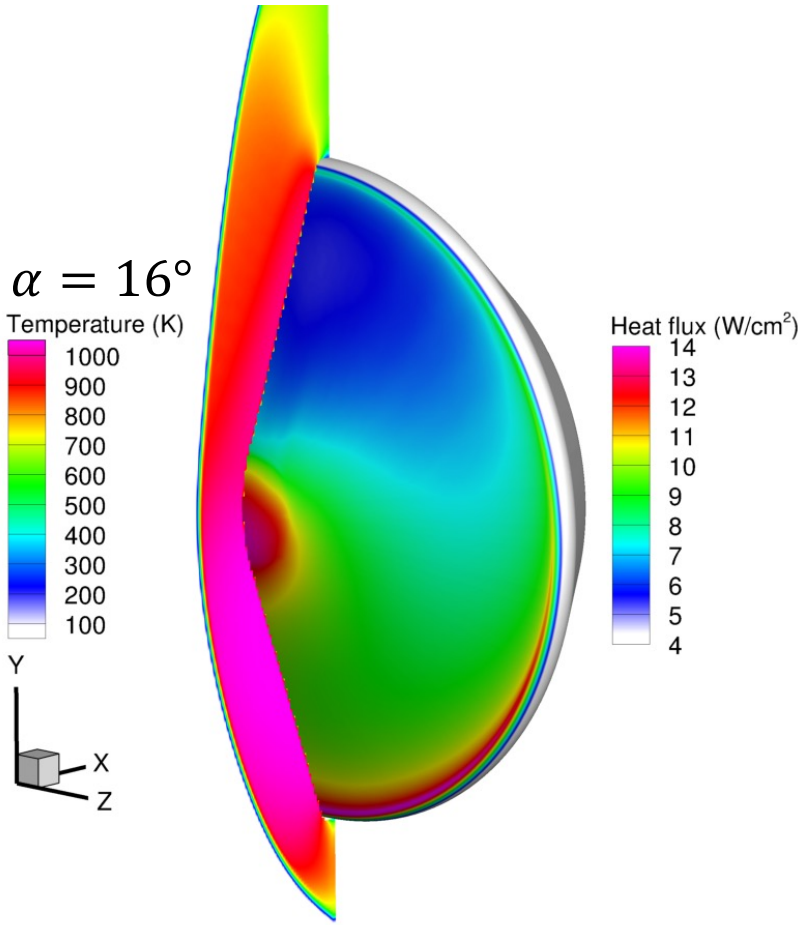


MSL Capsule, Perfect Gas

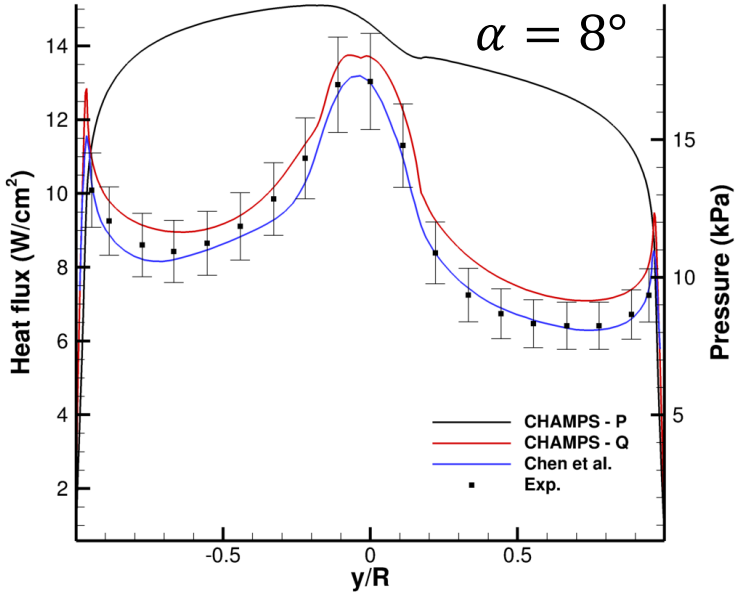
$\alpha = 8°$

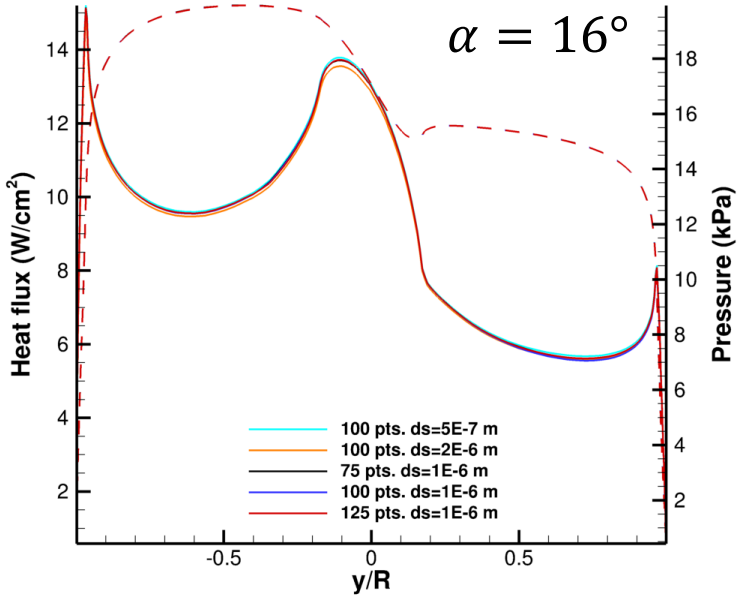


$\alpha = 16°$



Surface data at symmetry plane



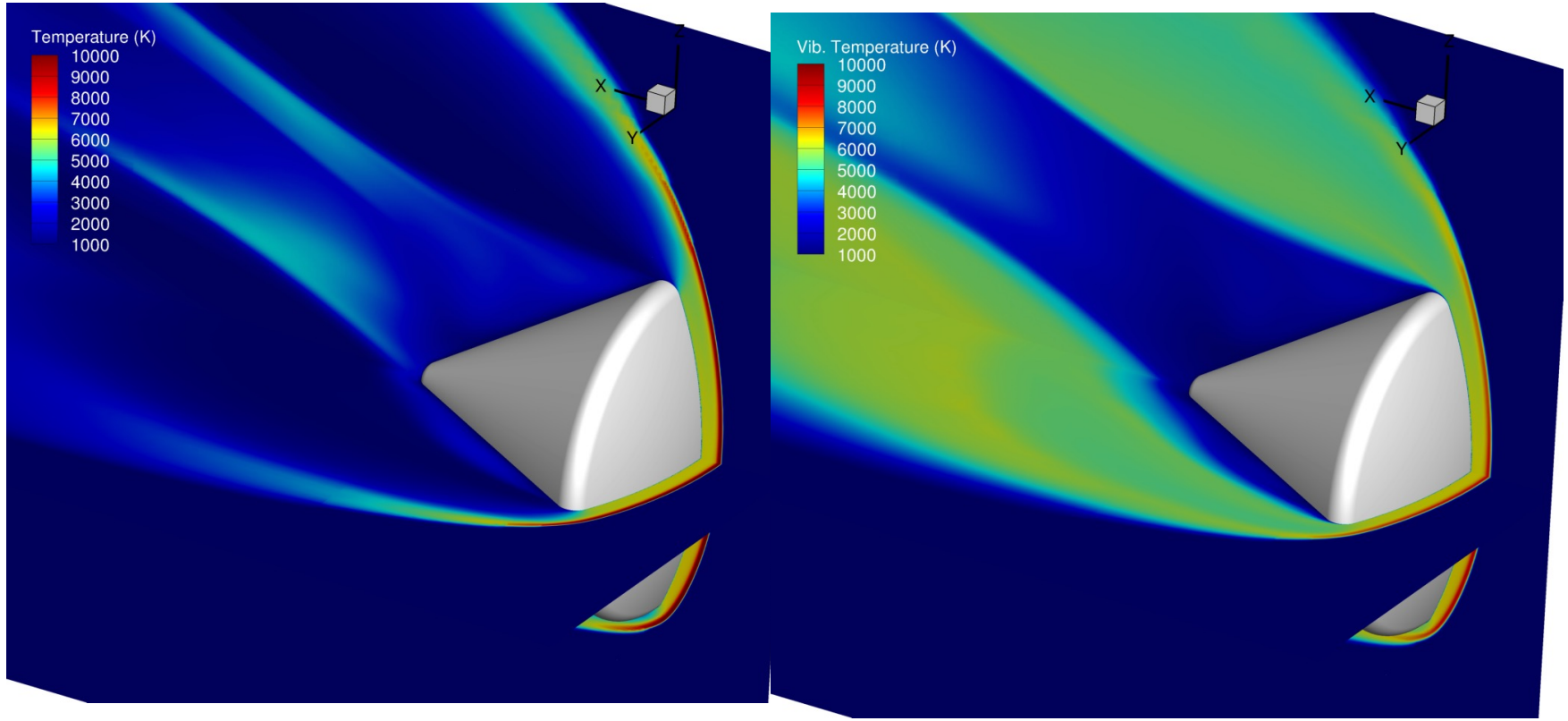


AS-202 Capsule

- AS-202 re-entry capsule at trajectory point t=4510 s (real flight condition)
- Comparison against Wright et al. (2006) with DPLR
- Radiative equilibrium surface with diffusion-limited, fully catalytic surface to atomic recombination
- **Focus:** Validation of NBS for 3D reacting flows and for fully catalytic surface boundary condition

Flow conditions

Parameter	Value
M_∞	25.6
ρ_∞ (kg/m^3)	1.69E-4
u_∞ (m/s)	7800
T_∞ (K)	230
α (deg.)	17.8
β (deg.)	2.5
$Re_{\infty,D}$	3.2E5

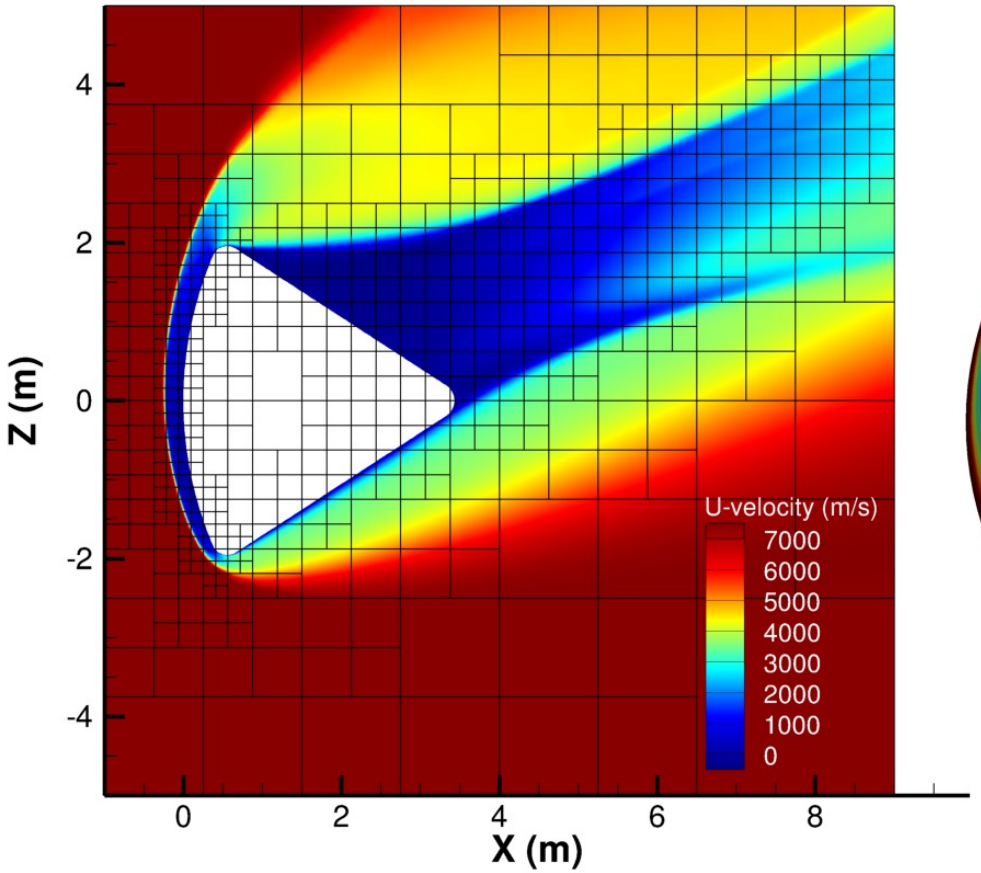


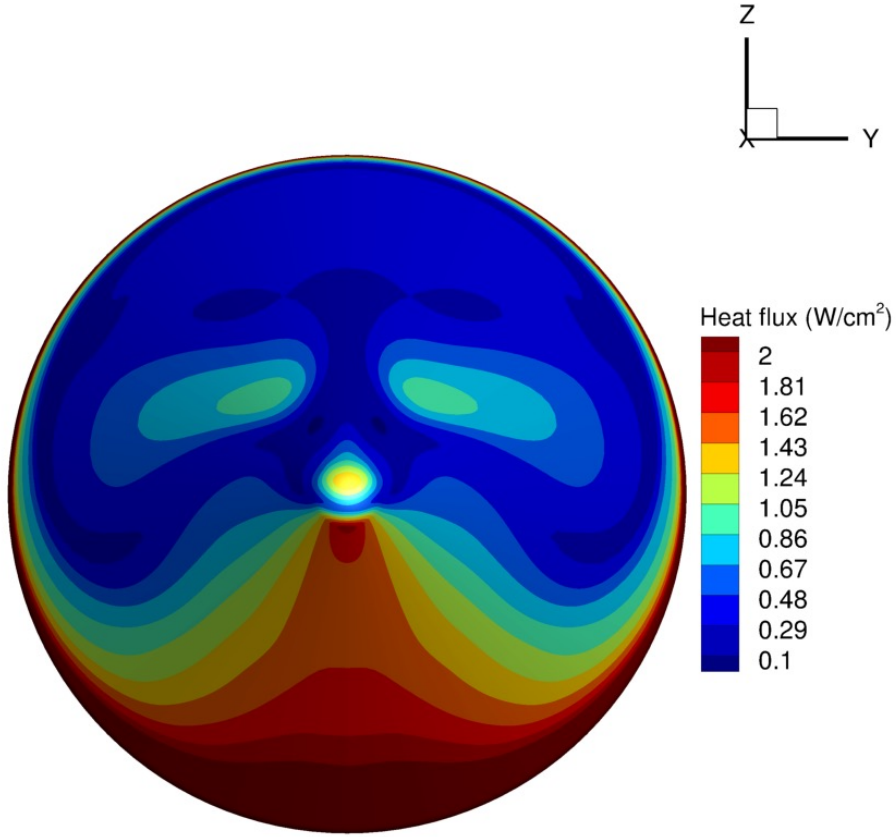
AS-202 Capsule

- AS-202 re-entry capsule at trajectory point t=4510 s (real flight condition)
- Comparison against Wright et al. (2006) with DPLR
- Radiative equilibrium surface with diffusion-limited, fully catalytic surface to atomic recombination

Flow conditions

Parameter	Value
M_∞	25.6
ρ_∞ (kg/m^3)	1.69E-4
u_∞ (m/s)	7800
T_∞ (K)	230
α (deg.)	17.8
β (deg.)	2.5
$Re_{\infty,D}$	3.2E5

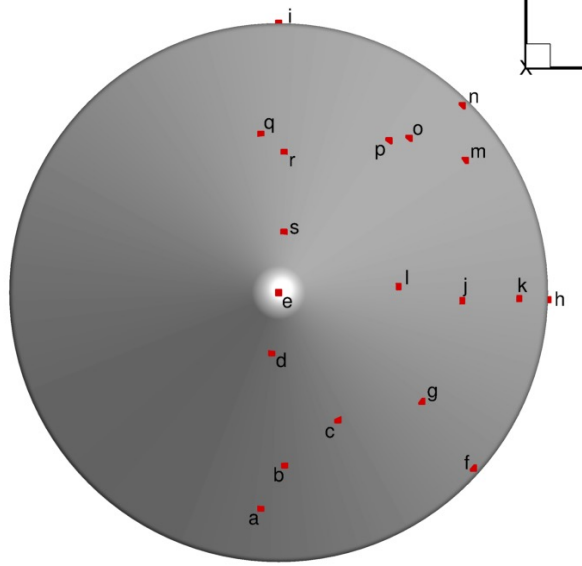


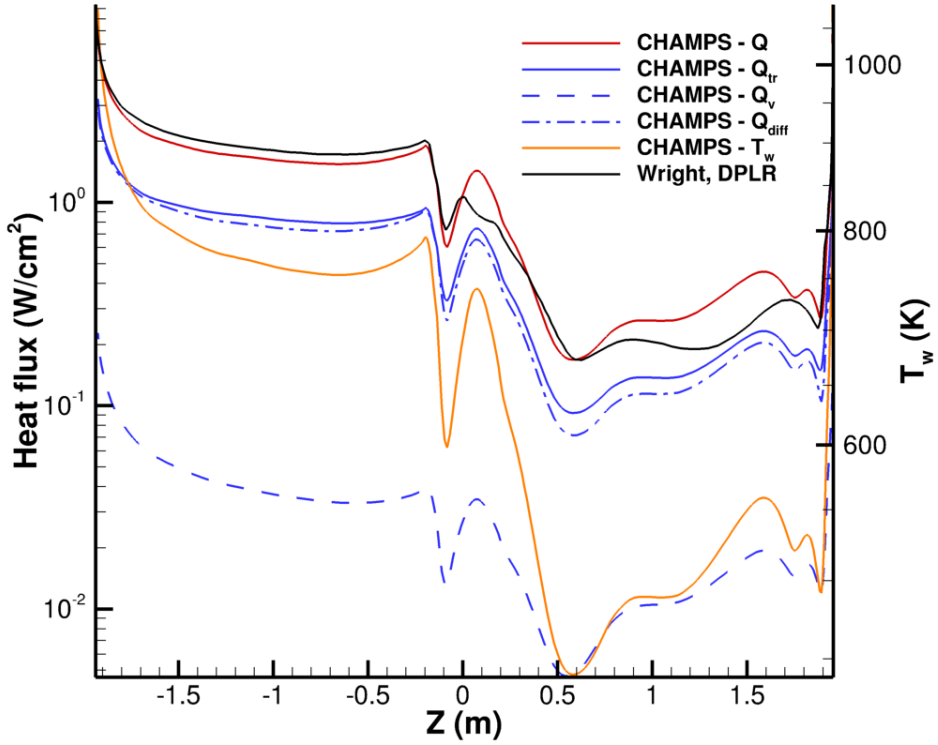


AS-202 Capsule

- AS-202 instrumented with 19 thermocouples on the aft body

	Calorimeter			Flight Data		DPLR	CHAMPS
Name	X (m)	Y (m)	Z (m)	Lower bound	Upper bound		
a	1.2080	-0.1286	-1.5638	1.4792	2.2198	2.2000	2.0037
b	1.6980	0.0437	-1.2501	1.2965	1.9340	1.9184	1.7175
c	2.0560	0.4304	-0.9229	0.9961	1.5097	1.4086	1.4547
d	2.9480	-0.0505	-0.4362	1.1624	1.7360	1.7515	1.5865
e	3.4310	0.0000	0.0000	1.2630	1.8736	1.0164	1.1498
f	0.6950	1.4136	-1.2728	1.6757	2.5143	3.0922	2.8240
g	1.6150	1.0393	-0.7888	0.6495	0.9695	1.0315	0.9784
h	0.5450	1.9551	-0.0512	7.3712	10.995	9.9716	8.8399
i	0.5450	0.0000	1.9558	N/A	N/A	4.5981	4.0829
j	0.9410	1.7419	-0.0426	0.3340	0.5128	0.3481	0.2562
k	1.5760	1.3288	-0.0580	0.2630	0.3909	0.3870	0.4332
l	2.2880	0.8666	0.0439	0.3268	0.4898	0.3068	0.3378
m	1.0680	1.3548	0.9592	0.2938	0.4423	0.3209	0.2818
n	0.6950	1.3333	1.3567	0.6188	0.9277	0.6110	0.4849
o	1.3660	0.9465	1.1201	0.2561	0.3839	0.3200	0.3170
p	1.5260	0.8009	1.1023	0.3281	0.4893	0.2865	0.2794
q	1.8430	-0.1289	1.1495	0.2582	0.3932	0.2111	0.2539
r	2.0560	0.0391	1.0176	0.2375	0.3460	0.2078	0.2249
s	2.9480	0.0383	0.4374	1.2824	1.9327	0.2414	0.2430





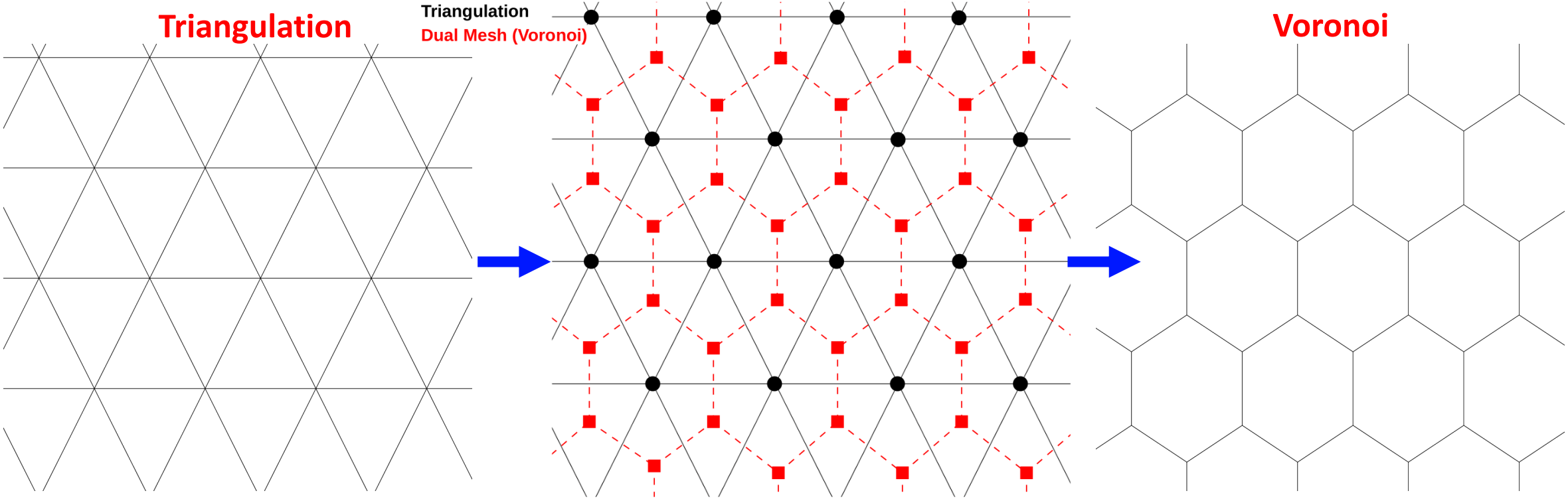
NBS-Cart Overview

- The NBS-Cart solver is particularly effective for when high fidelity results of trajectory sweeps are required
- For example, AS-202 capsule was simulated at 15 different trajectory points by Wright et al. (2006)
  - Each trajectory point provides a unique shock location and wake shear layer
  - A separate body-fitted grid was generated for each trajectory point to provide both shock and wake alignment
  - While some codes have developed mesh realignment algorithms for shock tracking at runtime, their implementation can be expensive and non-trivial
- NBS-Cart solver decouples the boundary layer grid generation from the off-body grid generation (retains high grid quality near the surface)
- Cartesian AMR is simple to implement and effective
  - Algorithmically simplistic in comparison since body alignment with the grid is not required
  - Provides an ideal analysis tool with minimal user intervention for geometry testing at various flight conditions

NBS Decoupled Convective Scheme (3D)

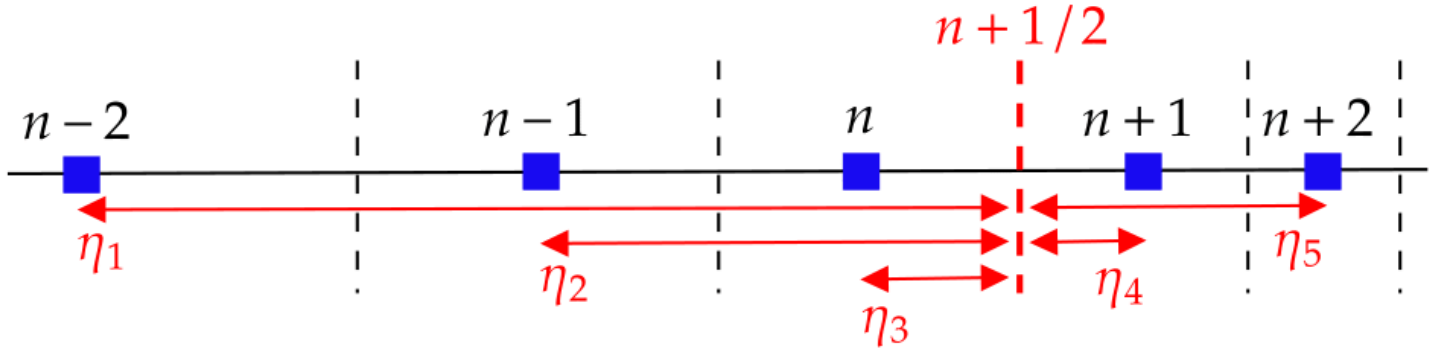
Improved Surface Grid Automation

- Quadrilateral/hexahedral grids are most common when considering viscous flow solutions due to improved solution quality
  - True for structured and unstructured solvers
- Triangulations are more readily automated but produce generally poor solutions
- Voronoi grids employed here to take advantage of improved automation via triangulations while retaining better solution reconstruction characteristics



NBS Convective Scheme

- Two numerical schemes are evaluated for the MSL validation test case:
  - Structured reconstruction (2nd order MUSCL)
  - Unstructured reconstruction (new numerical formulation developed for this work)
    - Decouple wall-normal and streamwise flux evaluations for convective scheme
    - Take advantage of structured wall-normal memory layout for higher order accuracy
    - **Wall-normal faces:**



    - 5th order WENO-based variable reconstruction to face based on signed distance
    - Modified Steger-Warming flux evaluation
    - Removes need for storage of metric terms
    - Gradient clouds re-computed during runtime for low memory overhead (GPU)

NBS Convective Scheme

- Two numerical schemes are evaluated for the MSL validation test case:
  - Structured reconstruction (2nd order MUSCL)
  - Unstructured reconstruction (new numerical formulation developed for this work)
    - Decouple wall-normal and streamwise flux evaluations for convective scheme
    - Take advantage of structured wall-normal memory layout for higher order accuracy
    - **Streamwise faces:**

$$q^L = q_P + \nabla q_P \cdot r_P$$
$$q^R = q_N + \nabla q_N \cdot r_N$$

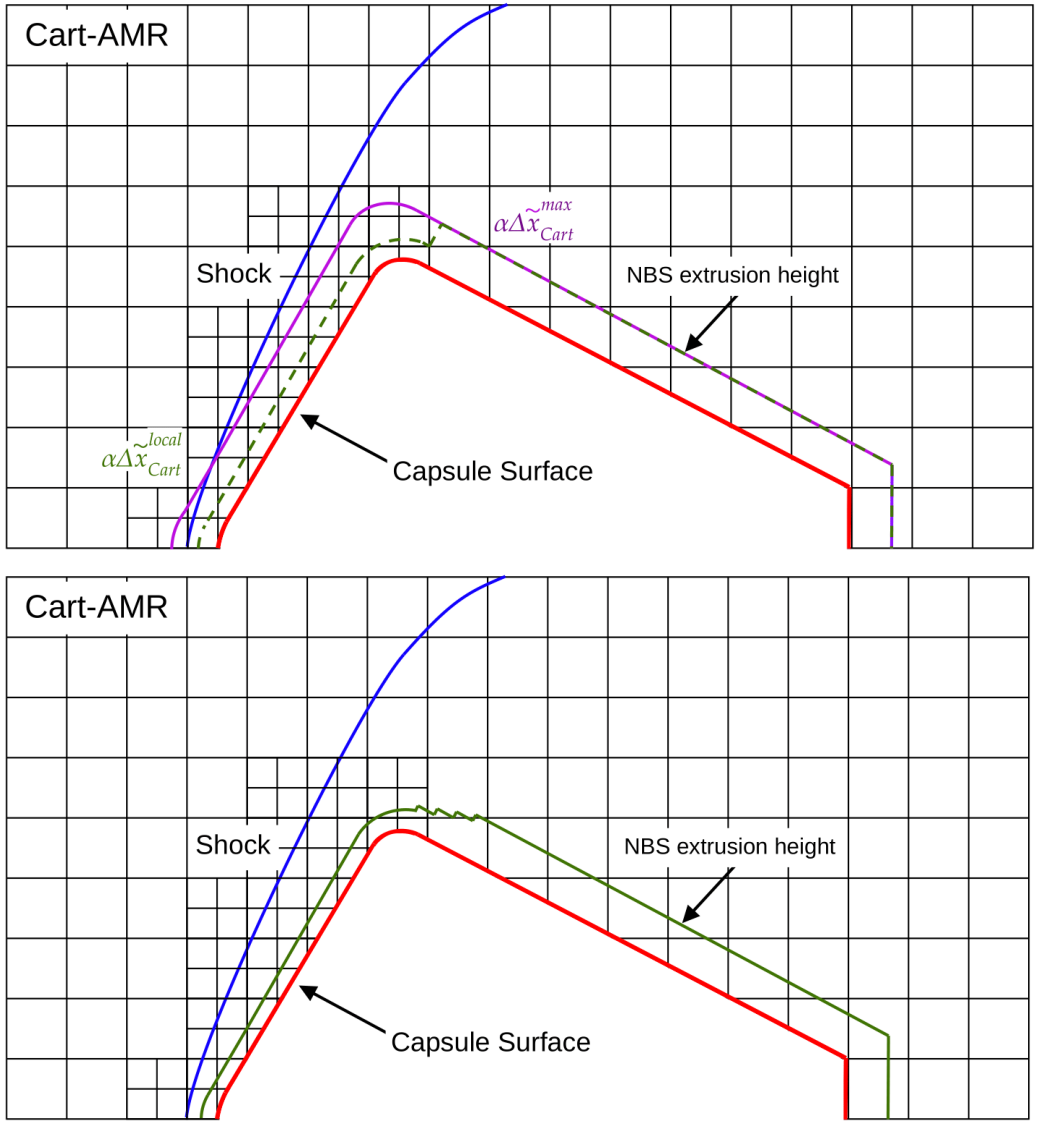
      - 2nd order Kinetic Energy and Entropy Preserving (KEEP) scheme (Kuya et al. 2020)

        OR

      - 2nd order MUSCL w/ modified Steger-Warming flux

NBS Grid Generation

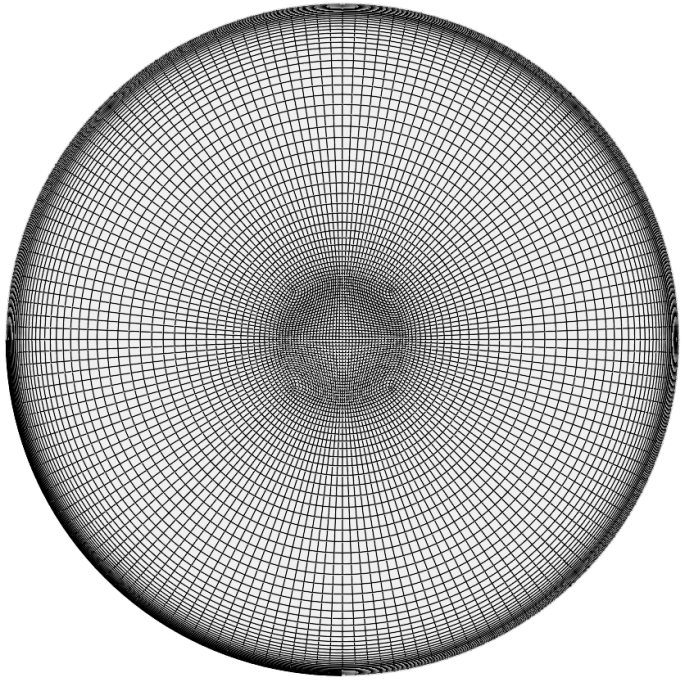
- Due to decoupling of wall-normal and streamwise flux evaluations, grid generation must be modified
- Must guarantee NBS rays remain orthogonal to the surface
- Switch to stair-stepped NBS extrusion to allow for orthogonal extrusion and variable boundary refinement



Case 1 – MSL Capsule, Perfect Gas

- Full MSL capsule forebody simulated at 0-degree AoA
- Validation against body-fitted solver of Chen et al. (2018)
- Validation against experimental campaign of Hollis and Collier (2008)
- **Focus:** Investigate decoupled convective scheme on various grid topologies

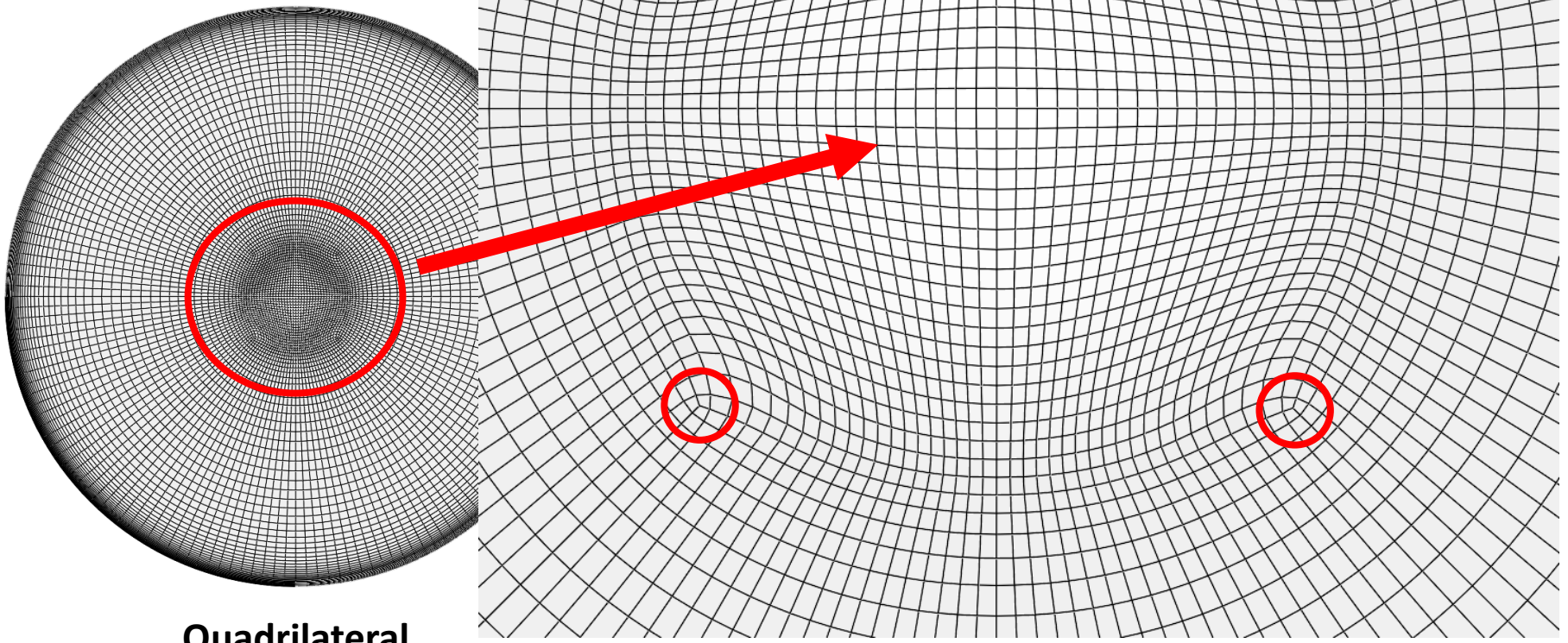
Parameter	Value
M_∞	9.47
p_∞ (Pa)	167.9
u_∞ (m/s)	1405.59
T_∞ (K)	54.8
T_w (K)	294.44
Re_∞ (1/m)	4.32E6



Quadrilateral

Case 1 – MSL Capsule, Perfect Gas

- ❑ Full MSL capsule fore
- ❑ Validation against bo
- ❑ Validation against exp
- ❑ **Focus:** Investigate de topologies



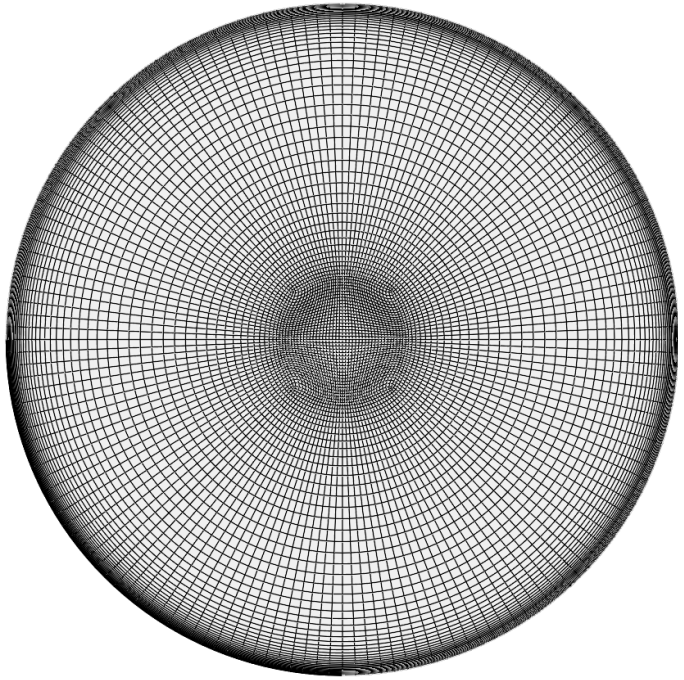
Quadrilateral

Parameter	Value
M_∞	9.47
p_∞ (Pa)	167.9
u_∞ (m/s)	1405.59
T_∞ (K)	54.8
T_w (K)	294.44
Re_∞ (1/m)	4.32E6

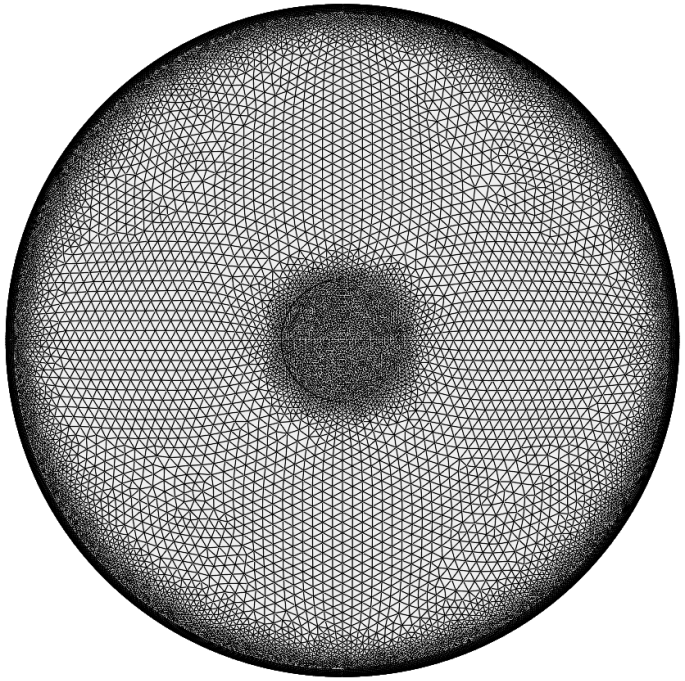
Case 1 – MSL Capsule, Perfect Gas

- Full MSL capsule forebody simulated at 0-degree AoA
- Validation against body-fitted solver of Chen et al. (2018)
- Validation against experimental campaign of Hollis and Collier (2008)
- **Focus:** Investigate decoupled convective scheme on various grid topologies

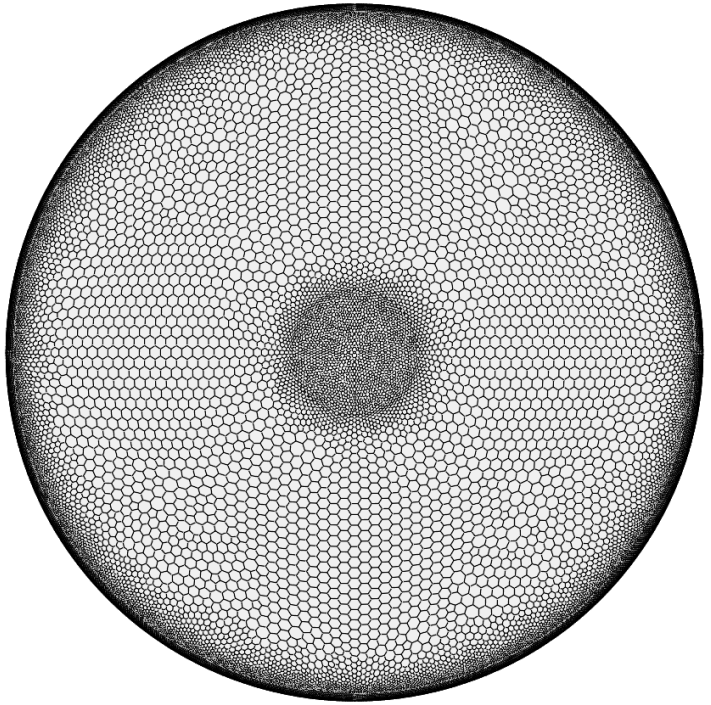
Parameter	Value
M_∞	9.47
p_∞ (Pa)	167.9
u_∞ (m/s)	1405.59
T_∞ (K)	54.8
T_w (K)	294.44
Re_∞ (1/m)	4.32E6



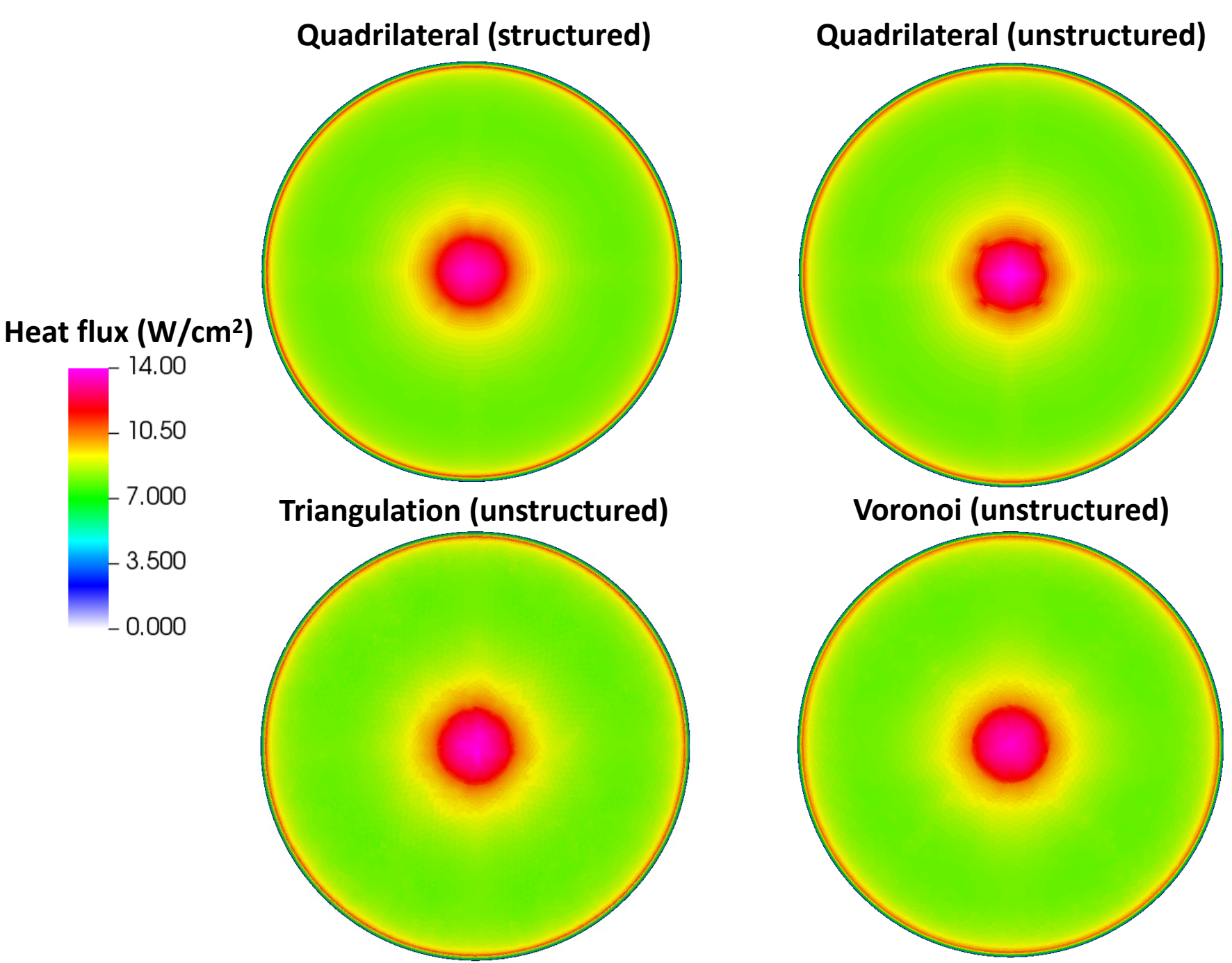
Quadrilateral



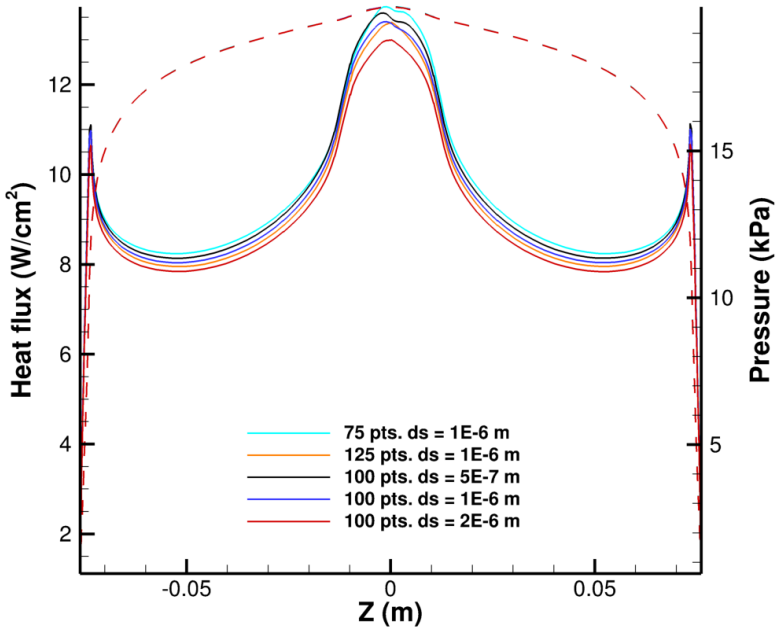
Triangulation



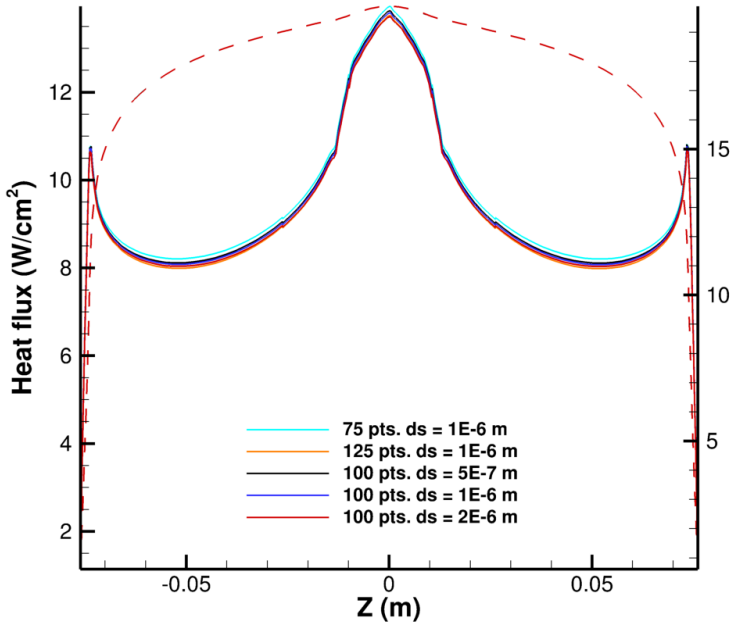
Voronoi


Quadrilateral (structured)
Quadrilateral (unstructured)
Heat flux (W/cm²)
14.00
10.50
7.000
3.500
0.000
Triangulation (unstructured)
Voronoi (unstructured)

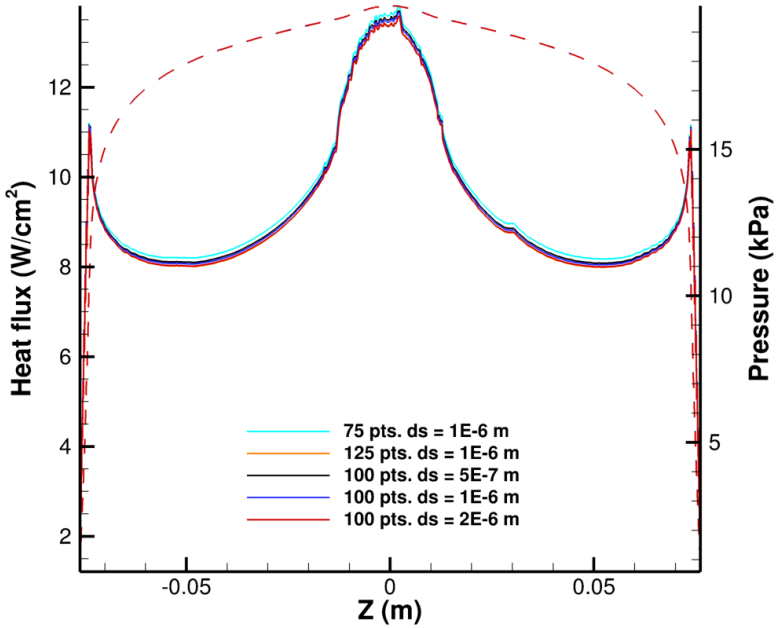
Quadrilateral (structured)



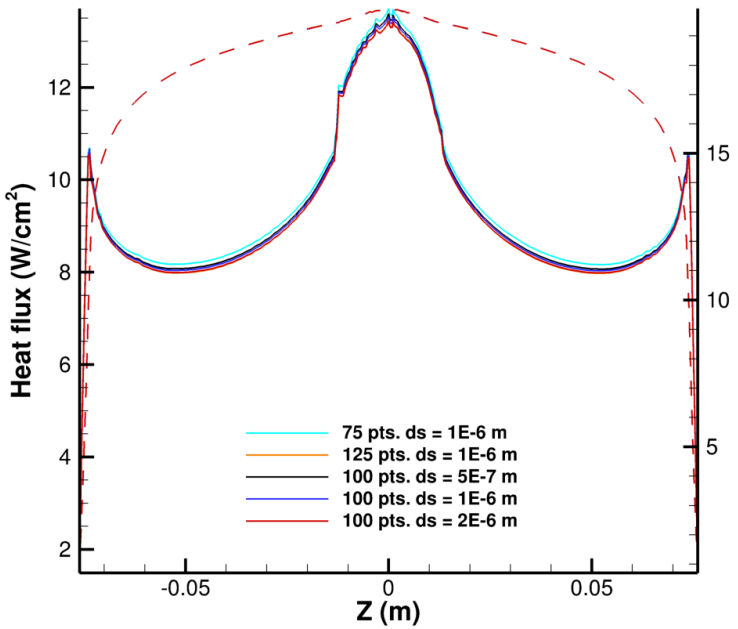
Quadrilateral (unstructured)

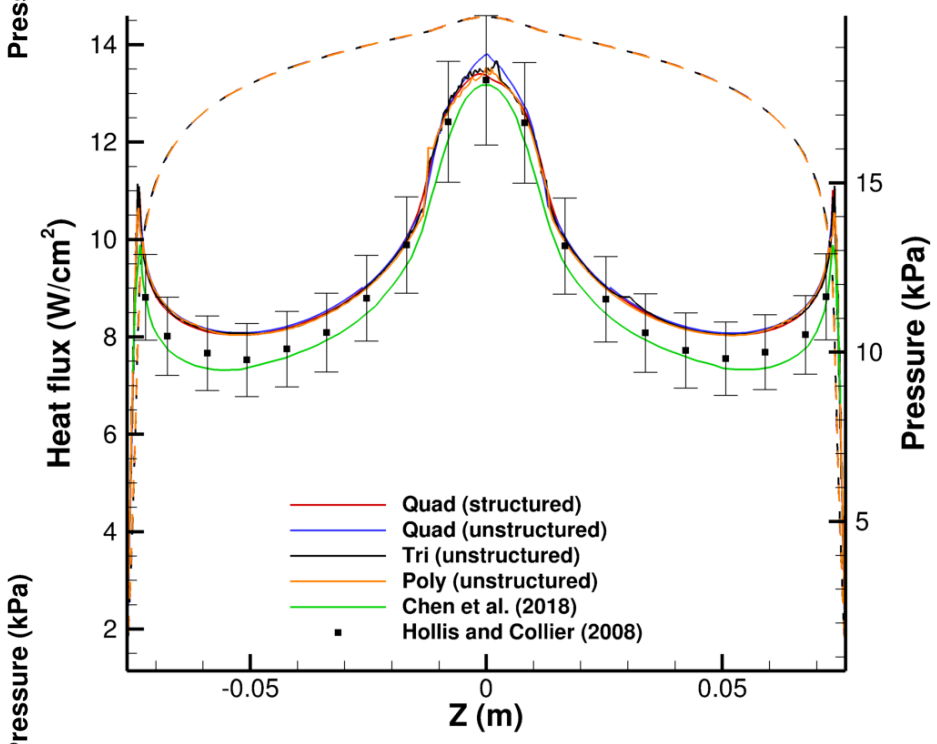


Triangulation (unstructured)



Voronoi (unstructured)



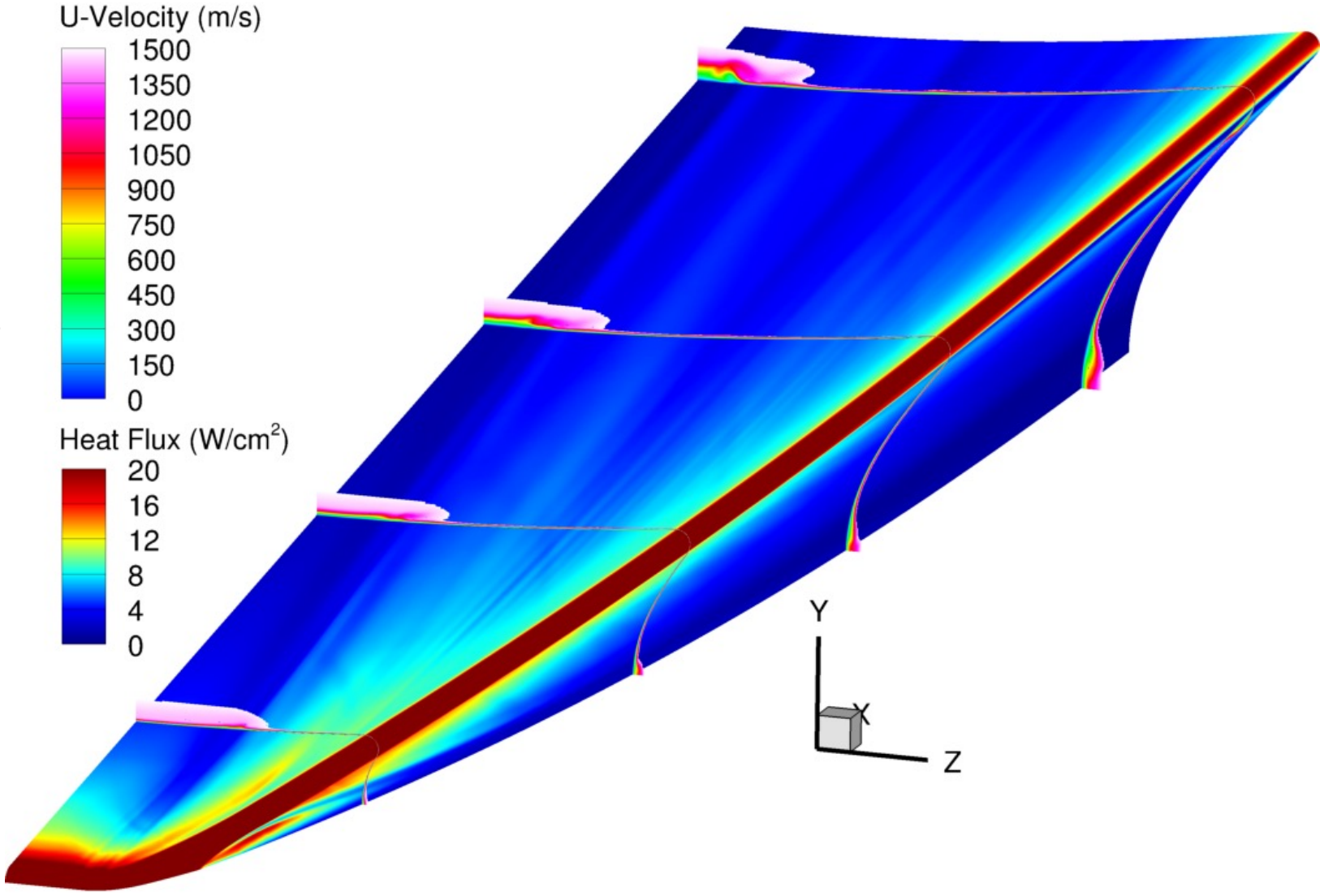


Decoupled convective scheme reaches the grid converged solution state much sooner!

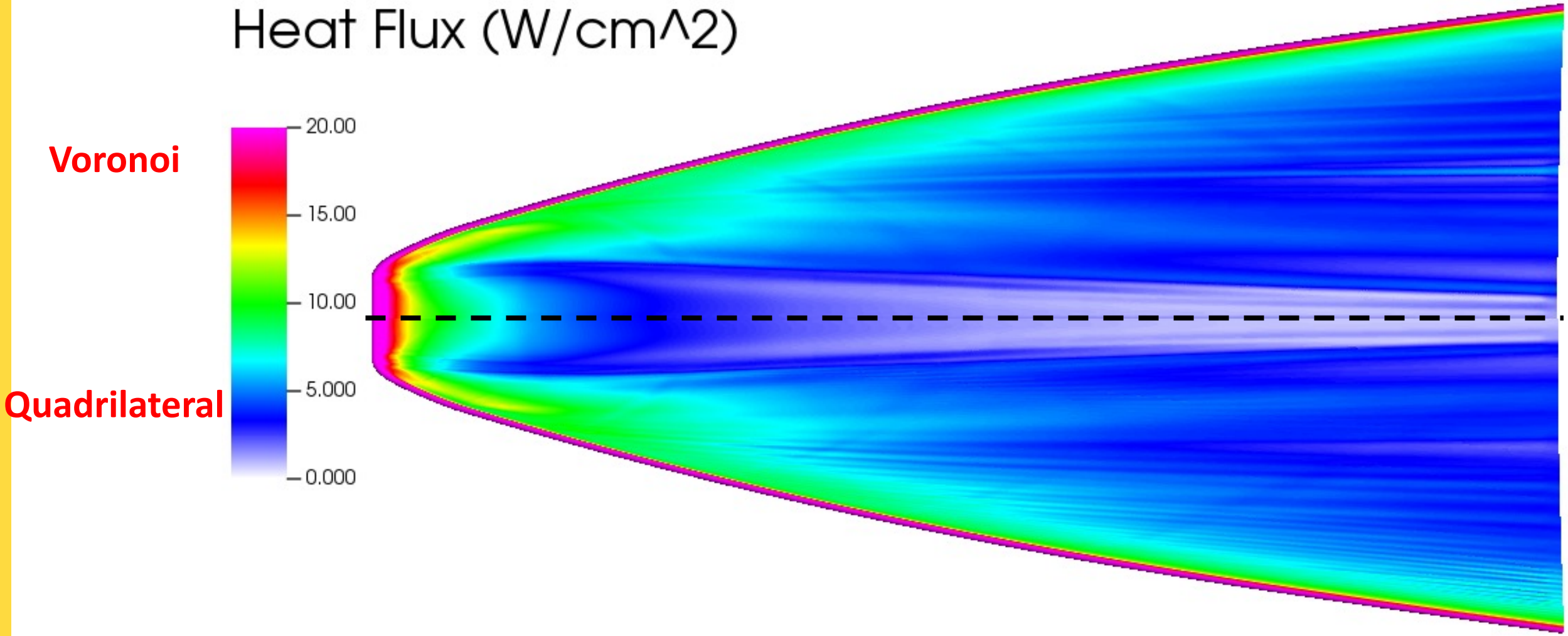
Case 2 – BOLT Vehicle

- Demonstration case for BOLT at ascent conditions
- Quadrilateral surface grid
- 63 M Cartesian points + 32M/46M NBS points = 95-109 M total grid points
- **Focus:** Can the new NBS scheme be used as a low-dissipation method for scale-resolving cases?

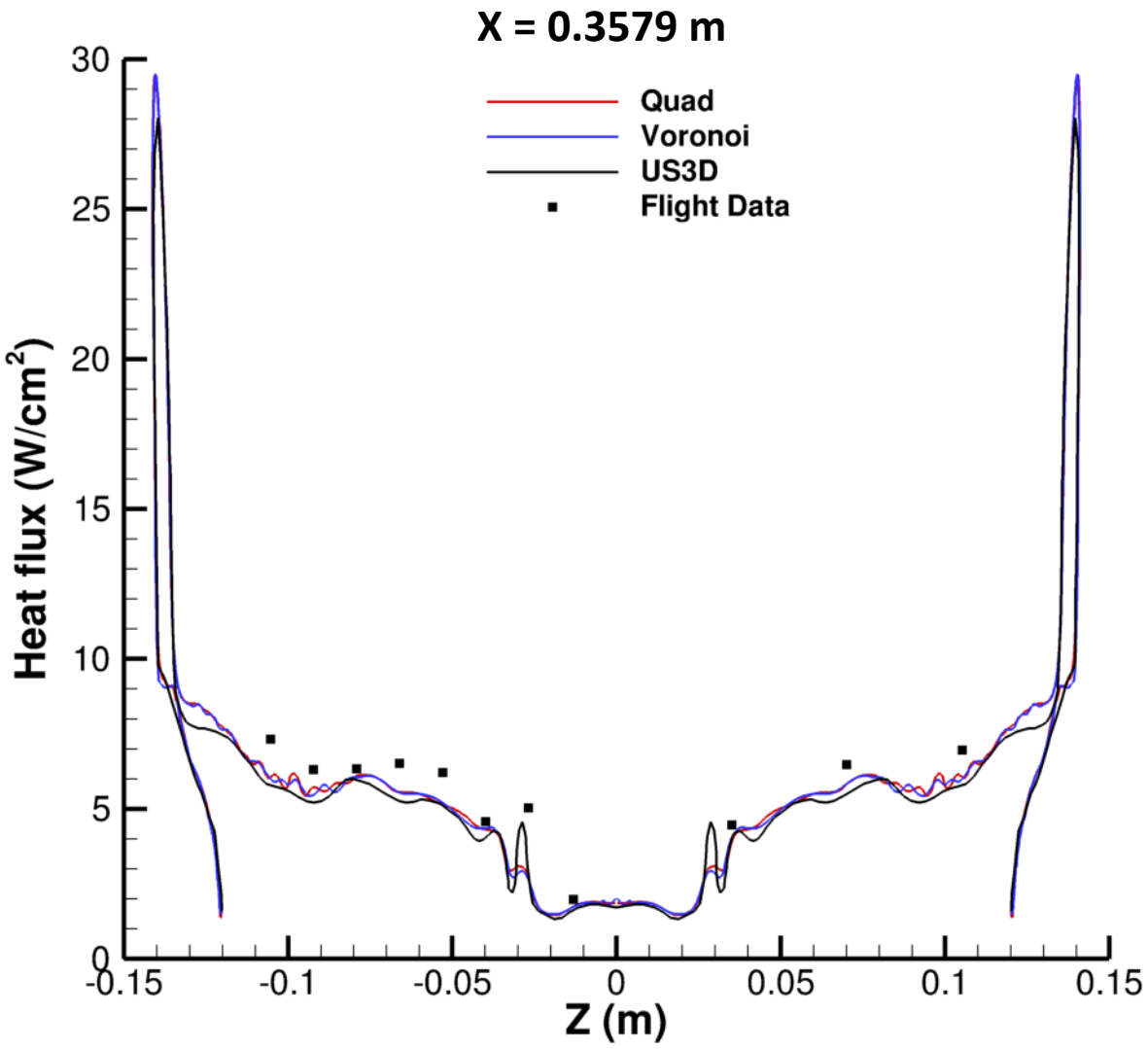
Parameter	Value
M_∞	6.0424
ρ_∞ (kg/m^3)	0.048302
u_∞ (m/s)	1768.5
T_∞ (K)	213.15
T_w (K)	390
Re_∞ (1/m)	6.0914E6

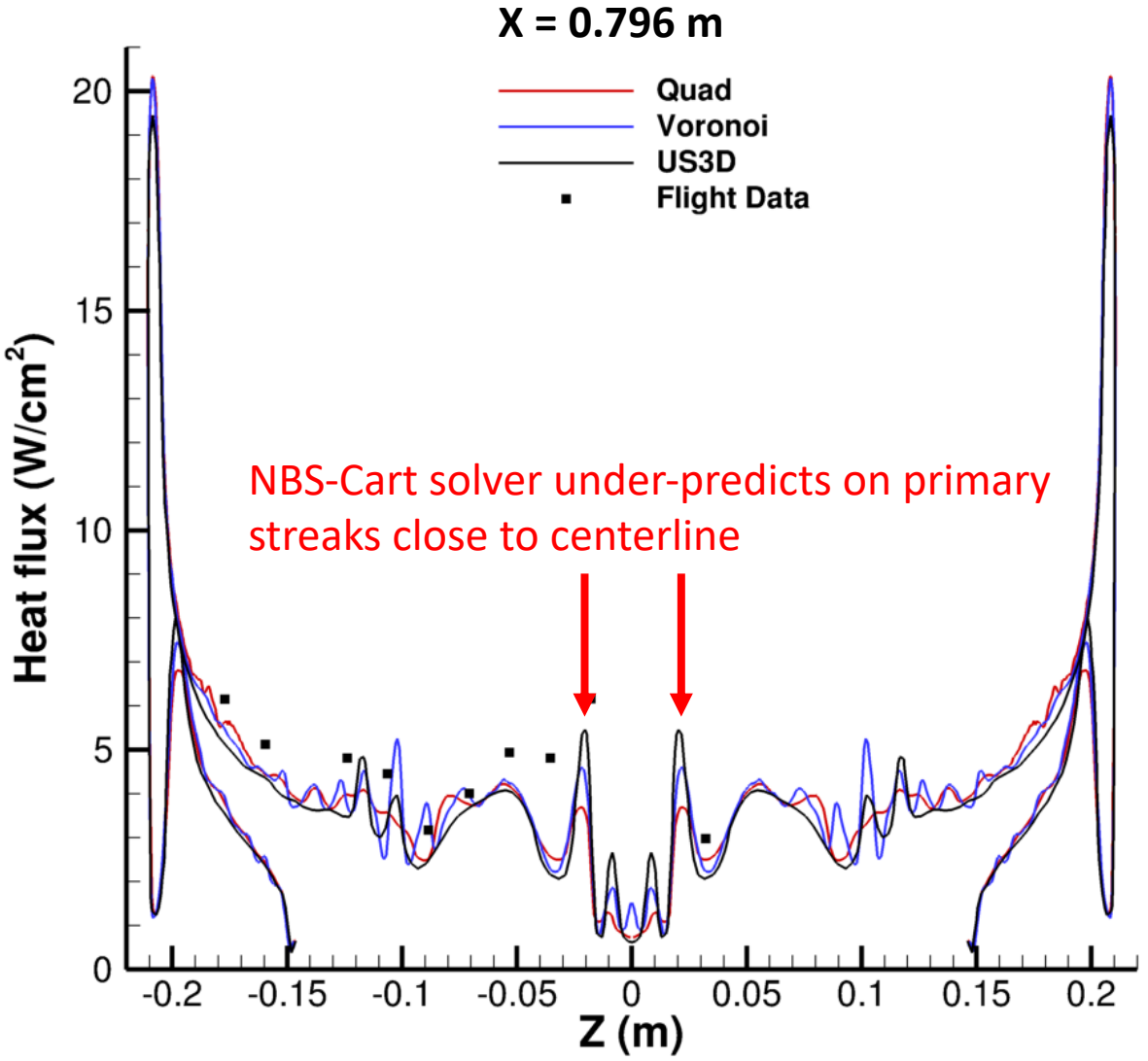


Case 2 – BOLT Vehicle

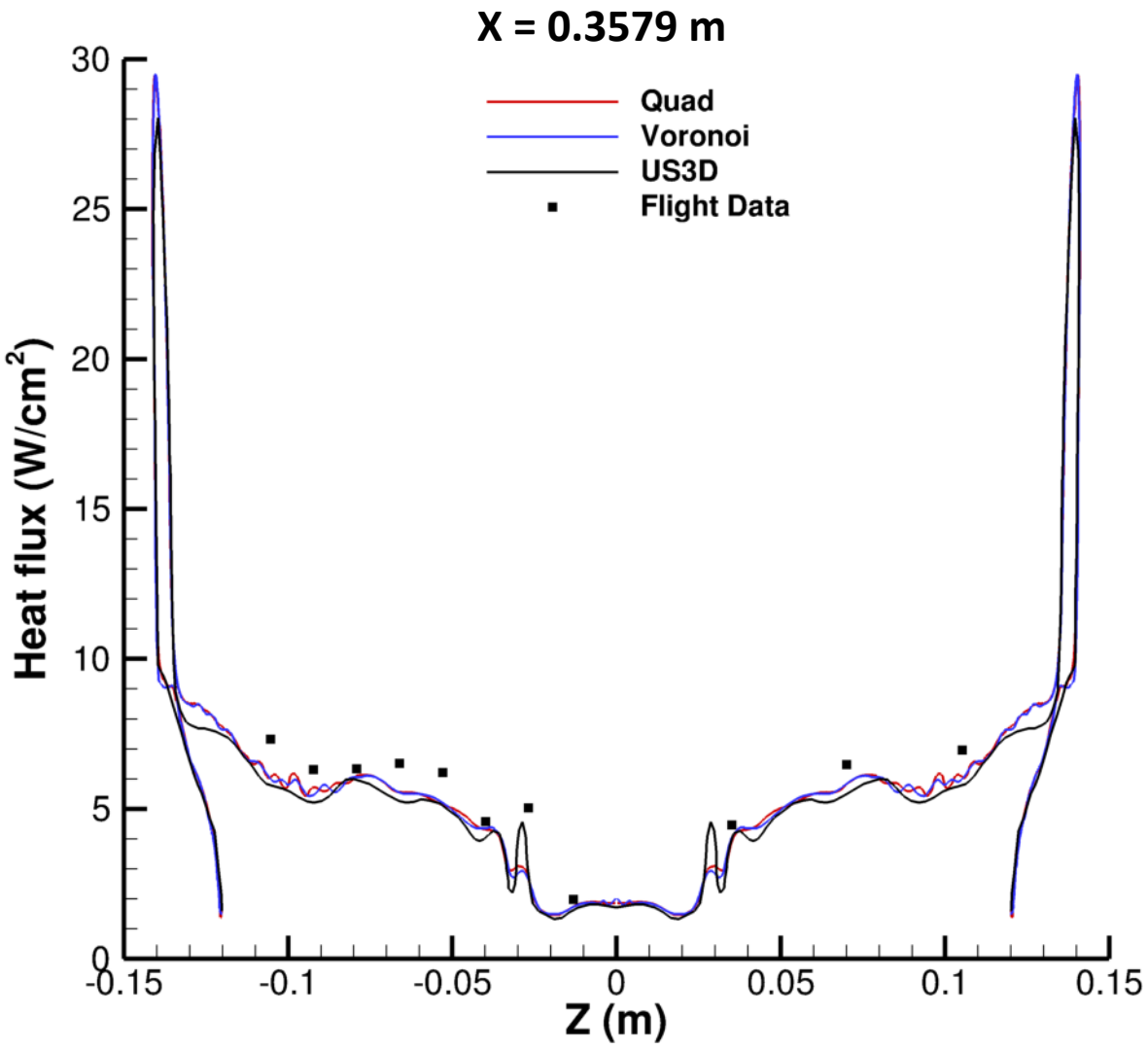


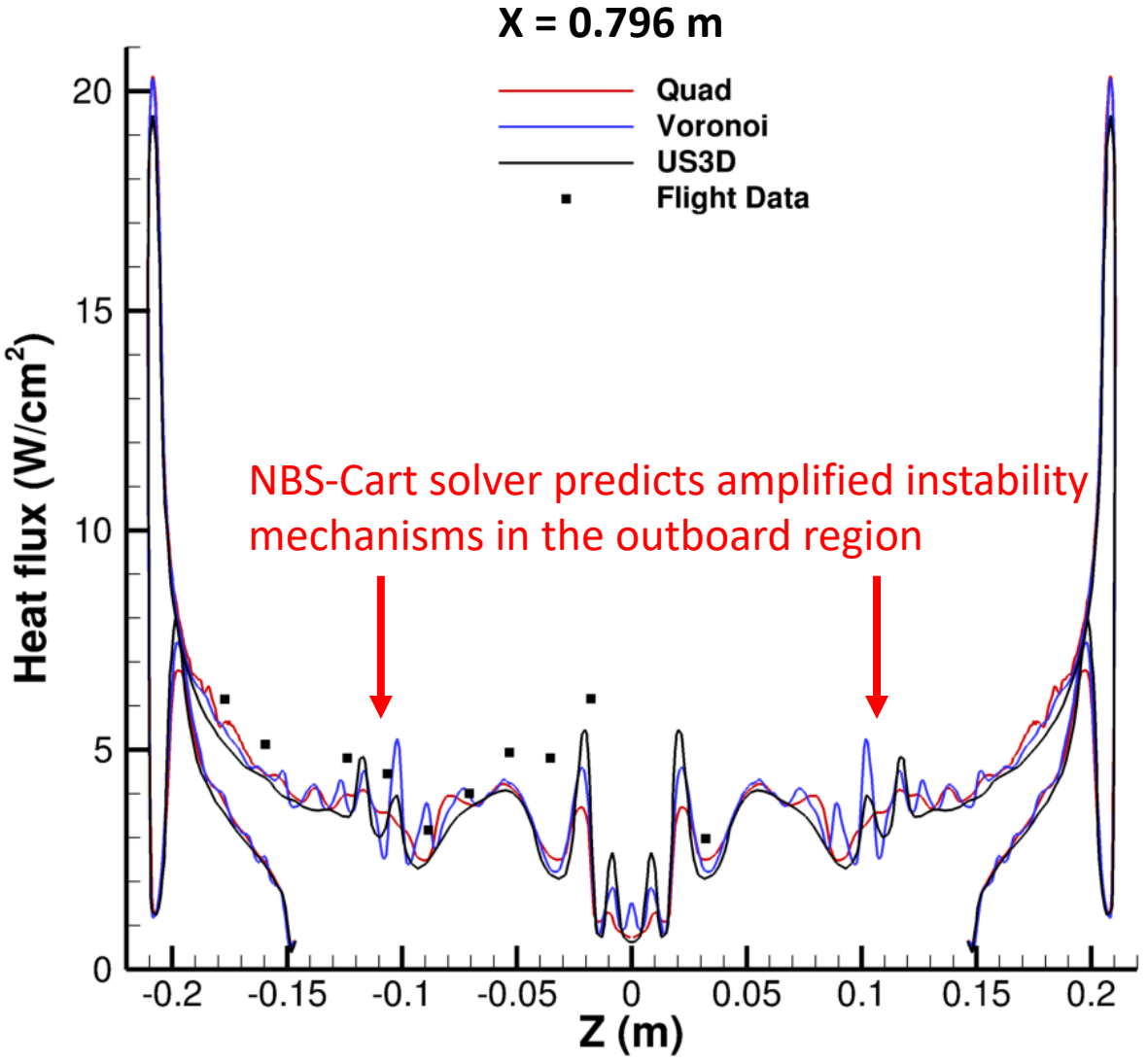
Case 2 – BOLT Vehicle





Case 2 – BOLT Vehicle





Conclusions

- Development of an NBS-Cart solver usable in 2D and 3D for scale-resolving simulations
  - Fully automated volume mesh generation within NBS
  - Robust numerical methods and time integration procedures for hypersonic shock capturing on non-aligned grids
  - Provides accurate and artifact-free heat flux predictions in low and high enthalpy environments
  - Effective for moving boundary and complex multi-physics problems
- NBS decoupled convective scheme provides a memory efficient numerical model that takes advantage of the structured wall-normal memory layout present for 2D and 3D applications

- The NBS-Cart solver increases CFD workflow automation by removing a significant bottleneck to the pre-processing mesh generation phase

Funding

- ❑ NASA EPSCoR RA Award (award no. 80NSSC19M0144) with Dr. Eric Stern
- ❑ NASA ACCESS (award no. 80NSSC21K1117) with Dr. Eric Stern
- ❑ Office of Naval Research (award no. N00014-23-1-2167) with Dr. Eric Marineau
- ❑ Naval Air Warfare Center Aircraft Division (award no. N00421-22-2-0001) with Dr. Joshua Butler and Dr. William Tyson
- ❑ DoD HPC Modernization Program (award no. FA700-19-2-0002) with. Dr. Russ Cummings
- ❑ University of Maryland Zaratan HPC system & University of Kentucky LCC HPC system